Mimicked Hydrogels for Bone Tissue Engineering in Orthopedic Applications

Atsadaporn Thangprasert

A Thesis Submitted in Partial Fulfillment of the Requirements for the Degree of Doctor of Philosophy in Biomedical Engineering

Prince of Songkla University

2019

Mimicked Hydrogels for Bone Tissue Engineering in Orthopedic Applications

Atsadaporn Thangprasert

A Thesis Submitted in Partial Fulfillment of the Requirements for the Degree of Doctor of Philosophy in Biomedical Engineering

Prince of Songkla University

2019

Thesis title	Mimicked Hydrogels for Bone Tissue Engineering in Orthopedic Applications
Author	Miss Atsadaporn Thangprasert
Major Program	Biomedical Engineering

Major Advisor

……...

(Assoc. Prof. Dr.Jirut Meesane)

Co-advisor:

……...

(Asst. Prof. Dr.Chittreeya Tansakul)

……...

(Asst. Prof. Dr.Nattawut Thuaksubun)

Examining Committee:

……Chairperson

(Assoc. Prof. Dr.Kawee Srikulkit)

…….……Committee

(Assoc. Prof. Dr.Jirut Meesane)

…….……Committee

(Asst. Prof. Dr.Chittreeya Tansakul)

…….……Committee

(Asst. Prof. Dr.Nattawut Thuaksubun)

…….……Committee

(Dr.Mattana Khangkhamano)

The Graduate School, Prince of Songkla University, has approved this thesis as partial fulfillment of the requirements for the Doctor of Philosophy Degree in Biomedical Engineering

…….…….

(Prof. Dr.Damrongsak Faroongsarng)

Dean of Graduate School

This is to certify that the work here submitted is the result of the candidate's own investigations. Due acknowledgement has been made of any assistance received.

……..Signature
(Assoc. Prof. Dr.Jirut Meesane)
Major Advisor

……..Signature
(Miss Atsadaporn Thangprasert)
Candidate

I hereby certify that this work has not been accepted in substance for any degree, and is not being currently submitted in candidature for any degree.

……..Signature
(Miss Atsadaporn Thangprasert)
Candidate

ชื่อวิทยานิพนธ์ โครงร่างเลียนแบบธรรมชาติประเภทไฮโดรเจลสำหรับวิศวกรรมเนื้อเยื่อกระดูก เพื่อการประยุกต์ใช้งานทางด้านโรคกระดูกและข้อ

ผู้เขียน นางสาวอัษฎาพร ตั้งประเสริฐ

สาขาวิชา วิศวกรรมชีวการแพทย์

ปีการศึกษา 2561

บทคัดย่อ

งานวิจัยนี้ได้ทำการออกแบบและสร้างโครงร่างวิศวกรรมเนื้อเยื่อเลียนแบบธรรมชาติประเภทไฮโดรเจล โดยไฮโดรเจลที่สร้างขึ้นนี้จะอาศัยการเลียนแบบโครงร่างภายนอกเซลล์ให้มีความใกล้เคียงกับเนื้อเยื่อธรรมชาติ เพื่อนำไปประยุกต์ใช้ในงานด้านกระดูกและข้อ ซึ่งโครงร่างวิศวกรรมเนื้อเยื่อในงานวิจัยชิ้นนี้ถูกสร้างขึ้น เพื่อทำหน้าที่ในการใช้งานสำหรับเป็น 1) วัสดุชีวภาพสำหรับต้นแบบในการประเมินโรค 2) วัสดุชีวภาพเพื่อใช้ในกระบวนการสร้างเนื้อเยื่อใหม่สำหรับผ่าตัด และ 3) วัสดชีวภาพเพื่อใช้ในการสร้างเป็นสัณฐานวิทยาของเนื้อเยื่อ โดยงานวิจัยแรกจะเป็นการสร้างโครงร่างวิศวกรรมแบบสามมิติที่เลียนแบบสภาวะการเกิดโรค Heterotopic ossification (HO) โดยสร้างจากเจลาติน, ไคโตซานและแคลเซียมฟอสเฟส ผลการทดลองแสดงให้เห็นว่า ไฮโดรเจลที่สร้างขึ้นจากส่วนประกอบของเจลาติน ไคโตซาน และแคลเซียมฟอสเฟตที่ใส่ในปริมาณต่างกันนี้ มีสมบัติทางกายภาพและสมบัติทางชีวภาพที่ สามารถนำไปใช้เป็นแบบจำลองสำหรับการวิเคราะห์โรค HO ได้ โครงร่างวิศวกรรมเนื้อเยื่อชนิดที่สองถูกสร้างขึ้นเพื่อใช้งานด้านกระบวนการสร้างเนื้อเยื่อใหม่ สำหรับงานทางด้านวิศวกรรมเนื้อเยื่อบริเวณส่วนผิวหน้าที่อยู่ระหว่างกระดูกอ่อนและกระดูกแข็งบริเวณข้อเข่า ไฮโดรเจลนี้ถูกสร้างขึ้นจากส่วนผสมของเจลาตินและพีวีเอโดยวิธีการเลียนแบบธรรมชาติ ผลการศึกษาแสดงให้เห็นว่า ไฮโดรเจลชนิดนี้มีสามารถทำให้เซลล์เกาะและเจริญเติบโตได้ นอกจากนี้เซลล์ที่เลี้ยงบนไฮโดรเจลชนิดนี้ยังสามารถหลั่งสารที่เป็นตัวบ่งชี้ของการสร้างกระดูกได้อีกด้วย ซึ่งเหมาะสมสำหรับการนำไปประยุกต์ใช้สำหรับเนื้อเยื่อกระดูกชั้นใต้ผิวกระดูกอ่อน และโครงร่างวิศวกรรมเนื้อเยื่อชิ้นสุดท้ายนั้น เป็นการสังเคราะห์พอลิเมอร์ประเภทไฮโดรเจลที่มีส่วนผสมของ PNIPAM ที่ตอบสนองกับอุณหภูมิและมีกรดไฮยาลูรอนิคที่เป็นองค์ประกอบของโครงสร้างภายนอกเซลล์ โดยพอลิเมอร์ไฮโดรเจลนี้จะทำหน้าที่เป็นโครงร่างสองมิติ (Two dimensional (2D) scaffolds) สำหรับสร้างแผ่นเนื้อเยื่อ ผลการทดลองพบว่า โครงร่างชนิดนี้จะถูกนำมาใช้ในการสร้างเป็นเยื่อบางๆเพื่อให้เซลล์เกาะ ผลการ

ทดลองพบว่าเซลล์สามารถเกาะได้ดีบนพอลิเมอร์ไฮโดรเจลที่สังเคราะห์ขึ้นและสามารถตอบสนองกับอุณหภูมิที่เปลี่ยนแปลงได้ แผ่นเนื้อเยื่อนี้สามารถนำไปใช้ในส่วนของกระดูกชั้นใต้ผิวกระดูกอ่อน และสามารถนำไปพัฒนาเพื่อสร้างเป็นสัณฐานวิทยาของเนื้อเยื่อที่มีความซับซ้อนในอนาคต จากผลการทดลองทั้งหมดแสดงให้เห็นว่าไฮโดรเจลที่สร้างขึ้นด้วยหลักการเลียนแบบธรรมชาติในงานวิจัยชิ้นนี้สามารถนำไปประยุกต์ใช้งานในโรคที่เกี่ยวข้องกับกระดูกและข้อได้

Thesis Title Mimicked Hydrogels for Bone Tissue Engineering in Orthopedic Applications

Author Miss Atsadaporn Thangprasert

Major Program Biomedical Engineering

Academic Year 2018

ABSTRACT

In this study, mimicked hydrogels are designed and fabricated for bone tissue engineering in orthopedic applications. Hydrogels in this research are used for 1) the model for diseases evaluation 2) biomaterial for surgery in bone tissue regeneration and 3) biomaterial for morphological formation of tissue. The first study is to fabricate hydrogels as model for evaluation of heterotopic ossification. Gelatin/chitosan/CCP was selected for hydrogel fabrication with the mimicking. The results showed that the mimicked gelatin/chitosan/CCP hydrogels had the suitable structure, physical and biological functionality for a model to evaluate heterotopic ossification. The second part is to fabricate and apply hydrogels for surgery to regenerate tissue at subchondral bone interface. Gelatin/PVA was fabricated into hydrogel based on the mimicking. The mimicked gelatin/PVA hydrogel demonstrated the good biological performance; cell adhesion and proliferation, the biomarkers referred to bone regeneration. This showed that the mimicked gelatin/PVA hydrogel for surgery to regenerate tissue at the subchondral bone interface. The third part is to synthesize the grafted hyaluronic acid (HA)-poly (*N*-isopropylacrylamide) (PNIPAM-COOH) thermo-responsive polymer via polymerization. This copolymer was created based on mimicked extracellular matrix (ECM) component of HA which had the thermo-responsive function of PNIPAM. The two dimensional (2D) hydrogel of HA-PNIPAM was used as substrate of the basement membrane ECM for morphological formation of cell sheet. The results demonstrate that cells well adhered, proliferated, and regulated into sheet on the substrate. This cell sheet is promising to tissue regeneration at the subchondrol bone. Furthermore, the cell sheet on substrate was detached and self-organized into the rolled form. This is the trigger idea as the model to engineer the complicate morphology of tissue for the future works. This research demonstrated that the mimicked hydrogel had the potential for orthopedic applications.

CONTENTS

	Page
ABSTRACT (THAI)	v
ABSTRACT (ENGLISH)	vii
ACKNOWLEDGEMENTS	viii
LIST OF TABLES	x
LIST OF FIGURES	xi
LIST OF ABBREVIATION AND SYMBOLS	xv
CHAPTER 1	1
CHAPTER 2	14
CHAPTER 3	37
CHAPTER 4	68
CHAPTER 5	93
APPENDIX	95
VITAE	101

LIST OF TABLES

Table		Page
4.1	Grafting yield, M_n, M_w, and PDI of synthesized polymers	78
4.2	The sol-gel transition temperature (^oC) of synthesized polymers (10%w/v)	81

LIST OF FIGURES

Figure		Page
1.1	The important components to make up the tissue engineering	2
1.2	Schematics of bone remodeling	4
1.3	Schematic illustration of bone tissue engineering process Stem cells isolated from the patient donor are differentiated into osteoblasts and cultivated in scaffolds *in vitro* before implantation at the defect site. Cell-free scaffold is also used by combination with nanoparticles or growth factors to enhance bone formation	5
2.1	**(**A) Blending of gelatin/chitosan/CCP without GA, (B) Blending of gelatin/chitosan/CCP with GA. Appearance of the hydrogels: (C) Control; (D) gelatin/chitosan/CCP (1:1:0.05); (E) (1:1:0.1); (F) (1:1:0.5); and (G) (1:1:1)	21
2.2	FT-IR spectra of the hydrogels: Control; gelatin/chitosan/CCP (1:1:0.05); (1:1/0.1); (1:1:0.5); and (1:1:1)	22
2.3	XRD diffraction of the hydrogels: Control; gelatin/chitosan/CCP (1:1:0.05); (1:1:0.1); (1:1:0.5); and (1:1:1)	23
2.4	Morphology of the hydrogels: (A) Control; (B), (F) gelatin/chitosan/CCP (1:1:0.05); (C, G) (1:1:0.1); (D, H) (1:1:0.5), and (E, I) (1:1:1)	24
2.5	Distribution of pore size: (A) Control; (B) gelatin/chitosan/CCP (1:1:0.05); (C) (1:1:0.1); (D) (1:1:0.5); and (E) (1:1:1)	26
2.6	Swelling behavior of the hydrogels: Control; gelatin/chitosan/CCP (1:1:0.05); (1:1:0.1); (1:1:0.5); and (1:1:1)	27
2.7	Calcium release of the hydrogels: Control, gelatin/chitosan/CCP (1:1:0.05); (1:1:0.1); (1:1:0.5); and (1:1:1)	28

LIST OF FIGURES (Continued)

Figure		Page
2.8	Cell viability on the hydrogels: Control; gelatin/chitosan/CCP (1:1:0.05); (1:1:0.1); (1:1:0.5); and (1:1:1) at days 3, 5, and 7.	29
2.9	Cell proliferation on the hydrogels: Control; gelatin/chitosan/CCP (1:1:0.05); (1:1:0.1); (1:1:0.5); and (1:1:1) at days 1, 3, 5, and 7.	31
3.1	Schematic illustration of gelatin/PVA hydrogel preparation	44
3.2	Gelatin/PVA hydrogels at different ratios (A) 100:0, (B) 70:30, (C) 50:50, (D) 30:70, and (E) 0:100	45
3.3	FT-IR spectra of gelatin/PVA hydrogels	46
3.4	Swelling graphs of gelatin/PVA hydrogels with different time period	47
3.5	Gelatin/PVA hydrogels after degradation in lysozyme enzyme	48
3.6	The mechanical properties of the gelatin/PVA hydrogels: (A) Stress at maximum load and (B) Young's modulus	49
3.7	Surface morphology of the gelatin/PVA hydrogels with different ratios at 200x magnification; (A) 100:0, (B) 70:30, (C) 50:50, (D) 30:70, and (E) 0:100. Insert indicates 1000x magnification	50
3.8	Pore size distribution of the gelatin/PVA hydrogels at different ratios; (A) 100:0, (B) 70:30, (C) 50:50, (D) 30:70, and (E) 0:100	50
3.9	The cell proliferation with different ratio of the gelatin/PVA hydrogels at day 1, 7, 14 and 21 with ostegenically induced cells.	51

LIST OF FIGURES (Continued)

Figure		Page
3.10	Cell adhesion and cell morphologies of the gelatin/PVA hydrogel at day 1 and day 14. Red arrows show examples of cell elongation	52
3.11	ALP activity at day 1, 7, 14, and 21 of the gelatin/PVA hydrogels: 100:0; 70:30; 50:50; 30:70; and 0:100	53
3.12	Alizarin red staining on the gelatin/PVA hydrogels at day14, and day 21, respectively. : (A, D, G) 50:50, (B, E, H) 30:70, and (C, F, I) 0:100. Blue arrows indicated the calcium nodules	54
3.13	Calcium release of the gelatin/PVA hydrogel measured at day 1, 7, 14, and 21	55
3.14	The chemical crosslink reactions of (A) gelatin, (B) gelatin/PVA, and (C) PVA with GA crosslinker in the gelatin/PVA hydrogels	56
3.15	Freeze thawing mechanism of hydrogel formation	57
4.1	Synthetic route of (A) HA-NH_2, (B) PNIPAM-COOH, and (C) HA-PNIPAM grafted-copolymer	72
4.2	^{1}H-NMR spectra of (a) HA-NH_2 and (b) PNIPAM-COOH	77
4.3	FT-IR spectra of HA-NH_2, NIPAM monomer, PNIPAM-COOH, HA-PNIPAM-3, and HA-PNIPAM-5	79
4.4	Viscosity behavior of the different synthesized polymer at 10% w/v concentration	80
4.5	DSC thermograms of PNIPAM-COOH, HA-PNIPAM-3, and HA-PNIPAM-5 in solution state (10% w/v)	81
4.6	Cell toxicity and cell proliferation of synthesized polymer	82

LIST OF FIGURES (Continued)

Figure		Page
4.7	(A) Cell sheet with PNIPAM hydrogel detached from the TPS surface after incubating at room temperature (B) Revised attachment of cell sheet with PNIPAM hydrogel on the TPS surface after incubation at 37^{o}C	83
4.8	Cell culturing at 10 min, day 3, and day 5 in PNIPAM-COOH, HA-PNIPAM-3, and HA-PNIPAM-5	84
4.9	Thermo-responsive behavior of HAPNIPAM copolymer for cell sheet membrane	87
4.10	The proposed model of engineered complicate tissue based on the smart basement membrane ECM (A) Morphological formation of two dimensional (2D) tissue (B) Morphological formation of three dimensional (3D) tissue	88

LIST OF ABBREVIATION AND SYMBOLS

ECM	=	Extracellular matrix
2D	=	Two dimension
3D	=	Three dimension
RGD	=	Arginine-Glycine-Aspartate
HO	=	Heterotopic ossification
OA	=	Osteoarthristis
CCP	=	Calcium phosphate
PVA	=	Poly (vinyl alcohol)
GA	=	Glutaraldehyde
HA	=	Hyaluronic acid
PNIPAM	=	Poly (*N*-isopropylacrylamide)
NIPAM	=	*N*-isopropylacrylamide
ADH	=	Adipic dihydrazine
MPA	=	3-Mercaptopropionic acid
EDC	=	1-Ethyl-3-(3-dimethylaminopropyl) carbodiimide
NHS	=	*N*-hydroxysuccinimide
AIBN	=	Azobisisobutyronitrile
MBA	=	*N*,*N*′-methylenebis(acrylamide)
DMSO	=	Dimethyl sulfoxide
HCl	=	Hydrochloric acid
NaCl	=	Sodium chloride
^{1}H-NMR	=	Proton nuclear magnetic resonance
GPC	=	Gel permeation chromatography
FT-IR	=	Fourier transform infrared

LIST OF ABBREVIATION AND SYMBOLS (Continued)

XRD	=	X-ray diffraction
DSC	=	Differential scanning calorimetry
LCST	=	Lower critical solution temperature
SEM	=	Scanning electron microscope
OD	=	Optical density
UV	=	Ultraviolet
ALP	=	Alkaline phosphatase
PBS	=	Phosphate buffer saline
FBS	=	Fetal bovine serum
MEM	=	Minimum Essential Medium Eagle
TPS	=	Tissue culture polystyrene
ANOVA	=	One-way analysis of variance
SD	=	Standard deviation
M_w	=	Weight average molecular weight
M_n	=	Number average molecular weight
PDI	=	Polydispersity index
GPa	=	Gigapascal
MPa	=	Megapascal
KPa	=	Kilopascal
N	=	Newton
μm	=	Micrometer
ml	=	Milliliter
mg	=	Milligram

CHAPTER 1
INTRODUCTION

1.1 Background and rationale

Many patients suffer from orthopedic disorders, especially in an aging populations. Many diseases such as fracture, osteoarthritis, osteoporosis, and osteogenesis imperfecta make bone dysfunction. These diseases cause the traumatic injury and induce bone defects or voids. Therefore, there are many researches focusing on effective models based on biomaterials to evaluate disease lead to create the new treatments (1). Some research designed the new surgical approach by implantation of performance biomaterials to regenerate the tissue at those defects (2). Furthermore, some researches are focused on to create morphology of tissue with the functional biomaterials (3). Therefore, in this research, the functional biomaterials were created for orthopedic applications.

Tissue engineering is the attractive approach which has been used for orthopedic applications (4). Mainly, there are three parts; 1) cells, 2) growth factors, and 3) scaffolds in tissue engineering. Especially, scaffolds are the functional biomaterials which show the function to support and enhance tissue engineering. To create the scaffolds is challenge for materials scientist and physician. Hence, to create scaffolds for orthopedic application was focused in this research.

Interestingly, the mimicking has been often used to create the scaffolds as effective models for disease evaluation and implantation (5). The mimicked function and structure which is similar to the natural tissue is used to fabricate the performance scaffolds (6). Therefore, this research was focused on the created mimicked scaffolds which had similar structure and function to the natural tissue.

Hydrogel is the attractive scaffolds which have been often used for tissue engineering for several years (7). Due to the unique physical and biological performance, hydrogel has been used to enhance new tissue formation (8). Especially, the mimicked hydrogel which has the structure and function similar to the natural tissue show the potential to promote the tissue regeneration (8). Hence, our research is emphasized on the mimicked hydrogel which is proposed for orthopedic application.

In this research, mimicked hydrogels were created for orthopedic application which was classified into three lines; 1) model for disease evaluation**,** 2) surgical application, and 3) created morphological tissue.

1.2 Review of literatures

1.2.1 Tissue engineering

Tissue Engineering is a discipline that focuses on the creation or regeneration of tissues. Aims of tissue engineering are to restore, maintain or improve the tissue structure and function. The basic approach of tissue engineering consists of cells that form tissue matrix, scaffolds to promote cell activity and tissue production, and signaling factors that regulate and induce cellular behavior (9). The concept of tissue engineering is shown in Figure 1.1.

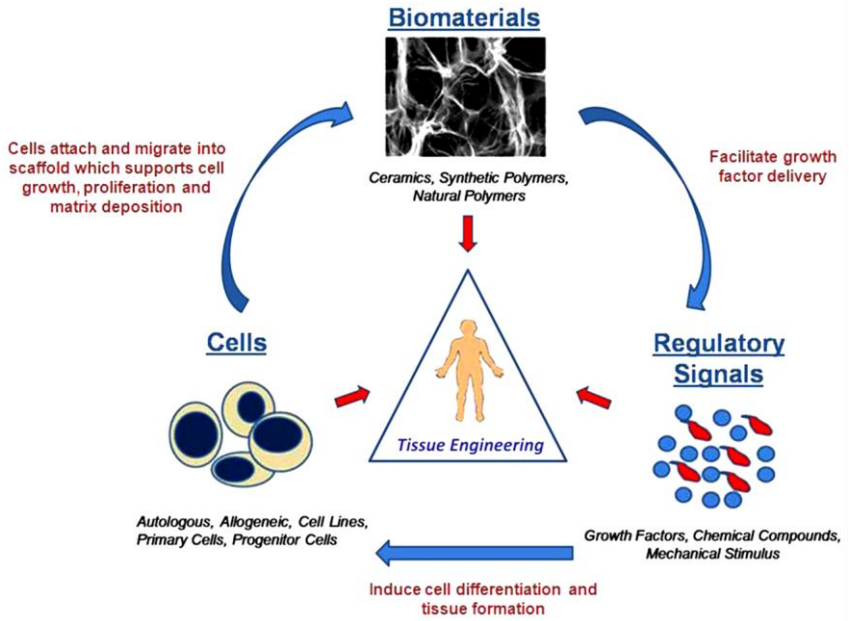

Figure 1.1 The important components to make up the tissue engineering (10)

1.2.2 Bone tissue engineering

Bone is a mineralized connective tissue made up of different types of bone cells: osteoblast, bone lining cells, osteocytes, and osteoclasts. Bone tissue composes of bone ECM and cells. Natural bone ECM consists of type I collagen, which is the fundamental mineral phase of bone. A mineral essential phase of bone is calcium phosphate or hydroxyapatite. Bone shows an essential functions in the body such as locomotion, provide structure of the body, support and protect soft tissues, minerals reservoir, and produce red and white blood cells. An imbalance between bone resorption and bone formations results in the bone diseases. Thus, bone remodeling is necessary process for bone fracture recovery, which help in maintains mineral homeostasis in the body and maintains the structural integrity of the skeleton (11).

Bone remodeling process take place on bone surface. This process starts with osteoclasts precursor cells, derived from hematopoietic stem cells, are recruited and activated to the remodeling sites. Multiple mononuclear cells fuse to form multinucleated preosteoclasts. These cells attach to the bone matrix and initiate resorption by secreting hydrochloric acid and proteolytic enzymes including cathepsin K, which can degrade bone matrix components (Activation phase). Then, osteoclasts dissolve the mineral matrix and the resorption cavities, called Howship's lacunae, are created. The growth factors stored in bone matrix are released (Resorption phase) and preosteoblasts are recruited. The resorption phase is stopped by the death of osteoclasts. During reversal phase, the bone resorption switches to bone formation. The resorption cavities containing many cells types (monocytes, osteocytes, and preosteoblasts), are recruited and start to form the new bone formation. In the formation phase, osteoblasts produces the new bone matrix and its mineralization. When the mineralization process is completed, osteoblasts undergo apoptosis, change into bone-lining cells or become buried in bone matrix and finally differentiate into osteocytes (12–14). The schematics of bone remodeling is shown in Figure 1.2

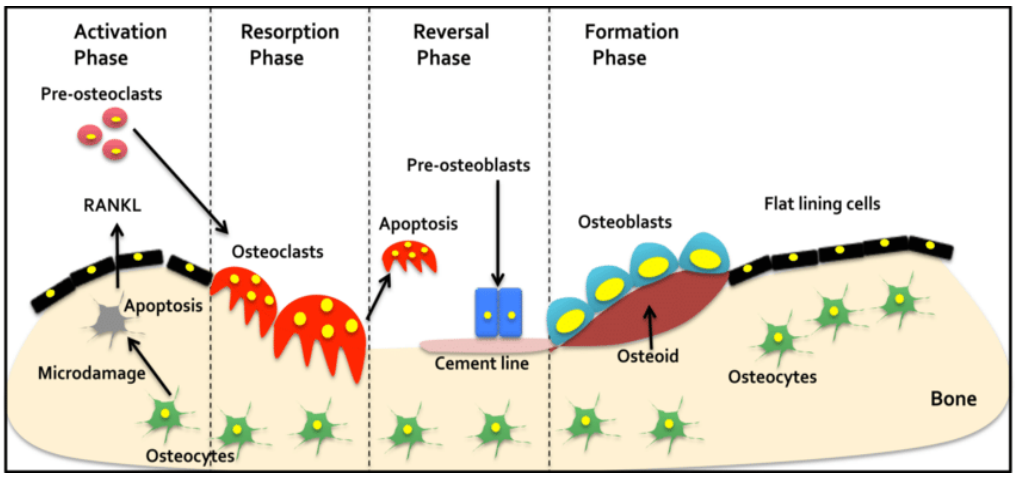

Figure 1.2 Schematics of bone remodeling (15)

Bone tissue engineering relates to the use of cells, biomaterial scaffolds, or the combination of cells, biomaterial scaffold, and bioactive molecules (Figure 1.3). The artificial extracellular matrix (ECM) or scaffolds are typically developed to engineer bone defect. These scaffolds mainly play the following roles: 1) serve as a framework for cell-cell and cell-tissue interactions to guide the new bone formation, 2) act as a carrier to transport the signaling molecules to the defect site, and 3) contribute to cell proliferation, differentiation, and metabolism (16). A variety of materials has been used to fabricate scaffolds for bone tissue implantations such as metal, ceramic, polymers (natural and synthetic), including their combinations. However, the lack of degradations and the difficulty of processability of metal and ceramics cause the limited usability in bone tissue engineering. In contrast, polymers have a great material to design and fabricate as a scaffold due to its flexibility. The structure and composition of polymer for scaffold fabrication can be altered to the specific desire (17).

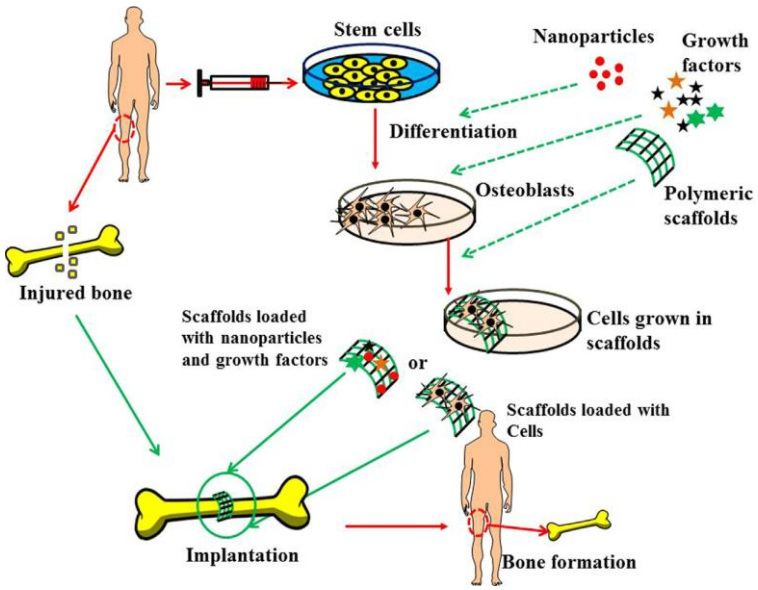

Figure 1.3 Schematic illustration of bone tissue engineering process. Stem cells isolated from the patient donor are differentiated into osteoblasts and cultivated in scaffolds *in vitro* before implantation at the defect site. Cell-free scaffold is also used by combination with nanoparticles or growth factors to enhance bone formation (18). After selecting suitable polymers to fabricate scaffolds, next step is to choose an appropriate process for the scaffold fabrication to optimize the mechanical properties, chemical properties and polymer miscibility. Moreover, this fabrication process has to produce pores with proper pore size, including interconnectivity for a specific application (19)

1.2.3 Scaffold properties in bone tissue engineering

Scaffolds are attractive to enhance the performance for tissue engineering. Requirements for an ideal scaffolds are focused as following

1. Biocompatibility

Biocompatibility is the primary requirements of any bone scaffolds. It has been defined as the ability of scaffolds to support cellular activity, including molecular signaling systems without any toxic or injurious effects to the host tissue. An ideal bone scaffolds must be able to support cell adhere, proliferate, and form ECM on its surface and pores. Moreover, it should induce the new bone formation and form blood vessels

in or around the implant tissue (20). A number of natural polymers such as collagen, gelatin, agarose, and chitosan are available for scaffold fabrication due to their good biocompatibility. However, some synthetic polymers such as poly (lactic acid) (PLA), poly (glycolid acid) PGA, and poly (lactic-co-glycolic) acid (PLGA) show a biocompatibility and are used to create scaffolds as well.

2. Mechanical properties

The mechanical properties of an ideal bone scaffolds should match with the host tissue. The implanted scaffolds must have sufficient mechanical properties as a function with time of implantation. Moreover, it must withstand to the load bearing and stress and to maintain the spaces for cell ingrowth and matrix production. Mechanical properties of bone is depends on the bone types. For example, Young's modulus of cortical bone is in the range of 15-20 GPa while in cancellous bone is between 0.1 to 0.2 GPa. Compressive strength of cortical bone is between 100 to 200 MPa and between 2 to 20 MPa for cancellous bone(20). The large variation in mechanical properties results in the difficult to design an ideal scaffold for bone tissue engineering.

Mechanical properties of scaffolds can be developed by combining scaffolds with ceramic materials such as hydroxyapatite and, β-tricalcium phosphate. According to Y. Tang *et al.*, the addition of hydroxyapatite particles in chitosan/poly(vinyl alcohol) scaffolds can improve the mechanical properties and cell adhesion on scaffolds (21).

3. Biodegradability

Scaffolds must be biodegradable to allow cells to produce ECM and to form the new bone formation. Controlling the degradation rate of scaffolds is an important characteristic since it should match with the rate of tissue growth. If scaffold degrades too quickly, it causes the mechanical failure of scaffolds. Conversely, if scaffold does not degrade or degrade too slow, it prevents the new tissue formation (22). The degradation rate of scaffold is based on the applications such as 3 to 6 months for cranio-maxillofacial tissue or 9 month or more for spinal fusion (20). Many research studies have proposed that using the different types different concentrations or different molecular weight of polymers can controlled the degradation rate of scaffolds.

According to E. Alsberg *et al*.,(23) increased the degradation rate can be tuned by decreased the size of polymer chain. In addition, the bi-product of degradation should be non-toxic or able to exit the body without interference with other organs (24).

4. Pore size

Pore structure is an important parameter to consider for scaffold development in tissue engineering. The pore size of scaffolds must be large enough for cell migration and small enough for cell binding to the scaffolds. If the pores are too large, the surface areas is decreased and then the cell adhesion is limited (25). The initial cell adhesion mediates all subsequent events such as cell growth, proliferation, and differentiation, If the pores are too small, it prevents cellular penetration, ECM production, and vascularization within scaffolds (19). Moreover, pore must be interconnected to allow cell growth, migration, nutrient and oxygen diffusion, and waste removal. Therefore, the balance between the optimal pore size and surface area is essential to create scaffolds in tissue engineering.

The mean pore sizes of scaffolds in the range of 20 µm to 1500 µm have been used in bone tissue engineering (26). Some research studies have proposed that the minimum pore size for bone ingrowth is 100-135 µm (27,28). Some studies have suggested that pore size ~300 µm is suitable for bone information and vascularization. Moreover, the pores are larger than ~300 µm, leading to the osteogenesis while the pores are smaller than ~300 µm can support osteochondral ossification (25). However, recent studies have suggested that the multi-scale porous scaffolds containing both micro (pore size > 20 µm) and macro (pore size > 100 µm) pore size can perform better scaffold performance for bone tissue engineering (20).

1.2.4 Hydrogels

Scaffolds can be fabricated into many forms, such as membranes, sponges, fibers, and hydrogels. In this research, we focused on hydrogels fabrication since many literatures shows its excellent biocompatibility with minimal inflammatory response or tissue damage. Hydrogel is a hydrophilic cross-linked network polymer. It can absorb fluid from 10-20 % up to thousand times of their dry weight. This ability allow cell adhesion, proliferation, and differentiation onto hydrogels (29). Based on the types of bonds between the polymer chains, the natural and synthetic polymers can be used to fabricate hydrogels by physical or chemical crosslinking networks. The physical networks have temporary junctions such as hydrophobic interaction, hydrogen bonding and polymer chain entanglements , whereas the chemical cross-linked networks have permanent junctions through covalent bonds (30).

Hydrogels can be created from natural polymers such as collagen, gelatin, chitosan, and alginate or from synthetic polymers such as poly (ethylene glycol) (PEG), poly (vinyl alcohol) (PVA), and poly (*N*-isopropylacrylamide) (PNIPAM). Moreover, hydrogels can be formed by the combinations of the natural and synthetic polymers. The synthetic polymers are chemically stronger than the natural polymers, resulting in slow degradation rate and good mechanical strength (30).

Hydrogels can be synthesized via many techniques such as physical crosslinking, chemical crosslinking, polymerization grafting, and irradiation polymerization. The modifications of hydrogels in term of polymer types, architecture, functions, size, different compositions and preparation processes make the hydrogels can be applied in many fields such as drug delivery systems, food additives, agriculture, pharmaceuticals, including tissue engineering (31).

The term of tissue engineering, hydrogels can be applied as cells transplantations, including in bone tissue engineering for bone repair and regenerations. For examples, inorganic hydroxyapatite and organic PLGA nanoparticles colloid gels have been prepared as injectable bone fillers. These biocompatible hydrogels can be utilized as an alternative surgical treatment (32). The injectable poly (aldehyde guluronate) (PAG) have been fabricated with the good mechanical stiffness and

controllable degradation rate. These hydrogels can be used as a bone precursor in tissue engineering (33).

At present, many research studies focus on the development of intelligent hydrogels with remarkable applications. However, some hydrogels are still incomplete and have many problems, such as degradation rate, mechanical properties, morphology, and biological activity that needs to be solved for bone tissue engineering.

1.2.5 Mimicked biomaterials

Mimicking is an attractive approach which has been used to build scaffolds for bone tissue engineering. Mimicked scaffolds have the structure and functionality similar to native ECM which can enhance bone healing. As mimicked hydrogels are capable to form two (2D) or three (3D) dimensional network with high porosity and absorb amount of water, which serve as a delivery vehicle. The mimicked hydrogels can support the cell-cell contact, cell-matrix interaction, cell proliferation and differentiation and their architecture can produce the shape of new bone formation. There are many studies associated to the mimicked hydrogels for bone tissue engineering. X. Fang et al., fabricated gelatin methycrylamide (GelMA) hydrogel by mimic both of physical architecture and chemical composition of native bone ECM by thermally induced phase separation technique. Gelatin-based hydrogel was selected to mimic natural ECM and 3D microstructure hydrogels was created. They proposed that this hydrogels can promote osteoblast differentiation and bone formation (34). According to T. Anada et al., the hydrogels constructed by 3D printing was fabricated and designed similar to cortical bone structure. This bone-mimetic 3D hydrogel consisted of the combination of GelMA and octacalcium phosphate (OCP) at the outer layer to mimic cortical shell. In addition, GelMA with human umbilical vein endothelial cells (HUVEC) was constructed at the inner layer to mimic bone marrow space and vascular formation. This hydrogel can stimulates the osteoblastic differentiation (35).

1.3 Objectives of this research

The objectives of this thesis can be divided into three parts as following

1. To fabricate and construct hydrogels based on mimicking approach
2. To test the physical and biological properties of hydrogels for bone tissue engineering
3. To evaluate hydrogels for orthopedic applications

1.4 Hypothesis

Bio-mimicked hydrogels will provide a suitable physical and biological properties for tissue engineering in orthopedic applications.

1.5 Expected Benefits

We expect that the created hydrogels in this study can be used as a biomaterials in bone tissue engineering for orthopedic applications. Moreover, we also hope that our hydrogels will be used as a pioneer materials and will be developed for better performance in future study.

1.6 References

1. Hinderer S, Brauchle E, Schenke-Layland K. Generation and Assessment of Functional Biomaterial Scaffolds for Applications in Cardiovascular Tissue Engineering and Regenerative Medicine. Adv Healthc Mater. 2015;4(16):2326–41.
2. Hutmacher DW. Scaffolds in tissue engineering bone and cartilage. In: Williams DF, editor. The Biomaterials: Silver Jubilee Compendium: Elsevier Science; 2000; (15):175–89.
3. Kusuhara H, Isogai N, Enjo M, Otani H, Ikada Y, Jacquet R, et al. Tissue engineering a model for the human ear: Assessment of size, shape, morphology, and gene expression following seeding of different chondrocytes. Wound Repair Regen. 2009;17(1):136–46.

4. Scaglione S, Quarto R. Clinical Applications of Bone Tissue Engineering. In: Santin M, editor. Strategies in Regenerative Medicine: Integrating Biology with Materials Design; 2009; (15):1–18.
5. Ino JM, Sju E, Ollivier V, Yim EKF, Letourneur D, Le Visage C. Evaluation of hemocompatibility and endothelialization of hybrid poly(vinyl alcohol) (PVA)/gelatin polymer films. J Biomed Mater Res B Appl Biomater. 2013 Nov 1;101(8):1549–59.
6. Lu T, Li Y, Chen T. Techniques for fabrication and construction of three-dimensional scaffolds for tissue engineering. Int J Nanomedicine. 2013;8:337–50.
7. El-Sherbiny IM, Yacoub MH. Hydrogel scaffolds for tissue engineering: Progress and challenges. Glob Cardiol Sci Pract. 2013 Dec 1;2013(3):38.
8. Lee J-H, Kim H-W. Emerging properties of hydrogels in tissue engineering. J Tissue Eng. 2018 Jan 1;9:2041731418768285.
9. Ma PX. Biomimetic materials for tissue engineering. Adv Drug Deliv Rev. 2008 Jan 14;60(2):184–98.
10. Murphy C, O'Brien F, Little D, Schindeler A. Cell-scaffold interactions in the bone tissue engineering triad. Anat Artic. 2013 Jan 1;120–32.
11. Velasco MA, Narváez-Tovar CA, Garzón-Alvarado DA. Design, Materials, and Mechanobiology of Biodegradable Scaffolds for Bone Tissue Engineering . BioMed Research International. 2015.
12. Kini U, Nandeesh BN. Physiology of Bone Formation, Remodeling, and Metabolism. In: Fogelman I, Gnanasegaran G, van der Wall H, editors. Radionuclide and Hybrid Bone Imaging: Springer; 2012; (15):29–57.
13. Hadjidakis DJ, Androulakis II. Bone Remodeling. Ann N Y Acad Sci. 2006;1092(1):385–96.
14. Bayliss L, Mahoney DJ, Monk P. Normal bone physiology, remodelling and its hormonal regulation. Surg Oxf. 2012 Feb 1;30(2):47–53.
15. Dole NS, Dole NS, D P. Genetic Determinants of Skeletal Diseases: Role of microRNAs. 2015 May..

16. Hao Z, Song Z, Huang J, Huang K, Panetta A, Gu Z, et al. The scaffold microenvironment for stem cell based bone tissue engineering. Biomater Sci. 2017 Jul 26;5(8):1382–92.
17. Liu X, Ma PX. Polymeric Scaffolds for Bone Tissue Engineering. Ann Biomed Eng. 2004 Mar 1;32(3):477–86.
18. Saravanan S, Leena RS, Selvamurugan N. Chitosan based biocomposite scaffolds for bone tissue engineering. Int J Biol Macromol. 2016 Dec 1;93:1354–65.
19. Salgado AJ, Coutinho OP, Reis RL. Bone Tissue Engineering: State of the Art and Future Trends. Macromol Biosci. 2004;4(8):743–65.
20. Bose S, Roy M, Bandyopadhyay A. Recent advances in bone tissue engineering scaffolds. Trends Biotechnol. 2012 Oct 1;30(10):546–54.
21. Tang Y, Du Y, Li Y, Wang X, Hu X. A thermosensitive chitosan/poly(vinyl alcohol) hydrogel containing hydroxyapatite for protein delivery. J Biomed Mater Res A. 2009;91A(4):953–63.
22. Turnbull G, Clarke J, Picard F, Riches P, Jia L, Han F, et al. 3D bioactive composite scaffolds for bone tissue engineering. Bioact Mater. 2018 Sep 1;3(3):278–314.
23. Alsberg E, Kong HJ, Hirano Y, Smith MK, Albeiruti A, Mooney DJ. Regulating Bone Formation via Controlled Scaffold Degradation. J Dent Res. 2003 Nov 1;82(11):903–8.
24. O'Brien FJ. Biomaterials & scaffolds for tissue engineering. Mater Today. 2011 Mar 1;14(3):88–95.
25. Murphy CM, Haugh MG, O'Brien FJ. The effect of mean pore size on cell attachment, proliferation and migration in collagen–glycosaminoglycan scaffolds for bone tissue engineering. Biomaterials. 2010 Jan 1;31(3):461–6.
26. Baksh D, Davies JE, Kim S. Three-dimensional matrices of calcium polyphosphates support bone growth in vitro and in vivo. J Mater Sci Mater Med. 1998 Dec 1;9(12):743–8.
27. Klawitter JJ, Bagwell JG, Weinstein AM, Sauer BW, Pruitt JR. An evaluation of bone growth into porous high density polyethylene. J Biomed Mater Res. 1976;10(2):311–23.

28. Hulbert SF, Young FA, Mathews RS, Klawitter JJ, Talbert CD, Stelling FH. Potential of ceramic materials as permanently implantable skeletal prostheses. J Biomed Mater Res. 1970;4(3):433–56.
29. Park J. The use of hydrogels in bone-tissue engineering. Med Oral Patol Oral Cirugia Bucal. 2011;16(1).
30. Ahmed EM. Hydrogel: Preparation, characterization, and applications: A review. J Adv Res. 2015 Mar 1;6(2):105–21.
31. Mahinroosta M, Jomeh Farsangi Z, Allahverdi A, Shakoori Z. Hydrogels as intelligent materials: A brief review of synthesis, properties and applications. Mater Today Chem. 2018 Jun 1;8:42–55.
32. Wang Q, Gu Z, Jamal S, Detamore MS, Berkland C. Hybrid Hydroxyapatite Nanoparticle Colloidal Gels are Injectable Fillers for Bone Tissue Engineering. Tissue Eng Part A. 2013 Jul 2;19(23–24):2586–93.
33. Lee KY, Alsberg E, Mooney DJ. Degradable and injectable poly(aldehyde guluronate) hydrogels for bone tissue engineering. J Biomed Mater Res. 2001;56(2):228–33.
34. Fang X, Xie J, Zhong L, Li J, Rong D, Li X, et al. Biomimetic gelatin methacrylamide hydrogel scaffolds for bone tissue engineering. J Mater Chem B. 2016 Feb 2;4(6):1070–80.
35. Anada T, Pan C-C, Stahl AM, Mori S, Fukuda J, Suzuki O, et al. Vascularized Bone-Mimetic Hydrogel Constructs by 3D Bioprinting to Promote Osteogenesis and Angiogenesis. Int J Mol Sci. 2019 Jan;20(5):1096.

CHAPTER 2
MIMICKED EXTRACELLULAR MATRIX OF CALCIFIED SOFT TISSUE BASED ON GELATIN/CHITOSAN/COMPOUNDED CALCIUM PHOSPHATE HYDROGELS TO DESIGN EX VIVO MODEL FOR HETEROTOPIC OSSIFICATION

Abstract

Heterotopic ossification is the abnormal growth of bone tissue formations within soft tissue. A mimicked extracellular matrix of calcified soft tissue based on; gelatin/chitosan/compounded calcium phosphate (gelatin/chitosan/CCP) hydrogel, is presented to design an ex-vivo model for evaluation of tissue formations in this research. Different ratios of CCP to gelatin/chitosan were prepared. The control was gelatin/chitosan at a ratio of 1:1. The other gelatin/chitosan/CCP ratios were 1:1:0.05, 1:1:0.1, 1:1:0.5, and 1:1:1. The mixtures were prepared into hydrogels by crosslinking with glutaraldehyde. The molecular, structural, and morphological characteristics of the hydrogels were observed by Fourier transform infrared, X-ray diffraction and scanning electron microscopy, respectively. The physical performance was assessed from the swelling behavior as well as calcium released. Biological performance was evaluated by cell viability and proliferation. The results demonstrated that; the molecules, structure and morphology of the hydrogels with CCP self-organized is similar to the extracellular matrix of in situ bone formation. Both the physical and biological performances of the hydrogels could enhance cell viability and proliferation, particularly in gelatin/chitosan/CCP (1:1:0.1). Finally, the results indicated that the hydrogels with CCP are promising to design extracellular matrix of calcified soft tissue as biomaterials of ex-vivo model for tissue evaluation of heterotopic ossification.

2.1 Introductions

Heterotopic ossification (HO) is the abnormal extra skeletal formation of bone within soft tissue or muscles, which results from musculoskeletal trauma, central nerve injury or spinal cord injury (1). In the early stage of HO patients are treated with medication. On the other hand, in the later stages medications become ineffective and patients are required to undergo surgical treatment. Previous research presented molecular and gene therapy for the disease of HO (2). Whilst animal models are generally used to evaluate the effectiveness of the molecules and genes, there are few reports of ex vivo models as a viable substitution for animal models for heterotopic ossification (3). We, therefore, used the ex vivo model for the evaluation of tissue formations of HO in the conduction of this research.

The ex vivo model, in this research, has the ability to promote cell behaviors similar to that of native tissue. Generally, the ex vivo model is fabricated with performance materials, which have both, physical and biological functionalities similar to the extracellular matrix of native tissue. However, one of the challenges for clinicians and biomaterials scientists is the creation of performance materials as ex vivo models. Therefore, the focus of this research is the construction of performance materials as an ex vivo model.

Calcified soft tissue is generated during the process of HO. Calcified soft tissue has an extracellular matrix that forms a bio-mineral structure. Previous research demonstrated that the extracellular matrix formation of calcified soft tissue affects orthopedic tissue disorder diseases, particularly in HO (4, 5). Hence, we focused on the extracellular matrix of calcified soft tissue in the design of an ex vivo model.

Mimicking is an attractive approach in the creation of high, biological performing biomaterials and previous research had succeeded in mimicked biomaterials that function as an extracellular matrix system during bone tissue formation (6). The materials were created with structural and biological functions of the native extracellular matrix system (7). Hence, utilizing a unique design approach, mimicking was selected to create an extracellular matrix of calcified soft tissue in this research.

Hydrogels are attractive biomaterials often used for biomedical applications, particularly in the application of tissue regeneration (8). Since, hydrogels have the unique ability to maintain a high amount of water, they have been used as biomaterials for cartilage tissue regeneration (9). Interestingly, some previous research applied hydrogels to be functional biomaterials as ex vivo models for the evaluation of tissue formation and molecular, gene screening for tissue disease treatments (10, 11). Based on those functionalities, hydrogels were selected as the basic biomaterials in the design of an ex vivo model for HO.

Calcium phosphate is a component in the extracellular matrix during soft tissue calcification and, generally, calcium phosphate is generated by the dynamic phenomenon of formation and resorption by either osteoblasts and osteoclasts, respectively (12, 13). The two components of calcium phosphate, during soft tissue calcification, are; hydroxyapatite and tricalcium phosphate (14). Hydroxyapatite and tricalcium phosphate are the insoluble and soluble phases, respectively, of calcified soft tissue (15). Based on soft tissue calcification, a compounded calcium phosphate (CCP) consisting of; hydroxyapatite and tricalcium phosphate, was chosen to be one of the components of the mimicked extracellular matrix in the creation of an ex vivo model within this research.

Gelatin is a hydrolysated collagen, which is often used in biomedical applications (16), this is due to its unique ability to induce tissue regeneration. The gel has been fabricated into scaffolds in many forms, for instance; two- and three-dimensional scaffolds, microspheres, nano-fibers as well as hydrogels (16). Gelatin hydrogels are often used in tissue engineering, with or without other components, to induce cartilage tissue formation (18, 19). Gelatin also has the biological functionality of a collagen in the extracellular matrix (20). Therefore, in this research gelatin was selected as the basic material for fabrication into hydrogels, so as to mimic the extracellular matrix of calcified soft tissue.

Chitosan is a positively charged polysaccharide, which also has unique biological functionality to induce tissue regeneration (21). Accordingly, chitosan has been fabricated into scaffolds for tissue engineering, particularly in cartilage tissue (22). Generally, chitosan enhances biological performance by adding bioactive molecules that can induce tissue formation (23). Chitosan is blended with other polymers to

manipulate the performance to fit the tissue formation (24, 25). Interestingly, chitosan has a physicochemical functionality similar to the polysaccharides in an extracellular matrix (26). Thus, in the conduction of our research, chitosan was chosen for blending with Gel to mimic the extracellular matrix of calcified soft tissue.

In this research, gelatin, chitosan, and CCP were blended and fabricated into hydrogels to mimic the extracellular matrix, which is similar to the system of calcified soft tissue. The structure, morphology along with performance of the hydrogels were characterized for use as an ex vivo model to evaluate tissue formation in HO.

2.2 Materials and Methods

2.2.1 Materials

Gelatin, for bacteriological purposes, was obtained from Sigma-Aldrich, whilst chitosan was obtained from Marine Bio Resources Co., Ltd. CCP powder was prepared by mixing β-tricalcium phosphate (>98% β-phase basis, Sigma Aldrich) with hydroxyapatite (reagent grade, Sigma Aldrich) at the ratio of 1:1. All other chemicals and reagents were analytical grade and used without further purification.

2.2.2 Preparation of gelatin/chitosan/CCP hydrogels

A gelatin solution of 1.2 wt.% was prepared by dissolving the solution into deionized water and stirring for 2hr. A chitosan solution of 1.2 wt.% was prepared by dissolving this into 0.1 M CH_3COOH (27) and then stirred and filtered to remove the undissolved particles. The gelatin and chitosan solutions were added into the CCP dispersion solutions in 0.1 M CH_3COOH with different weight percent of CCP. The mixtures were then stirred again to obtain homogeneous dispersions. A glutaraldehyde (GA) stock solution (50%) was diluted and used at 0.1 wt.% (28). After which, it was slowly added into the gelatin/chitosan/CCP mixtures, while stirring, for 3mins. The gelatin/chitosan hydrogels, with the addition of CCP, were prepared at ratios of 1:1:0.05, 1:1:0.1, 1:1:0.5, and 1:1:1. A gelatin/chitosan solution without CCP was used as the control.

2.2.3 Fourier transform infrared spectroscopy (FT-IR) characterization

FT-IR spectra of composite hydrogels were carried out using the attenuated total reflectance mode on an FT-IR spectrometer (Equinox 55, Bruker, Ettlingen, Germany). The dried hydrogels were scanned in the ranges of 4000 to 400 cm^{-1}.

2.2.4 X-ray diffraction (XRD) characterization

The XRD patterns of the hydrogels were obtained using the XPert MPD (Philips, the Netherlands). The samples were studied at 2θ range of 5-90^{o} with a scan step size of 0.05 and second of scan step time.

2.2.5 Hydrogel morphologies

The structural morphologies of the gelatin/chitosan/CCP hydrogels, with different weight ratios, were observed by a scanning electron microscope (SEM) (Quanta 400, FEI, Brno, Czech Republic). The hydrogel samples were coated with gold using a gold sputter coater machine (SPI Supplies, Division of Structure Probe Inc., Westchester, PA, USA), before the SEM analysis.

2.2.6 Pore size and distribution

The pore size distribution of the hydrogels was measured from the SEM images using the ImageJ program. The pore size distributions of all hydrogel samples were calculated using the Origin 8.1 program (OriginLab, USA) with different pore size ranges.

2.2.7 Swelling analysis

The dried hydrogels were prepared by being freeze dried for the swelling test. The dried hydrogels were weighed, then immersed in a phosphate buffer saline (PBS) solution at 37 ^{o}C over different time periods. The wet samples were taken from the PBS solution, any excess water was removed by filter paper. The wet weight was obtained in this process, while the percent swelling ratio was calculated by the following equation (29):

$$\text{Swelling ratio} = (W_t - W_d)/W_d$$

Where; W_t and W_d are the masses of the swollen hydrogels as well as the dried hydrogels, respectively. Four samples were repeated for the swelling analysis for each composition.

2.2.8 Calcium release analysis

A calcium, release analysis of the hydrogels was studied using Biovision's Colorimetric Calcium Assay Kit (30). The hydrogels were immersed in a PBS solution and pipetted at 50 µL into a 96-well plate. A chromogenic reagent (90 µL) and calcium assay buffer (60 µL) were then added into the solution samples under mixing. The solution mixtures were incubated for 10mins at room temperature and protected from light. The optical density was measured at 575 nm. The calcium concentration was calculated from the ratio between; the calcium sample amount and the sample volume added into the 96-well plate.

2.2.9 MC3T3-E1 cell culture

Before, the MC3T3-E1 osteoblast cell culture a glycine solution was used to remove the non-reacted GA cross-linking agent on the hydrogels and subsequently the hydrogels were soaked in absolute ethanol for 24 h. MC3T3-E1 osteoblast cells were seeded at $2x10^5$ cells on the gelatin/chitosan/CCP hydrogels and cultured in alpha MEM medium (Gibco, Invitrogen, Carlsbad, CA, USA) containing 1% penicillin/streptomycin, 0.1% Fungizone and 10% fetal bovine serum. The MC3T3-E1 cultures were kept in a 37^{o}C incubator with 5% CO_2. The media was changed every 2-3 days, after culturing the cells (31)

2.2.10 Cell viability

The cell viability of the hydrogels was observed under fluorescence microscope, after nucleic acid staining (Hoechst 33342). The hydrogels, containing the osteoblast cells, were soaked twice in PBS solution and then 1mL of fresh medium and 5 µL of dye were added. The hydrogels were kept away from light and incubated for 5mins at room temperature. The blue fluorescence of the cell nuclei appeared after staining (32).

2.2.11 Cell proliferation assay (PrestoBlue: at days 1, 3, 5, and 7)

Cell proliferation of the gelatin/chitosan/CCP hydrogels was examined by PrestoBlue reagent on days; 1, 3, 5 and 7. PrestoBlue is a resazurin-based compound that is reduced by mitochondrial activity in viable cells. The reduced resazurin is a pink color that can be detected using the fluorometric method. PrestoBlue was prepared by mixing with the media at a ratio of 1:10 and then added into the hydrogels, after washing the hydrogels with 1x PBS. All samples were incubated at 37 ^{o}C for 1hr and then the florescence was measured at a wavelength of 570 nm (33).

2.2.12 Statistical analysis

In this research, 5 samples were selected for testing. The results are presented as mean ± standard deviation. All data were statically analyzed using one-way ANOVA (SPSS 16.0 software package). A P value < 0.05 was accepted as statistically significant.

2.3 Results and Discussion

2.3.1 Molecular and structural organization of hydrogels

After, the gelatin, chitosan, and CCP were mixed GA was then added to the mixtures to form the hydrogels (Figures 2.1A and B). The results showed that the turbidity of the hydrogels increased as the amount of CCP increased (Figures 2.1C to G). The hydrogel at a gelatin/chitosan/CCP ratio of 1:1:1 had the most turbidity. The results demonstrated that CCP induced light scattering, which in turn caused the increased turbidity (34). The induced scattering possibly came from the different aggregation sizes of the CCP as well as distribution in the texture of the hydrogels (35). Interestingly, the results indicated that the different ratios of the gelatin/chitosan/CCP hydrogels represented different extracellular matrices of calcified soft tissue. The hydrogel, without CCP represented a similar period to the organic template formation of the extracellular matrix. On the other hand, hydrogels with different amounts of CCP were similar to the different stages of calcium deposition on the organic template of the extracellular matrix.

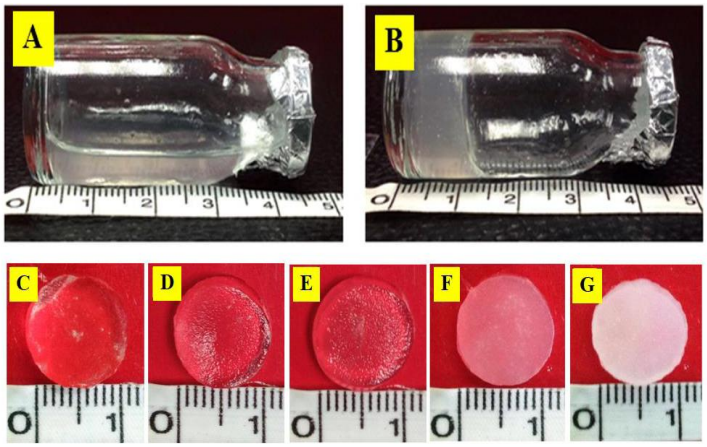

Figure 2.1 (A) Blending of gelatin/chitosan/CCP without GA, (B) blending of gelatin/chitosan/CCP with GA. Appearance of the hydrogels: (C) Control; (D) gelatin/chitosan/CCP (1:1:0.05); (E) (1:1:0.1); (F) (1:1:0.5); and (G) (1:1:1)

The molecular and structural organizations of the mimicked extracellular matrices of the freeze dried hydrogels were evaluated by FT-IR and XRD. The FT-IR spectrum showed mainly that the ⁻OH groups came from the molecular characteristics of the gelatin and chitosan. The wave number results of the hydroxyl groups or -OH stretching of the control and the gelatin/chitosan/CCP ratios of 1:1:0.05, 1:1:0.1, 1:1:0.5 and 1:1:1 were at around 3276, 3282, 3282, 3269 and 3269 cm^{-1}, respectively (Figure 2.2). The -OH wave number was higher in the lower amounts of CCP (0.05 and 0.1) than that of the hydrogel without CCP. This indicated that the ⁻OH groups of the hydrogels at those ratios had more mobility than the hydrogel without CCP. This indicated that the water molecules, which generally interact with the ⁻OH groups were pulled out by the CCP. Therefore, the -OH groups had more mobility (36). The -OH wave number was lower in the hydrogels with higher amounts of CCP (0.5 and 1) than those of the hydrogel without CCP. This indicated that the ⁻OH in those ratios of hydrogel had low mobility, which came from molecular interaction (37). The results indicated that the water molecules around the gelatin and chitosan were pulled out by a certain amount of CCP. Interestingly, the excess amounts of CCP interacted with those ⁻OH groups, which in turn led to low mobility. Based on the FT-IR characterization,

the results demonstrated that the molecular organization of the gelatin/chitosan/CCP interacted mainly with the –OH groups.

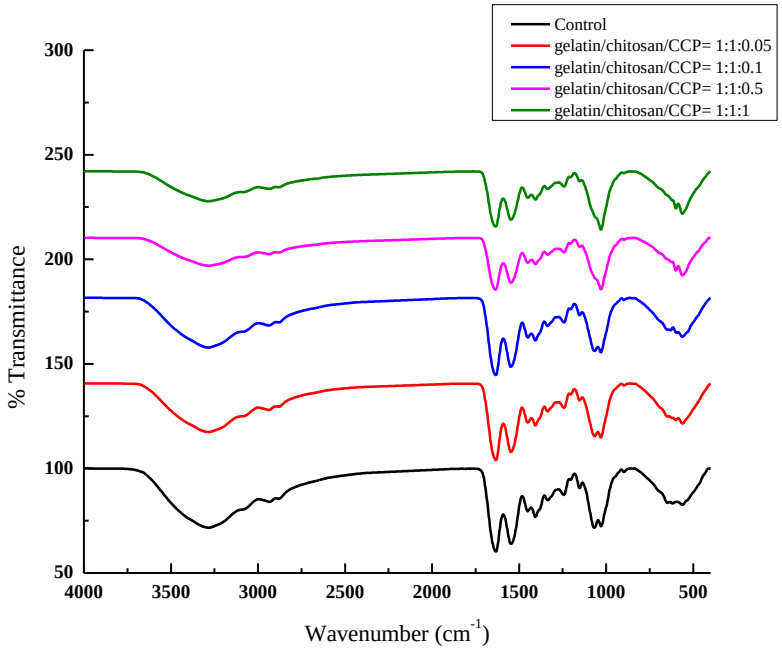

Figure 2.2 FT-IR spectra of the hydrogels: Control; gelatin/chitosan/CCP (1:1:0.05) (1:1:0.1) (1:1:0.5) and (1:1:1)

XRD diffraction was used for the structural characterization of the different hydrogels (Figure 2.3). These results indicated that the hydrogels without CCP had broad peaks of XRD, which represented an amorphous organization. The results of the hydrogels with lower amounts of CCP (0.05 and 0.1) showed broad peaks, which had small, sharp peaks at around 33 degrees. This represented the CCP in those hydrogels. The XRD diffraction of the hydrogels with higher amounts of CCP (0.5 and 1) had predominantly sharp peaks at around 25, 27 and 33 degrees of CCP, which was distributed in the texture of the hydrogels. Based on the XRD characterization, the results demonstrated that the CCP was appeared in the matrix of the gelatin/chitosan. This additionally demonstrated, that the structure of the hydrogels with CCP was similar to the extracellular matrix of calcified soft tissue.

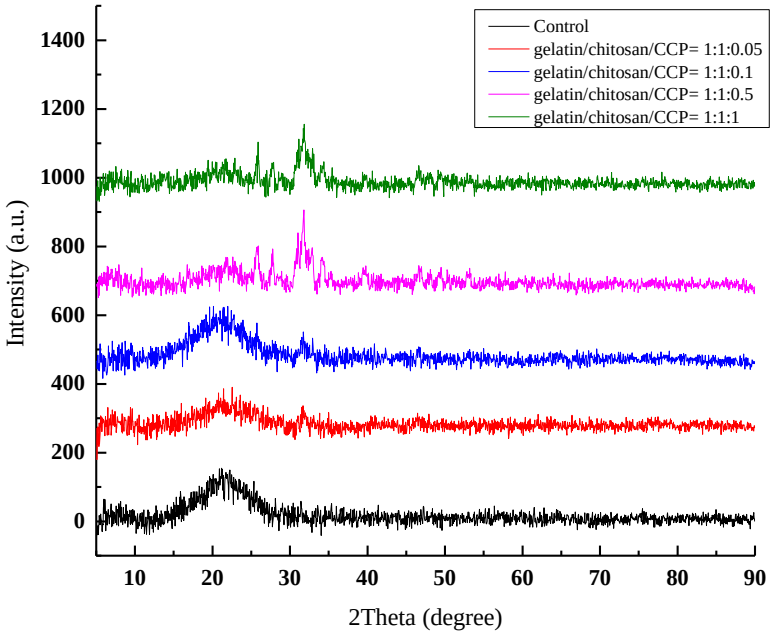

Figure 2.3 XRD diffraction of the hydrogels: Control; gelatin/chitosan/CCP (1:1:0.05); (1:1:0.1); (1:1:0.5); and (1:1:1)

According to the molecular and structural characterizations, the results demonstrated that the molecules of gelatin/chitosan/CCP self-organized via ⁻OH interaction. The organization of gelatin/chitosan/CCP had the structure of an organic substrate of gelatin and chitosan, which was deposited by the minerals of CCP. Previous research demonstrated that; the extracellular matrix of calcified soft tissue was formed via the molecular organization of biomacromolecules of proteins, proteoglycans and glycosaminoglycans (38). Biomacromolecules self-organized into a sophisticated structure, incorporated with mineral molecules of calcified soft tissue (39). In this research, the results showed that those biomacromolecules of gelatin/chitosan were incorporated with mineral molecules of CCP and organized themselves via molecular interaction. This is similar to the structure of extracellular matrix organization during soft tissue calcification.

2.3.2 Morphologies of the hydrogels

SEM was used to observe the morphological structure of the gelatin/chitosan/CCP hydrogels at different ratios. The hydrogel without CCP showed

a smoother surface than that of hydrogels with CCP. Small particles of CCP were distributed on the surface of the porous walls in the case of hydrogels with CCP (Figures 2.4B, C, D, and E). This was especially true, for the hydrogels containing higher amounts of CCP (gelatin/chitosan/CCP [1:1:0.5] and [1:1:1]) as the particles were distributed over, almost the entire surface of the porous walls. These results contributed to the above explanation, whereas, the hydrogels with CCP had the structure of calcified soft tissue.

The structural formation of the extracellular matrix during soft tissue calcification shows bio-mineralization of both organic and inorganic materials (40). During soft tissue calcification; collagen, proteoglycans and glycosaminoglycans are the organic materials, which serve as a template for the inorganic deposition of calcium phosphate. The results indicated that the gelatin/chitosan performed as a template for deposition of CCP. This was similar to the structural formation of the extracellular matrix during soft tissue calcification (41).

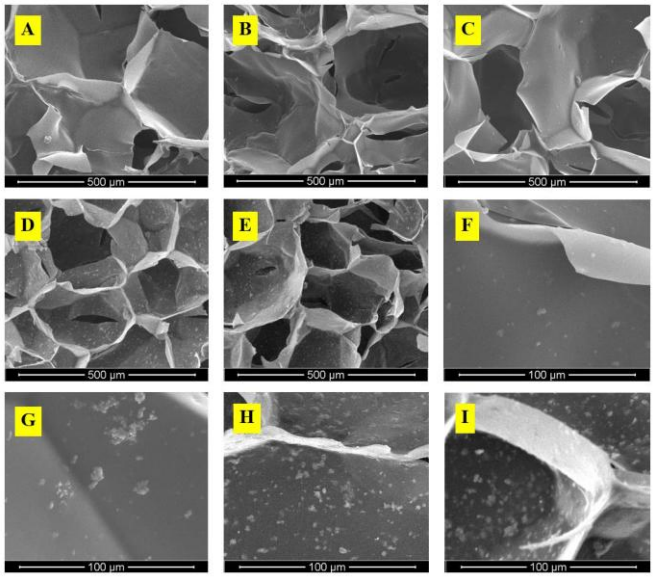

Figure 2.4 Morphology of the hydrogels: (A) Control; (B, F) gelatin/chitosan/CCP (1:1:0.05); (C, G) (1:1:0.1); (D, H) (1:1:0.5), and (E, I) (1:1:1)

The mean pore sizes along with pore size distributions of the hydrogels were assessed (Figure 2.5). The mean pores sizes of the gelatin/chitosan/CCP ratios of 1:1:0.01, 1:1:0.05, 1:1:0.1 and 1:1:1 were; 90.7, 80.8, 86.8, 75.5 and 72.6 µm, respectively. The mean pore sizes of the hydrogels with CCP were smaller than that of

the hydrogel without CCP. Increasing the amount of CCP decreased the mean pore size. The hydrogel with the highest amount of CCP (gelatin/chitosan/CCP [1:1:1]) had the smallest, mean pore size. This possibly came from intensive interaction between the CCP particles and the gelatin/chitosan causing this interaction to lead to a reduction in the pore size.

The pore size distributions of the control along with the gelatin/chitosan/CCP ratios of 1:1:0.01, 1:1:0.05, 1:1:0.1 and 1:1:1 were in the ranges of around; 70 to 110, 50 to 110, 80 to 100, 50 to 100 and 50 to 100 μm, respectively. Notably, a gelatin/chitosan/CCP ratio of 1:1:0.1 had the narrowest range of pore size distribution. That narrow range implied a homogeneous porous formation, which possibly came from the components that self-organized into a regular and stable structure. Contrary to that, the control and the gelatin/chitosan/CCP ratios of 1:1:0.05, 1:1:0.5 and 1:1:1 had wide pore size distributions, which represented a heterogeneous porous formation. This came from an irregular and unstable structure of said hydrogels. The results indicated that mimicking the extracellular matrix of calcified soft tissue based on hydrogels of gelatin/chitosan/CCP with certain amounts of CCP had an effect on the regular structural porous formation. Overall, the pore size range of the mimicked extracellular matrix was 50-100 μm which was suitable for osteoblast insertion (42).

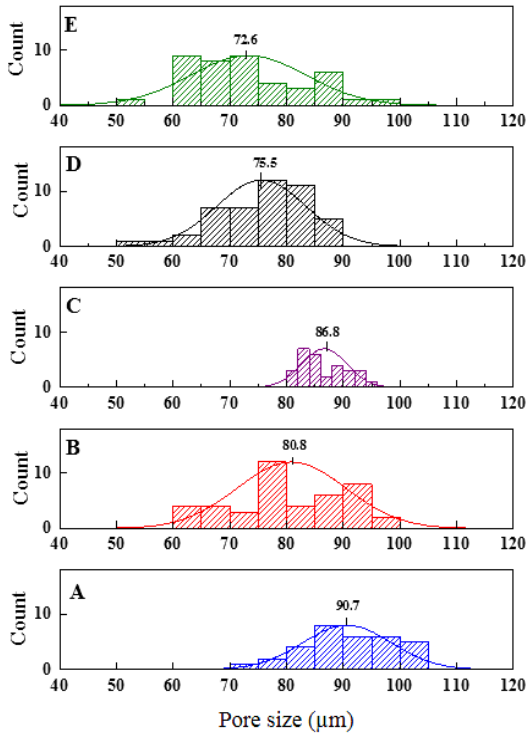

Figure 2.5 Distribution of pore size: (A) Control; (B) gelatin/chitosan/CCP (1:1:0.05); (C) (1:1:0.1); (D) (1:1:0.5); and (E) (1:1:1)

2.3.3 Physical behaviors of the gelatin/chitosan/CCP hydrogels

The swelling ratio and calcium release of the hydrogels were evaluated for their physical behaviors of mimicked extracellular matrix of calcified soft tissue. The swelling ratios of the hydrogels, including the control and the gelatin/chitosan/CCP ratios of 1:1:0.05, 1:1:0.1, 1:1:0.5 and 1:1:1 are shown in Figure 2.6. The hydrogel without CCP had a higher swelling ratio than that of the hydrogels with CCP because, the hydrogel without CCP had a regular pore size distribution and large pores. The swelling behavior of the hydrogels reached a steady state in the time period of; 5 to 10 minutes. The hydrogel without CCP along with those with higher amounts of CCP, in particular the gelatin/chitosan/CCP ratio of 1:1:1, approached a steady state earlier than the others. The swelling ratio of the hydrogel without CCP, which reached an early steady state, was probably due to the rapid water uptake into the morphological structure of the regular pore size distribution as well as it having large pores. In contrast to this, the hydrogel with the highest amount of CCP had an early starting point of

steady state possibly occurring due to the molecular and structural characteristics coupled with the organization, which had the unique component of CCP inducing water adsorption. Interestingly, previous research demonstrated that the extracellular matrix had different components, molecular and structural characteristics, organization and morphological structures during different stages of soft tissue calcification (43, 44). The extracellular matrix also showed different swelling behaviors of calcified soft tissue (44).

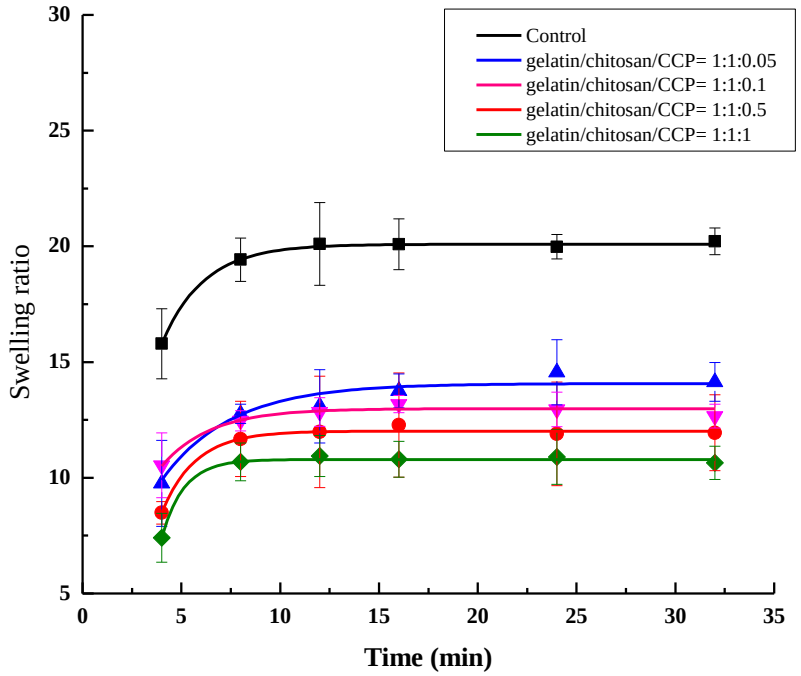

Figure 2.6 Swelling behavior of the hydrogels: Control; gelatin/chitosan/CCP (1:1:0.05); (1:1:0.1); (1:1:0.5); and (1:1:1)

The amount of calcium release was measured (Figure 2.7). These results showed that; the early state, burst release of calcium for the gelatin/chitosan/CCP ratio of 1:1:0.05 had a lower amount of calcium than the others. Furthermore, that ratio had a lower rate of burst release than the others. That ratio of 1:1:0.05 approached the steady state of calcium release in the time periods of 40 to 60 minutes, which was longer than the others. This possibly occurred because the calcium was firmly trapped in the gelatin/chitosan matrix. Oppositely, the calcium release period of the gelatin/chitosan/CCP at ratios of 1:1:0.1, 1:1:0.5, and 1:1:1 approached a steady state earlier than those at a ratio of 1:1:0.05. This was possibly from excess calcium, which self-organized into an unstable interaction causing rapid release (45).

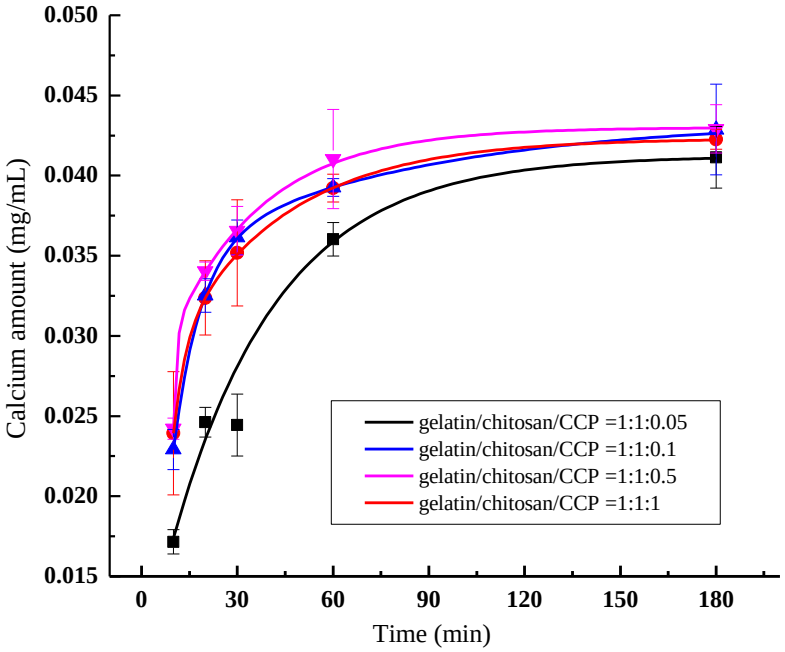

Figure 2.7 Calcium release of the hydrogels: Control, gelatin/chitosan/CCP (1:1:0.05); (1:1:0.1); (1:1:0.5); and (1:1:1)

Therefore, according to the physical behavior results, including the swelling behavior and calcium release, the hydrogels with CCP showed a behavior that was similar to the extracellular matrix of calcified soft tissue. In addition, the hydrogels with CCP might have the effect of enhancing tissue regeneration. To clarify this hypothesis, biological performance testing was undertaken.

2.3.6 Biological performances of the gelatin/chitosan/CCP hydrogels

In this research, cell viability as well as proliferation were assessed to evaluate the biological performance of the mimicked extracellular matrix. Cell viability of the osteoblasts was observed at days; 3, 5 and 7 (Figure 2.8). The blue spheres on the hydrogels were the nuclei of the cells. The hydrogel without CCP showed some cell aggregations that adhered in an irregular distribution on the surface at all-time points. This indicated that the gelatin and chitosan affected the aggregation and distribution of the osteoblasts. The aggregations and distribution come from the unstable, structural formation of gelatin and chitosan, which affected the cell aggregation similar to a spheroid formation.

The hydrogels with CCP had good distributions of cells on the surface at all-time points. This demonstrated that the CCP was able to enhance cell adhesion on the hydrogels. The hydrogels with CCP showed more cell distribution at day 5 than at day 7. This was due to the calcium, which could enhance cell viability (46). The results showed that the hydrogels with CCP were suitable for cell viability.

Interestingly, the gelatin/chitosan/CCP ratio of 1:1:0.1 showed a denser cell distribution than the others. This was possibly due to the suitable amount of CCP along with the regular, porous structure of the hydrogel being able to enhance cell viability.

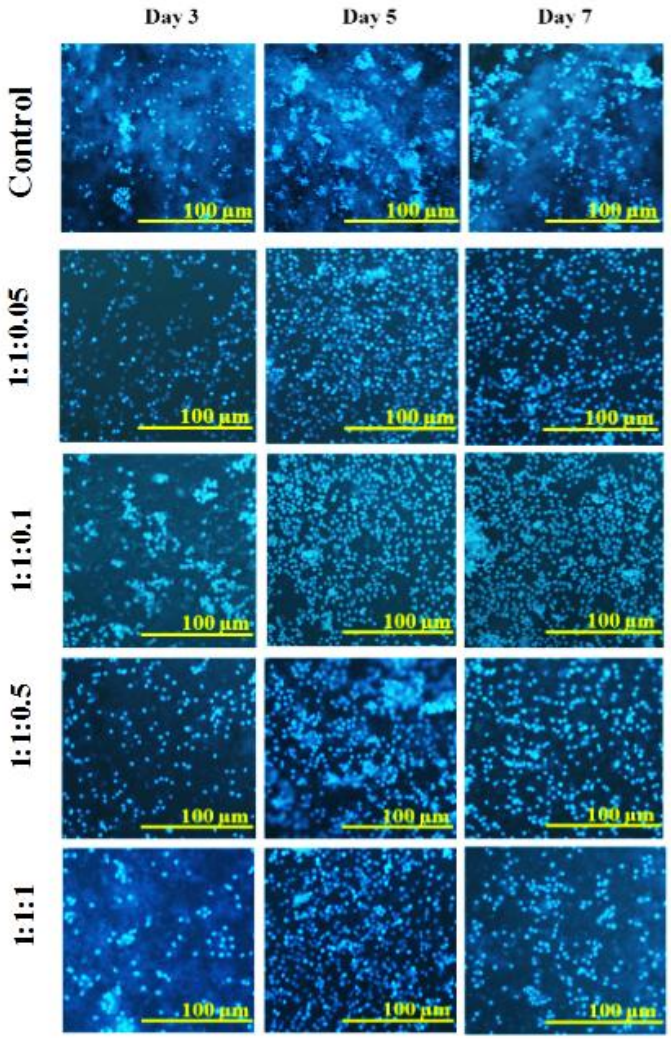

Figure 2.8 Cell viability on the hydrogels: Control; gelatin/chitosan/CCP (1:1:0.05); (1:1:0.1); (1:1:0.5); and (1:1:1) at days 3, 5, and 7

The biological performance was also assessed from cell proliferation. There were no differences in cell proliferation at days 1 and 5 for all ratios. However, the gelatin/chitosan/CCP ratios of 1:1:0.5 and 1:1:1 at day 3 showed more cell proliferation of osteoblasts than those hydrogel without CCP (Figure 2.9). After day 5, cell proliferation for all ratios decreased because, the hydrogels had eroded. The hydrogels with CCP had more cell proliferation than those hydrogel without CCP at day 7. Especially, the gelatin/chitosan/CCP at a ratio of 1:1:0.1, which had a greater, more unique cell proliferation than the others. This was possibly due to suitable amounts of components along with regular porous formations of the gelatin/chitosan/CCP at a ratio of 1:1:0.1. According to previous reports, suitable organic and inorganic materials in the extracellular matrix coupled with a structural, porous formation can induce osteoblast proliferation (43, 47).

The results, in this research, indicated that; the structural stability, regular morphology and a certain amount of mimicked extracellular matrix, particularly in the sample of gelatin/chitosan/CCP (1:1:0.1), performed suitability for the induction of osteoblast proliferation. This indicated that; gelatin/chitosan/CCP (1:1:0.1) is fit to be an ex vivo model of HO. Interestingly, different periods of soft tissue calcification showed different amounts of deposited calcium phosphate on an organic template (48). Furthermore, there are different amounts of calcium phosphate in different types of soft tissue in HO (49). Therefore, selection of a suitable model for the type of soft tissue as well as the period of soft tissue calcification needs to be considered before evaluation for use in screening for molecular and gene therapy in HO.

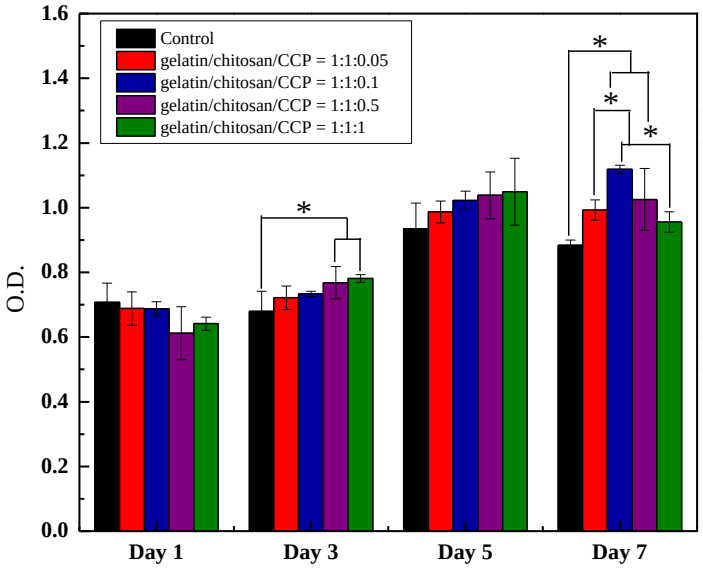

Figure 2.9 Cell proliferation on the hydrogels: Control; gelatin/chitosan/CCP (1:1:0.05); (1:1:0.1); (1:1:0.5); and (1:1:1) at days 1, 3, 5, and 7. The symbol (*) presented significant changes (*$p < 0.05$)

2.4 Conclusions

A mimicked extracellular matrix of calcified soft tissue based on hydrogels of gelatin/chitosan/CCP was presented as a performance system for the design of an ex vivo model of HO. For molecular and structural organization, the mimicked extracellular matrix showed embedded calcium phosphate in a matrix of gelatin and chitosan, which was similar to calcified soft tissue. In the case of physical performance, the different ratios of components in the mimicked extracellular matrix had an effect on the behavior of swelling and calcium release. The biological performance of gelatin/chitosan/CCP hydrogels showed a certain functionality to enhance cell viability and proliferation, particularly in the gelatin/chitosan/CCP at a ratio of 1:1:0.1. This research indicated that the mimicked, calcified soft tissue of those hydrogels with CCP has promise for use as an ex vivo model of HO. The gene expression of the osteoblasts on the mimicked extracellular matrix of calcified soft tissue is an important area for future research. Finally, the screening of specific molecules as well as genes for treatment of diseases by the ex vivo model is our goal.

2.5 Acknowledgments

This work was partially supported by the Institute of Biomedical Engineering, Faculty of Medicine, Prince of Songkla University. A. Thangprasert would like to acknowledge the scholarship supported by the Development and Promotion of Science and Technology Talents Project (DPST).

2.6 References

1. Kaplan FS, Glaser DL, Hebela N, Shore EM. Heterotopic Ossification : Journal of the American Academy of Orthopaedic Surgeons. 2004 Mar 12(2):116-25.
2. Olabisi RM, Lazard ZW, Franco CL, Hall MA, Kwon SK, Sevick-Muraca EM, et al. Hydrogel Microsphere Encapsulation of a Cell-Based Gene Therapy System Increases Cell Survival of Injected Cells, Transgene Expression, and Bone Volume in a Model of Heterotopic Ossification. Tissue Eng Part A. 2010 Jul 30;16(12):3727–36.
3. Rumi MN, Deol GS, Singapuri KP, Pellegrini VD. The origin of osteoprogenitor cells responsible for heterotopic ossification following hip surgery: An animal model in the rabbit. J Orthop Res. 2005 Jan 1;23(1):34–40.
4. McCarthy EF, Sundaram M. Heterotopic ossification: a review. Skeletal Radiol. 2005 Oct 1;34(10):609–19.
5. Sawyer JR, Myers MA, Rosier RN, Puzas JE. Heterotopic ossification: Clinical and cellular aspects. Calcif Tissue Int. 1991 May 1;49(3):208–15.
6. Hutmacher DW. Scaffolds in tissue engineering bone and cartilage. Biomaterials. 2000 Dec 15;21(24):2529–43.
7. Sharma B, Elisseeff JH. Engineering Structurally Organized Cartilage and Bone Tissues. Ann Biomed Eng. 2004 Jan 1;32(1):148–59.
8. Caló E, Khutoryanskiy VV. Biomedical applications of hydrogels: A review of patents and commercial products. Eur Polym J. 2015 Apr;65:252–67.
9. Kisiday J, Jin M, Kurz B, Hung H, Semino C, Zhang S, et al. Self-assembling peptide hydrogel fosters chondrocyte extracellular matrix production and

cell division: Implications for cartilage tissue repair. Proc Natl Acad Sci. 2002 Jul 23;99(15):9996–10001.

10. Chai YC, Carlier A, Bolander J, Roberts SJ, Geris L, Schrooten J, et al. Current views on calcium phosphate osteogenicity and the translation into effective bone regeneration strategies. Acta Biomater. 2012 Nov;8(11):3876–87.
11. Seibel MJ, Robins SP, Bilezikian JP. Dynamics of Bone and Cartilage Metabolism: Principles and Clinical Applications. Academic Press; 2006. 945.
12. Detsch R, Hagmeyer D, Neumann M, Schaefer S, Vortkamp A, Wuelling M, et al. The resorption of nanocrystalline calcium phosphates by osteoclast-like cells. Acta Biomater. 2010 Aug;6(8):3223–33.
13. LeGeros RZ, Properties of Osteoconductive Biomaterials: Calcium Phosphates. Clinical Orthopaedics and Related Research. 2002 Feb;(395):81-98.
14. Peng Z, Peng Z, Shen Y. Fabrication and Properties of Gelatin/Chitosan Composite Hydrogel. Polym-Plast Technol Eng. 2011 Jul 15;50(11):1160–4.
15. Dunn JCY, Chan W-Y, Cristini V, Kim J s., Lowengrub J, Singh S, et al. Analysis of Cell Growth in Three-Dimensional Scaffolds. Tissue Eng. 2006 Apr 1;12(4):705–16.
16. Ibusuki S, Fujii Y, Iwamoto Y, Matsuda T. Tissue-Engineered Cartilage Using an Injectable and in Situ Gelable Thermoresponsive Gelatin: Fabrication and in Vitro Performance. Tissue Eng. 2003 Apr 1;9(2):371–84.
17. Chung C, Burdick JA. Engineering Cartilage Tissue. Adv Drug Deliv Rev. 2008 Jan 14;60(2):243–62.
18. Lutolf MP, Hubbell JA. Synthetic biomaterials as instructive extracellular microenvironments for morphogenesis in tissue engineering. Nat Biotechnol. 2005 Jan;23(1):47–55.
19. Berger J, Reist M, Mayer JM, Felt O, Gurny R. Structure and interactions in chitosan hydrogels formed by complexation or aggregation for biomedical applications. Eur J Pharm Biopharm. 2004 Jan;57(1):35–52.

20. Francis Suh J-K, Matthew HWT. Application of chitosan-based polysaccharide biomaterials in cartilage tissue engineering: a review. Biomaterials. 2000 Dec 15;21(24):2589–98.
21. Kim SE, Park JH, Cho YW, Chung H, Jeong SY, Lee EB, et al. Porous chitosan scaffold containing microspheres loaded with transforming growth factor-β1: Implications for cartilage tissue engineering. J Controlled Release. 2003 Sep 4;91(3):365–74.
22. Puppi D, Chiellini F, Piras AM, Chiellini E. Polymeric materials for bone and cartilage repair. Prog Polym Sci. 2010 Apr;35(4):403–40.
23. Neves SC, Moreira Teixeira LS, Moroni L, Reis RL, Van Blitterswijk CA, Alves NM, et al. Chitosan/Poly(ε-caprolactone) blend scaffolds for cartilage repair. Biomaterials. 2011 Feb;32(4):1068–79.
24. Tibbitt MW, Anseth KS. Hydrogels as extracellular matrix mimics for 3D cell culture. Biotechnol Bioeng. 2009 Jul 1;103(4):655–63.
25. Nagahama H, Maeda H, Kashiki T, Jayakumar R, Furuike T, Tamura H. Preparation and characterization of novel chitosan/gelatin membranes using chitosan hydrogel. Carbohydr Polym. 2009 Mar 17;76(2):255–60.
26. Shi J, Xing MMQ, Zhong W. Development of Hydrogels and Biomimetic Regulators as Tissue Engineering Scaffolds. Membranes. 2012 Feb 14;2(1):70–90.
27. Zhu M, Feng Q, Sun Y, Li G, Bian L. Effect of cartilaginous matrix components on the chondrogenesis and hypertrophy of mesenchymal stem cells in hyaluronic acid hydrogels. J Biomed Mater Res B Appl Biomater. 2016 Jul 1.
28. Liu X, Zhao M, Lu J, Ma J, Wei J, Wei S. Cell responses to two kinds of nanohydroxyapatite with different sizes and crystallinities. Int J Nanomedicine. 2012;7:1239–50.
29. Thein-Han WW, Saikhun J, Pholpramoo C, Misra RDK, Kitiyanant Y. Chitosan–gelatin scaffolds for tissue engineering: Physico-chemical properties and biological response of buffalo embryonic stem cells and transfectant of GFP–buffalo embryonic stem cells. Acta Biomater. 2009 Nov;5(9):3453–66.

30. Boncler M, Różalski M, Krajewska U, Podsędek A, Watala C. Comparison of PrestoBlue and MTT assays of cellular viability in the assessment of anti-proliferative effects of plant extracts on human endothelial cells. J Pharmacol Toxicol Methods. 2014 Jan;69(1):9–16.
31. Yamane S, Sugawara A, Watanabe A, Akiyoshi K. Hybrid Nanoapatite by Polysaccharide Nanogel-templated Mineralization. J Bioact Compat Polym. 2009 Mar 1;24(2):151–68.
32. Okay O, Oppermann W. Polyacrylamide−Clay Nanocomposite Hydrogels: Rheological and Light Scattering Characterization. Macromolecules. 2007 May 1;40(9):3378–87.
33. Kačuráková M, Smith AC, Gidley MJ, Wilson RH. Molecular interactions in bacterial cellulose composites studied by 1D FT-IR and dynamic 2D FT-IR spectroscopy. Carbohydr Res. 2002 Jun 12;337(12):1145–53.
34. Ruoslahti E, Yamaguchi Y. Proteoglycans as modulators of growth factor activities. Cell. 1991 Mar 8;64(5):867–9.
35. Landis WJ. The strength of a calcified tissue depends in part on the molecular structure and organization of its constituent mineral crystals in their organic matrix. Bone. 1995 May 1;16(5):533–44.
36. Poole AR1, Kojima T, Yasuda T, Mwale F, Kobayashi M, Laverty S. Composition and Structure of Articular Cartilage: A Template for Tissue Repair. Clinical Orthopaedics and Related Research. 2001 Oct;(391 Suppl):S26-33.
37. Ferreira AM, Gentile P, Chiono V, Ciardelli G. Collagen for bone tissue regeneration. Acta Biomater. 2012 Sep;8(9):3191–200.
38. O'Brien FJ, Harley BA, Yannas IV, Gibson LJ. The effect of pore size on cell adhesion in collagen-GAG scaffolds. Biomaterials. 2005 Feb;26(4):433–41.
39. Olszta MJ, Cheng X, Jee SS, Kumar R, Kim Y-Y, Kaufman MJ, et al. Bone structure and formation: A new perspective. Mater Sci Eng R Rep. 2007 Nov 28;58(3–5):77–116.
40. Tabata Y, Yamada K, Miyamoto S, Nagata I, Kikuchi H, Aoyama I, et al. Bone regeneration by basic fibroblast growth factor complexed with biodegradable hydrogels. Biomaterials. 1998 Apr 1;19(7):807–15.

41. Kirschner CM, Anseth KS. Hydrogels in healthcare: From static to dynamic material microenvironments. Acta Mater. 2013 Feb;61(3):931–44.
42. Rezwan K, Chen QZ, Blaker JJ, Boccaccini AR. Biodegradable and bioactive porous polymer/inorganic composite scaffolds for bone tissue engineering. Biomaterials. 2006 Jun;27(18):3413–31.
43. Bongio M, van den Beucken JJJP, Nejadnik MR, Leeuwenburgh SCG, Kinard LA, Kasper FK, et al. Biomimetic modification of synthetic hydrogels by incorporation of adhesive peptides and calcium phosphate nanoparticles: in vitro evaluation of cell behavior. Eur Cell Mater. 2011 Dec 17;22:359–76.
44. Maeno S, Niki Y, Matsumoto H, Morioka H, Yatabe T, Funayama A, et al. The effect of calcium ion concentration on osteoblast viability, proliferation and differentiation in monolayer and 3D culture. Biomaterials. 2005 Aug;26(23):4847–55.
45. Towler DA. Inorganic Pyrophosphate. Arterioscler Thromb Vasc Biol. 2005 Apr 1;25(4):651–4.
46. Gerber H-P, Ferrara N. Angiogenesis and Bone Growth. Trends Cardiovasc Med. 2000 Jul;10(5):223–8.

CHAPTER 3
MIMICKED HYBRID HYDROGEL BASED ON GELATIN/PVA FOR TISSUE ENGINEERING IN SUBCHONDRAL BONE INTERFACE FOR OSTEOARTHRITIS SURGERY

Abstract

Osteoarthritis (OA) is a degenerative joint disease of the articular cartilage and extends to subchondral bone. Although, many studies mention the regeneration of both cartilage and subchondral bone, the interface between these soft and hard tissue should be highlighted since it plays a significant role in OA as well. In this work, gelatin/PVA hydrogels in different ratios of 100:0, 70:30, 50:50, 30:70, and 0:100 were prepared by chemical and freeze-thaw physical crosslinking. The molecular organization and morphology were characterized and observed by FT-IR and SEM, respectively. The physical properties of swelling ratio, degradation rate, and compressive strength were evaluated. The hydrogels were cultured with osteoblasts before evaluation of cell adhesion and proliferation, alkaline phosphatase activity (ALP), and calcium deposition and content. The results showed that gelatin/PVA formed hydrogels via crosslinking of chemical bonding and molecular interaction. The morphology demonstrated that pore sizes decreased as the proportion of PVA increased and the swelling ratio and degradation rate increased as the proportion of gelatin increased. The compressive strength increased as the proportion of PVA increased. The biological function tests showed that gelatin/PVA hydrogels supported cell adhesion and proliferation, ALP activity, calcium deposition and content. Finally, the gelatin/PVA ratio of 30:70 demonstrated suitable structural formation, physical properties, and biological functions to induce tissue engineering at subchondral bone interface for OA surgery.

3.1 Introduction

Osteoarthritis (OA) is the chronic disease found in older patients. The feature of OA is the degradation and lesion of joint tissues, involving articular cartilage, subchondral bone, and the synovial membrane (1). The major characteristic of OA is articular cartilage breakdown, which results in joint pain, swelling, and mobility disability. Numerous surgical approaches such as microfracture, autologous chondrocyte implantation (ACI), and graft transplantation have been attempted to regenerate cartilage when medical treatment fails. Alternatively, tissue engineering approaches using biomaterial scaffolds have become a promising intervention to regenerate the loss of cartilage in OA. This tissue engineering scaffold provides a three-dimensional (3D) structure for cell growth and differentiation in non-immune diseases (2). An ideal artificial scaffold for tissue engineering must provide sufficient mechanical stability, biocompatibility, biodegradability, suitable porosity for cell growth and blood invasion, fit the size and shape of the defect, and mediate cell-cell signaling and interaction (3).

Many types of materials and methods of scaffold fabrication have been implemented to recapitulate microenvironments present during development or in adult tissue to induce the formation of cartilaginous constructed with biochemical and mechanical properties of native tissue (4). Gelatin is a polypeptide derived from the hydrolysis of collagen and shows similar properties as extracellular matrix (ECM) in native tissue. It contains a large number of the tripeptide Arg-Gly-Asp (RGD) motifs which can interact with integrin of the cell surface that results in the enhancement of cell adhesion to the matrix (5). Due to brittleness, less flexibility, and the fast degradation rate of a gelatin hydrogel, modifications of the gelatin with other materials are needed. Poly (vinyl alcohol) or PVA is a water soluble synthetic polymer. It shows many good properties such as availability, biocompatibility, biodegradability, and elastic and compressive mechanical properties. The tiny pores in PVA hydrogels are capable of storing a large amount of water which allows a PVA hydrogel to act as a lubricant similar to the surface of cartilage (6). It was reported that gelatin/PVA hydrogels showed decent mechanical and biological properties for this application (7). Moreover, many works proposed that mixing PVA as composite material or PVA

scaffold can enhance mechanical properties of scaffold (8–11). In this work, the combination of gelatin with PVA should increase the mechanical properties of pure gelatin hydrogels to promote cell adhesion, cell proliferation, or important biomarkers of pure PVA hydrogels for cartilage tissue engineering.

A number of studies have focused on the preparation and characterization of gelatin scaffolds or PVA scaffolds or both for cartilage tissue engineering (6,8,12–14). The result demonstrated that gelatin and PVA were shown to be biologically compatible biomaterials and they increased cell growth. Moreover, differentiated cells regulate biomarkers and gene expressions which are essential to identify chondrocyte differentiation and cartilage formation. Interestingly, gelatin/PVA scaffolds have not been promoted only for cartilage regeneration. However, these scaffolds are appropriate for the interfacial microstructure between the cartilage in the calcified zone and the subchondral bone, which is beneath the calcified zone of cartilage and play a potential role during OA degenerative as well (15). The porosity of the subchondral bone interface could maintain the matrix without breakdown and promote cell and mineralization for new bone interface (16). The optimal scaffold fills the defect and promotes tissue formation at the subchondral bone interface (17). Hence, this research focused on the scaffold which can enhance tissue formation at the subchondral bone interface.

The basic materials of PVA and gelatin were selected with the mimicking concept for scaffold fabrication into hydrogels. The molecular organization, morphological structure, and the physical and biological performance of the gelatin/PVA hydrogels were characterized observed, and tested. Finally, one of the hydrogels of gelatin/PVA was evaluated as a promising cartilage scaffold to enhance the tissue engineering of subchondral bone at the interface for OA surgery.

3.2 Materials and methods

3.2.1 Preparation of gelatin/PVA hydrogels

Gelatin solution was prepared by dissolving gelation powder (Sigma-Aldrich, for bacteriological purposes) in deionized water to get a concentration of 7% w/v and stirred at 50^{o}C for 1 h. A 7% PVA (Mw = 145,000 and degree of hydrolysis $\geq$ 98%,

Merck, Darmstadt, Germany) solution was also prepared in deionized water and stirred at 90^{o}C for 2-4 h to get complete dissolution. The gelatin and PVA solutions were mixed at ratios of 100:0, 70:30, 50:50, 30:70, and 0:100. The glutaraldehyde (GA) at concentration of 0.1% was added into the mixture of gelatin and PVA solution, stirred until a homogenous solution was obtained and poured into 48-well plate. Then, the gelatin/PVA hydrogels were frozen at -20^{o}C for 12 h and thawed at room temperature for 12 h. The freeze-thaw procedure was carried out in 5 cycles to reach a stable shape. After the freeze-thawing cycles, the gelatin/PVA hydrogels were soaked with 0.1 M glycine for 2 h to neutralize GA.

3.3 Characterization of hydrogels

3.3.1 Fourier transform infrared spectroscopy (FT-IR) characterization

FT-IR spectra of the composite hydrogels were carried out using the attenuated total reflectance mode on an FT-IR spectrometer (Equinox 55, Bruker, Ettlingen, Germany). The dried hydrogels were scanned in the range of 4000 to 400 cm^{-1}.

3.3.2 Morphology and pore size measurement

The morphology of the hydrogels was observed using scanning electron microscope (SEM, TM3030Plus, Tabletop microscope, Hitachi). Before the SEM analysis, the hydrogel samples were coated with gold using a gold sputter coater machine (SPI Supplies, Division of Structure Probe Inc., Westchester, PA, USA). The pore sizes in each group of gelatin/PVA hydrogels were randomized (n=100) and the average of pore sizes was calculated using ImageJ software.

3.3.3 Swelling testing

The swelling behavior of the hydrogels was measured at different time periods in phosphate buffer solution (PBS) at 37^{o}C. The hydrogels were removed out from the PBS, excess water was wiped off by filter water and the wet weight was determined immediately. The dry weight of the hydrogels was obtained after freeze-drying. The swelling ratio was calculated using the equation

$$\text{Swelling ratio} = (W_t - W_d)/W_d$$

When W_t and W_d are the weight of the swollen hydrogels and dried hydrogels, respectively (18).

3.3.4 Degradation behavior

Degradation of the gelatin/PVA hydrogels was carried out by measuring the weight loss. The gelatin/PVA hydrogels were freeze-dried, weighed, and immersed in lysozyme at a concentration of 2 mg/ml. A weight comparison was performed before and after the enzymatic degradation using this equation (19).

% weight loss = (Initial weight – weight after degradation)/Initial weight x 100

3.3.5 Mechanical testing

Compressive testing of the gelatin/PVA hydrogels was performed by applying a strain rate of 0.2 mm/min using a universal testing machine (Lloyd model LRX-Plus, Lloyd Instrument Ltd., London, UK). The hydrogels (n=6) were cut into sizes of 10 mm diameter with a 5 mm thickness. The testing machine had a static load cell of 10 N at rate of 2 mm/min and stopped at a strain 40%.

3.3.6 Cell culture

MC3T3-E1 cells were cultured in α-modified minimal essential medium (α-MEM) (Gibco, Invitrogen, Carlsbad, CA, USA) supplemented with 1% penicillin/ streptomycin, 0. 1% Fungizone, and 10% fetal bovine serum (FBS). Before cell seeding, the samples were sterilized by UV light for 1 h and immersed into the cultured medium for 24 h. Hydrogels were seeded with $1x10^5$ cells density in 30 µl expansion medium. After 2 h of cell seeding, 500 µl of osteogenic differentiation medium was added into each hydrogel, cultivated at 37 ºC with 5% CO_2 for up 3 weeks, and the medium was changed every 3-4 days.

To prepare the osteogenic differentiation medium, α-MEM was supplemented with penicillin/ streptomycin, fungizone, FBS, 10 mM β-glycerophosphate, 50 mg/mL ascorbic acid, and 100 nM dexamethasone.

3.3.7 Cell proliferation

The cell proliferation of gelatin/PVA hydrogels without osteogenic differentiation medium were measured using PrestoBlue reagent (PrestoBlue® cell viability regent, Invitrogen, USA) at day 1, 7, 14 and 21. Initially, the hydrogels were washed twice with 1xPBS solution. The PrestoBlue solution was prepared by mixing with the medium at a ratio of 1:10 and added into the hydrogels. The gelatin/PVA hydrogels were then incubated for 1 h at 37ºC, A quantity of 200 µl of the solution was transferred into 96-well plate, and the absorbance was measured at wavelength of 570 nm.

3.3.8 Cell attachment

MC3T3-E1 cell attachment seeded on the gelatin/PVA hydrogels was observed at day 1 and day 14 by SEM. The hydrogels were fixed with 3.5% formaldehyde solution, washed with distilled water, and freeze dried. Before the SEM analysis, the hydrogels were coated with gold and the cell viability was observed by SEM (SEM, TM3030Plus, Tabletop microscope, Hitachi).

3.3.9 Mineralization assay

Alizarin red staining was used to determine the mineralized bone matrix after osteogenic differentiation. The cells on the gelatin/PVA hydrogels cultivated for day 14 and day 21 were fixed with 4% formaldehyde for 10 min. A 2% (w/v) solution of alizarin red (Sigma-Aldrich, USA) was added and kept in the dark for 20 min. The hydrogels stained with alizarin red were then washed several times with deionized water to remove the excess stain and the mineralize nodule were observed under a microscope.

3.3.10 Alkaline phosphatase (ALP) analysis

The ALP activity of the cells seeded hydrogels was determined at day1, 7, 14, and 21 after culturing the cells in osteogenic differentiation medium. The gelatin/PVA hydrogels were washed twice with PBS and then frozen at -80^{o}C until the ALP analysis. To perform the ALP analysis, the lysing solution (1% Triton-X in PBS) was added into each hydrogel, incubated on ice, and freeze-thawed in 3 cycles. Aliquots of the ALP assay were measured using alkaline phosphatase liquicolor (AMP Buffer, IFCC, Human, Germany) according to the manufacturer's instructions. During the reaction, ALP hydrolyzes the colorless ρ-nitrophenylphosphate to form the yellow product of ρ-nitrophenol (20). The rate of ρ-nitrophenol is proportional to the ALP activity. The absorbance was measured at the wavelength of 405 nm. Each experiment was performed in triplicates and the relative ALP activity was expressed in U/I.

3.3.11 Calcium colorimetric assay

Another aliquot of the lysed cell solution was used to determine calcium content. The calcium qualitative assay was measured according to the manufacturer's instruction (Biovision, Milpitas, CA, USA). Briefly, the lysed cell solution was pipetted (50 µl) into a 96-transparent-well plate. Then, chromogenic reagent (90 µl) and calcium assay buffer (60 µl) were added into the solution samples under mixing and incubated for 10 min at room temperature in the dark. The optical density was measured at wavelength of 575 nm. The calcium concentrations was calculated by the ratio of the calcium content and the sample volume.

3.3.12 Statistic analysis

All data were statically analyzed using one-way ANOVA, Turkey's HDS test (SPSS 20.0 software package). The data are presented as mean ± standard deviation was shown. P values less than 0.05 were considered to be significant.

3.4 Results

3.4.1 Preparation and gelation of gelatin/PVA

The schematic illustration of the gelatin/PVA hydrogel is shown in Figure 3.1. The gelatin/PVA hydrogels were prepared in two step method. The first step was to generate covalently chemical crosslinking using the GA crosslinker. The next step was the formation of the physical crosslinking in the hydrogels using the freeze-thaw method. The morphology of pure gelatin exhibited a translucent gel. Addition of the PVA solution showed white opaque structures. The morphologies of the gelatin/PVA hydrogels at different ratios was presented in Figure 3.2.

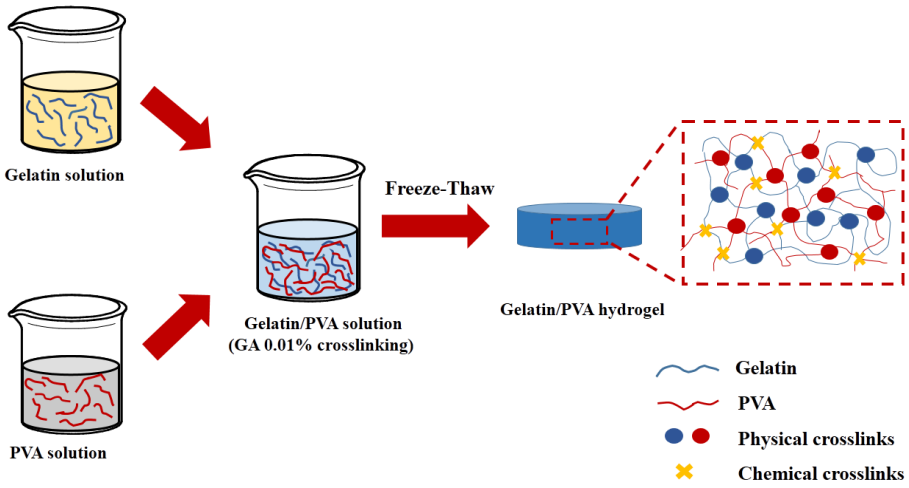

Figure 3.1 Schematic illustration of gelatin/PVA hydrogel preparation

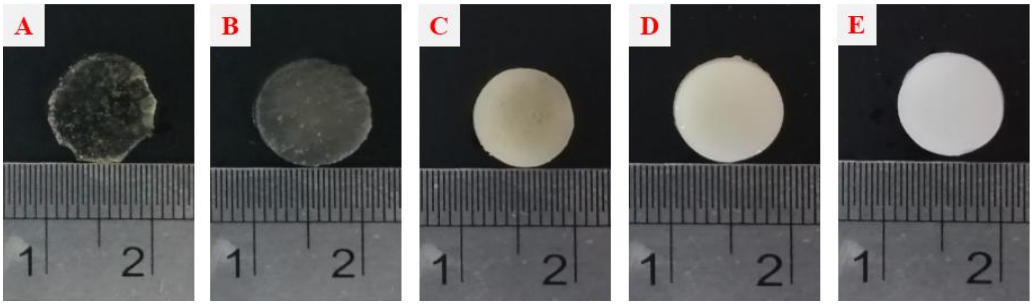

Figure 3.2 Gelatin/PVA hydrogels at different ratios (A) 100:0, (B) 70:30, (C) 50:50, (D) 30:70, and (E) 0:100

3.4.2 FT-IR characterization of gelatin/PVA hydrogels

The molecular and structural organization of the gelatin/PVA hydrogels with different concentrations after freeze-drying were studied using FT-IR measurement. The gelatin, gelatin/PVA and PVA hydrogels showed different spectra in the region of 800-3500 cm^{-1} as (Figure 3.3).

The gelatin spectra showed C-H stretching vibration of the protein that appeared at wavenumbers 2915 cm^{-1} and 2850 cm^{-1}. The peaks in the range of 3100-3500 cm^{-1} were due to N-H stretching of secondary amide including O-H stretching vibration. Moreover, N-H bending appeared in the wavenumber of 1500 -1550 cm^{-1} (21). The hydroxyl groups (O-H) stretching in the hydrogels showed a broad peak at wavenumber in the region of 3000-3600 cm^{-1}. This hydroxyl groups indicated existence of intermolecular and intramolecular hydrogen bonding of PVA and gelatin. CH_2 bending appeared at wavenumber at 1400-1450 cm^{-1}. The bands at 1000-1100 cm^{-1} was attributed to the reaction of the aldehyde groups of GA with hydroxyl groups of PVA, forming acetal groups (O-C-O vibration) (22). The more intense absorption peak in this region was observed as the amount of PVA increased. Moreover, the band at 1630-1650 cm^{-1} and 1530-1550 cm^{-1} in 100:0, 70:30, 50:50, and 30:70 gelatin/PVA hydrogel were related to the formation of imine (C=N), which came from the interaction between amine group of gelatin and aldehyde groups of GA. The broad peak of this region (1630-1650 cm^{-1}) was exhibited due to the overlapping with the bands of C=O stretching vibration peaks in amide I (about 1630 cm^{-1}) of uncrosslinked gelatin (23). The lower intensity of this characteristic peak appeared in the higher PVA amount. Interestingly, there was no characteristic peak of aldehyde (C=O) obtained from the GA

crosslinker at 1700 cm^{-1} in the FTIR spectrum which indicated no residual GA existed in the hydrogels (24).

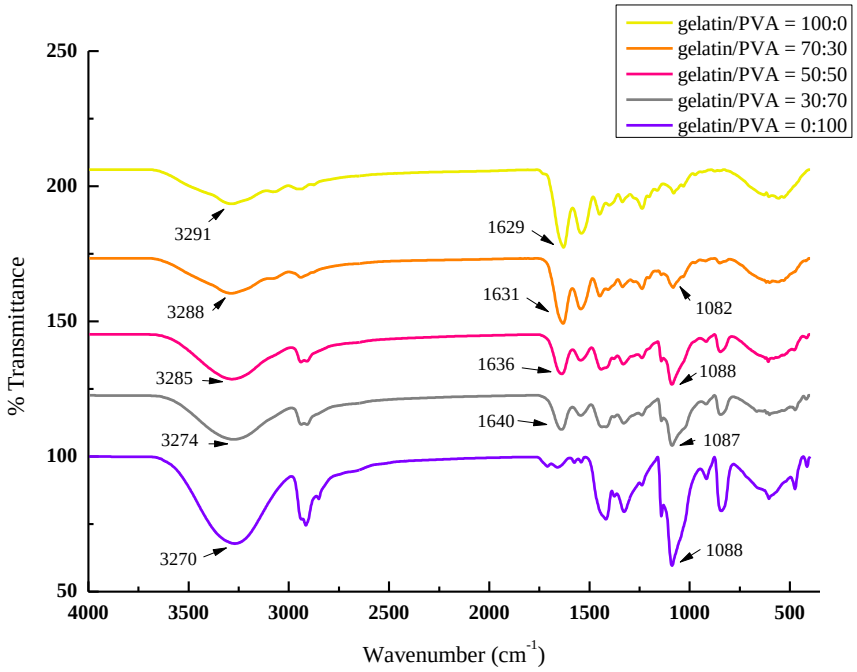

Figure 3.3 FT-IR spectra of gelatin/PVA hydrogels

3.4.3 Swelling behavior of gelatin/PVA hydrogels

The swelling behavior of a hydrogel network is an important factor when fabricating hydrogels because it is necessary to have high water adsorption and retention capacity. Moreover, this factor affects solute diffusion, mechanical properties and molecular mobility of a hydrogel (25). Swelling behaviors of gelatin/PVA hydrogel with different concentrations were studied at different time periods from 1 min to 180 min (Figure 3.4). All groups of hydrogels swelled rapidly in the first few minutes. This reason was due to the pores in the hydrogels and the hydrophilicity of the polymers. The swelling ratio started to saturate after a long time due to the equilibrium of water absorption. The hydrogels that contained pure gelatin (100:0) and gelatin/PVA at ratio 70:30 had highest swelling ratio. Conversely, hydrogels containing higher amount of PVA (50:50, 30:70, and 0:100) showed low swelling ratios.

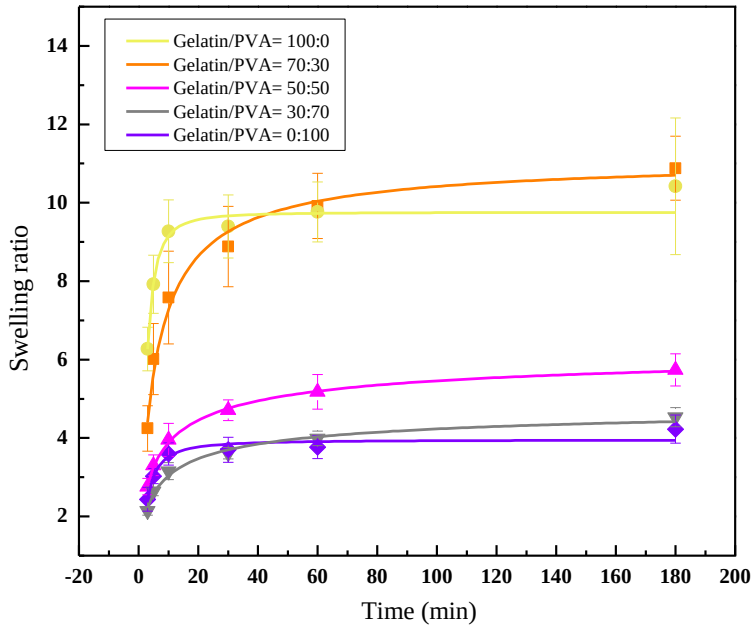

Figure 3.4 Swelling graphs of gelatin/PVA hydrogels with different time period

3.4.4 Degradation behavior of gelatin/PVA hydrogels

The degradation behavior of gelatin/PVA hydrogels with different concentration ratios were studied by measuring the weight loss (Figure 3.5). All groups of gelatin/PVA hydrogels showed high degradation rate at the starting point. The 100:0 and 70:30 gelatin/PVA hydrogels were completely degraded in the lysozyme solution at day 5 and day 8, respectively. The weight loss of gelatin/PVA hydrogels with ratios of 50:50, 30:70 and 0:100 decreased after day 32. However, these three groups maintained their shape during the degradation testing. The results suggested that the addition of PVA into the gelatin/PVA hydrogel decreased the degradation rates of hydrogel and provided hydrogel shape stability.

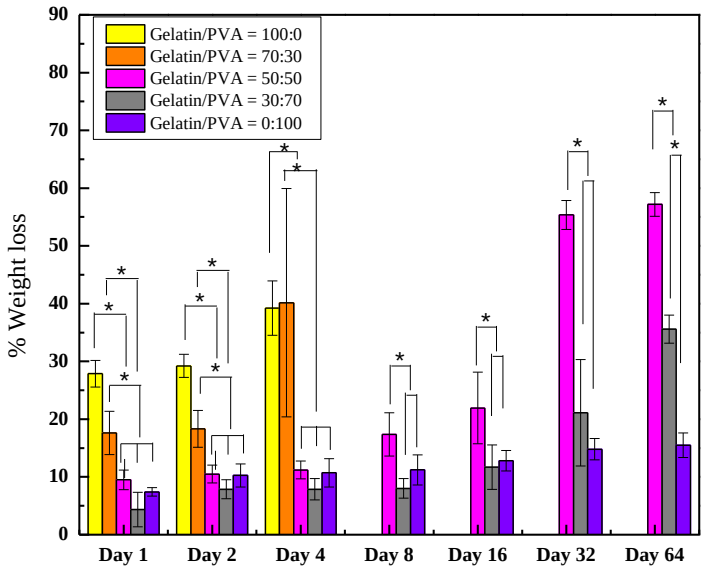

Figure 3.5 Gelatin/PVA hydrogels after degradation in lysozyme enzyme. The symbol (*) presented significant changes (*$p < 0.05$)

3.4.5 Mechanical properties of gelatin/PVA hydrogels

The mechanical properties of a hydrogel are important requirement for cartilage tissue engineering. When compressed, a hydrogel should not be easily broken or fractured. Therefore, the mechanical properties of the gelatin/PVA hydrogels underwent compressive testing. The compressive stress and Young's moduli of the gelatin/PVA hydrogels in wet state are showed in Figure 3.6. The pure gelatin hydrogel showed the lowest compressive stress and Young's modulus at the limitation of 40% strain. In contrast, higher PVA content in the hydrogels increased the compressive stress and Young's modulus of the gelatin/PVA hydrogels.

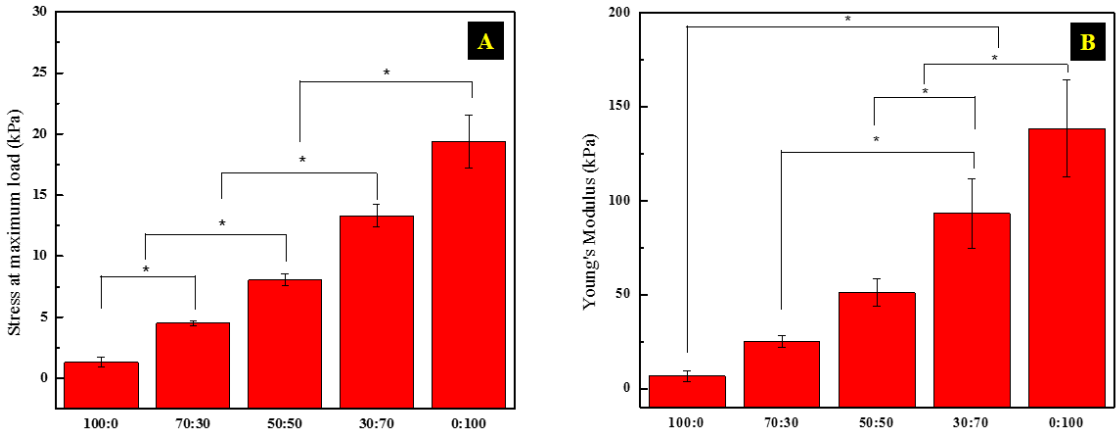

Figure 3.6 The mechanical properties of gelatin/PVA hydrogels: (A) stress at maximum load and (B) Young's modulus. The symbol (*) presented significant changes (*$p < 0.05$)

3.4.6 Morphological observations and analysis of gelatin/PVA hydrogels

The pore size of hydrogels is important in facilitating cell binding, migration, and ingrowth. Moreover, the pore size can allow nutrient and oxygen transportation to the inside of the hydrogels (26). The SEM images of the porous structures of the gelatin/PVA hydrogels are revealed in Figure 3.7. Gelatin/PVA hydrogels with a ratio of 100:0 had the largest pore size compared to the other groups at the same magnification. Adding PVA into the gelatin hydrogels made the pore sizes smaller. Moreover, the interconnected pores were also appeared in all hydrogel groups. The pore size distribution of 100 pores was also studied using ImageJ software (Figure 3.8). The pore size of the gelatin/PVA hydrogels with higher PVA content showed smaller pore sizes.

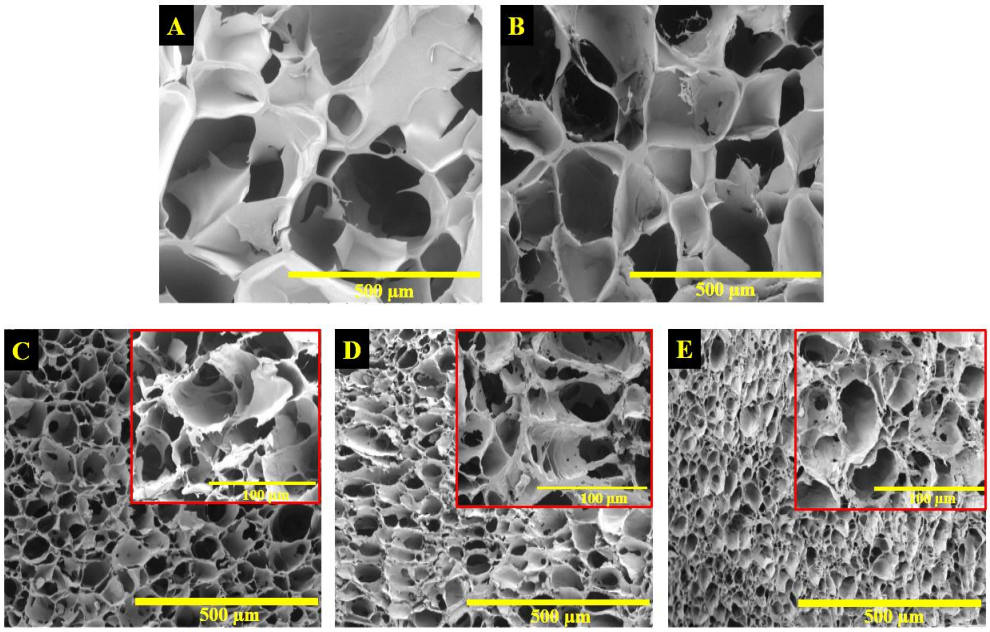

Figure 3.7 Surface morphology of gelatin/PVA hydrogels with different ratios at 200x magnification; (A) 100:0, (B) 70:30, (C) 50:50, (D) 30:70, and (E) 0:100. Insert indicates 1000x magnification

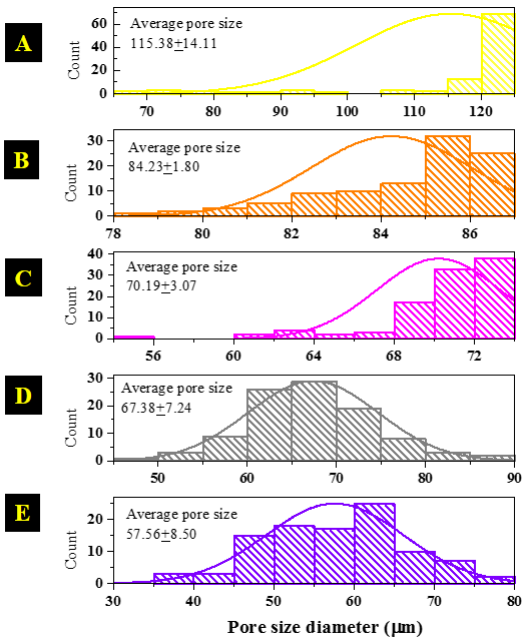

Figure 3.8 Pore size distribution of the gelatin/PVA hydrogels at different ratios; (A) 100:0, (B) 70:30, (C) 50:50, (D) 30:70, and (E) 0:100

3.4.7 Osteoblast proliferation on gelatin/PVA hydrogels

Cell proliferation of the gelatin/PVA hydrogels was evaluated to determine the biological performance. The hydrogel structure and properties such as morphology, surface functional groups, mechanical properties, stiffness, degradation, and molecular structures affect cell attachment and cell proliferation of the hydrogels (27).

The cell proliferation efficiency of the gelatin/PVA hydrogels was studied using PrestoBlue reagent and measured at day 1, 7, 14, and 21 in the absent of osteogenic differentiation. (Figure 3.9). The results showed that cell proliferation of the gelatin/PVA hydrogel increased from day 1 to day 7 and decreased at day 21. Pure gelatin hydrogels showed the highest cell proliferation at day 1. However, the pure gelatin hydrogels completely dissolved in the culture medium at day 5 which resulted in no cell proliferation following day 5. At day 7, the gelatin/PVA hydrogels at the ratio of 70:30 showed the highest cell proliferation. However, the hydrogels in this group also dissolved. In the other three groups, no significant difference on cell proliferation were observed.

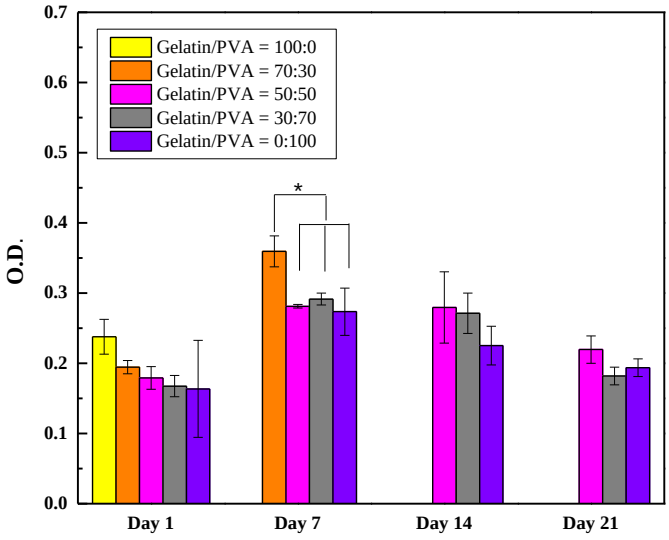

Figure 3.9 The cell proliferation with different ratio of the gelatin/PVA hydrogels at day 1, 7, 14 and 21 with ostegenically induced cells. The symbol (*) indicated significant changes (*$p < 0.05$)

3.4.8 Osteoblast attachment on gelatin/PVA hydrogels

Cell attachment on the hydrogels was observed at day 1 and day 14 after cell culturing (Figure 3.10). At day 1, most of the cells adhered, elongated, and aggregated along the walls of the pores. Some cells extended across the pores and connected to neighboring cells. Moreover, few cells penetrated into the pore of the hydrogels. At day 14, the cells spread and grew almost to confluence on the surface area. In the 0:100 gelatin/PVA hydrogel, it was nearly covered by cultured cells because of the smallest pore size.

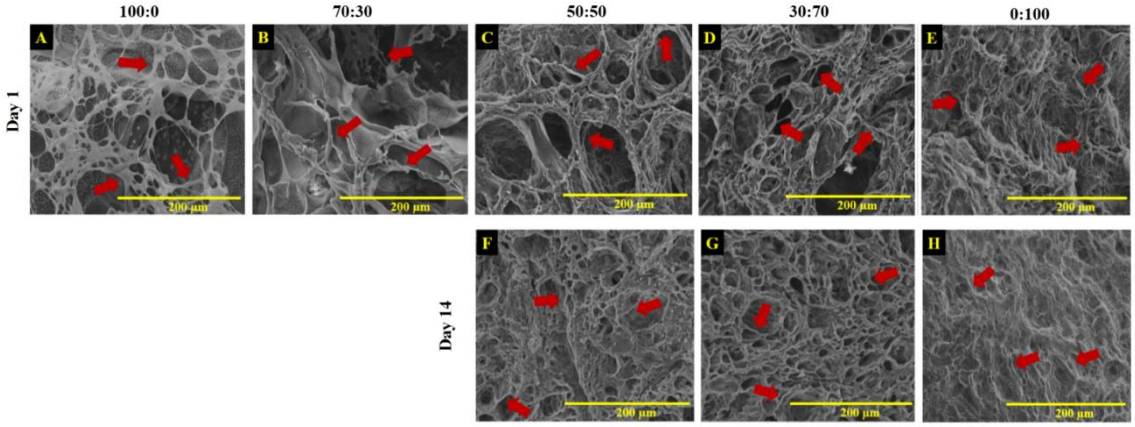

Figure 3.10 Cell adhesion and cell morphologies of the gelatin/PVA hydrogel at day 1 and day 14. Red arrows show examples of cell elongation

3.4.9 ALP activity from cultured osteoblasts on gelatin/PVA hydrogels

After culturing osteoblast on the gelatin/PVA hydrogels, ALP activity was measured. ALP activity initiates the mineralization process which was measured to evaluate the biological performance of bone formation. In this study, the ALP contents secreted from the MC3T3-E1 cells was determined on days 1, 7, 14 and day 21 in osteogenic differentiation medium (Figure 3.11). No significant difference in the ALP activity were observed between the samples at any time point measurement except at day 7.

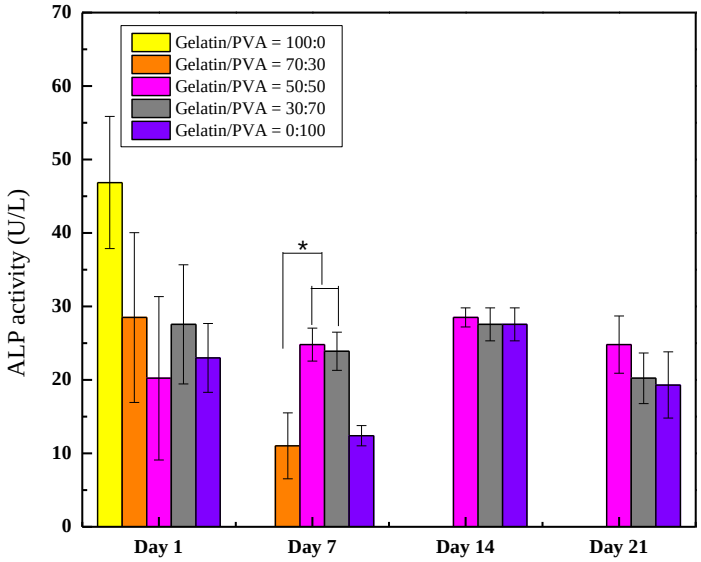

Figure 3.11 ALP activity at day 1, 7, 14, and 21 of the gelatin/PVA hydrogels: 100:0; 70:30; 50:50; 30:70; and 0:100. The symbol (*) presented significant changes (*$p < 0.05$).

3.4.10 Calcium deposition on cultured osteoblast hydrogels of gelatin/PVA

After day 14 and day 21 of cell culturing in osteogenic differentiation medium, the cell-seeded hydrogels were stained with alizarin red to indicate the mineralized nodules. The gelatin/PVA hydrogels without cells were used as control groups at all experiment times. The results showed that the quantity of calcium content increased at the cultured time point. The 50:50 and 30:70 gelatin/PVA hydrogels had greater densities of calcium deposition than the hydrogels without gelatin, i.e. 0:100 (Figure 3.12).

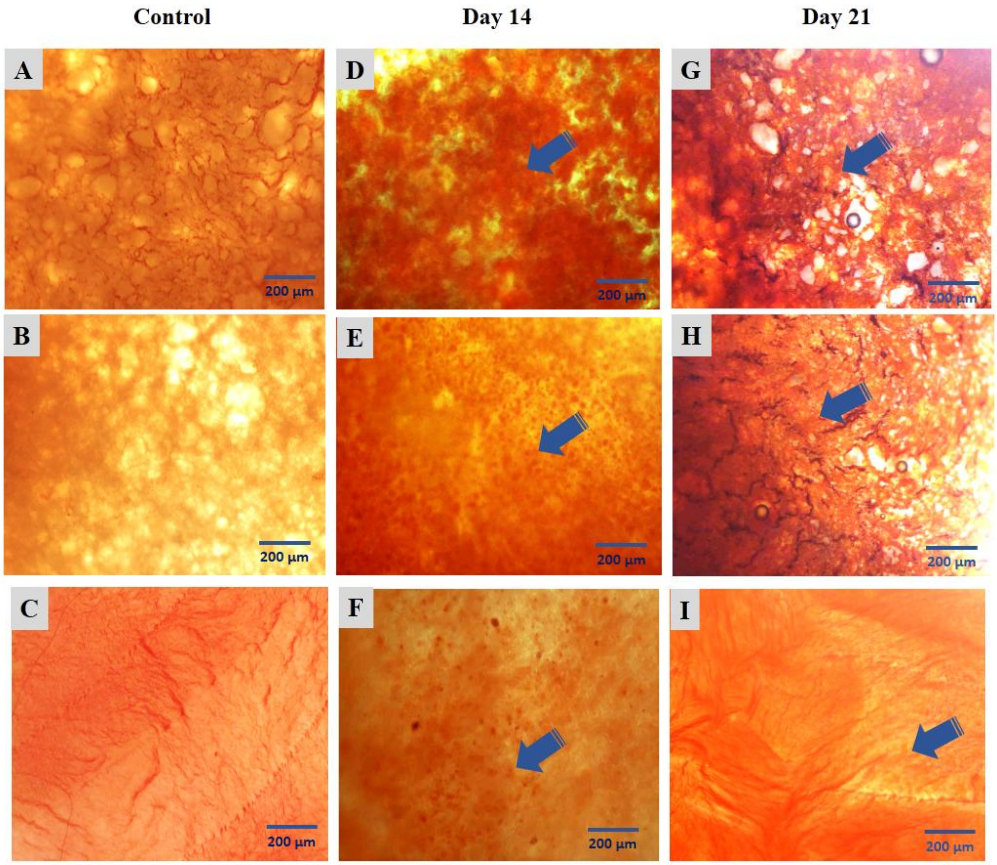

Figure 3.12 Alizarin red staining on the gelatin/PVA hydrogels at day14, and day 21, respectively. : (A, D, G) 50:50, (B, E, H) 30:70, and (C, F, I) 0:100. Blue arrows indicated the calcium nodules

3.4.11 Calcium contents on the cultured osteoblast hydrogels of gelatin/PVA

In order to determine the calcium accumulation synthesized by the osteoblasts, the supernatants were collected and the calcium content were measured. Figure 3.13 presents the calcium content of the hydrogels measured at day 1, 7, 14, and 21. No significant differences of calcium content were observed in any of the gelatin/PVA hydrogels at day 1 and day 7 in the cell lysates. Notably, the calcium contents of the 50:50 and 30:70 gelatin/PVA hydrogels increased while the 0:100 gelatin/PVA hydrogel had the lowest calcium content at day 21.

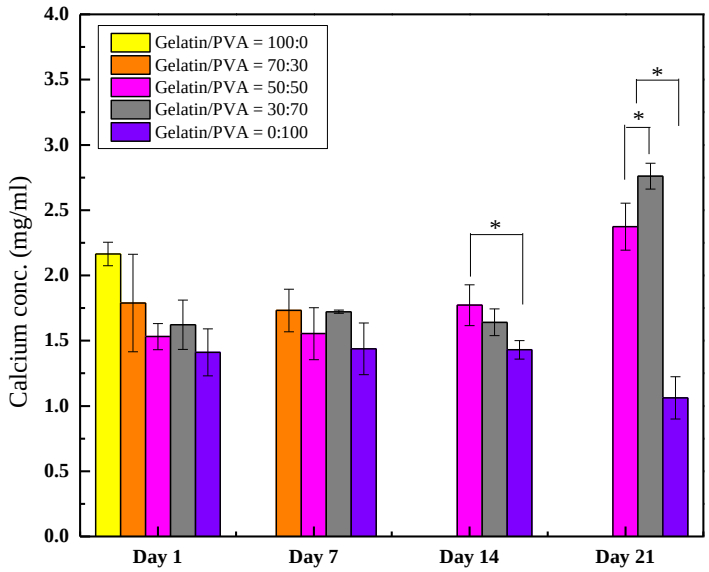

Figure 3.13 Calcium release of the gelatin/PVA hydrogel measured at day 1, 7, 14, and 21. The symbol (*) presented significant changes (*$p < 0.05$)

3.5 Discussions

3.5.1 Molecular and structural formation of mimicked hybrid hydrogels of gelatin/PVA

Gelatin/PVA hybrid hydrogels were fabricated using the chemical and physical crosslinking technique for cartilage tissue engineering that focused on the subchondral bone interface. Excellent mechanical and biological properties were observed from the successful crosslinks in the materials. Three types of chemical crosslinks in polymer chains using GA crosslinking agent in gelatin/PVA hydrogels were formed (Figure 3.14). First, a GA molecule reacts with an amino groups of lysine residues to form imine bonds in gelatin chains. Second, addition of GA to the gelatin/PVA solution caused the crosslinking between a lysine residue (-NH_2) of gelatin chains and a hydroxyl groups of PVA chains. The last reaction occurs when a GA molecule reacts with two hydroxyl groups of adjacent PVA chains, forming acetal bridge (28). The physical crosslinks to form polymer crystallites in the gelatin/PVA hydrogels were induced by cyclic freeze-thaw processing. Figure 3.15 shows the freeze-thaw mechanism of hydrogel formation. The freeze-thawed hydrogel are formed by dissolving the polymers in the solvent and freezing the solution. Ice crystals then formed in the freezing step. The size of the ice

crystals increase as the temperature decreases which results in the gelatin and PVA polymer chains coming into close contact with each other (12). As the ice-crystal melt during the thawing, the pores in the gel are formed (29). Repeating the freeze-thaws cycles can increase the crystalline domain which increases the physical crosslink density and leads to increased chain stiffness in the hydrogels (30). As a consequence of different ratios of gelatin/PVA contents, the degree of crosslinking controls the mechanical and biological properties.

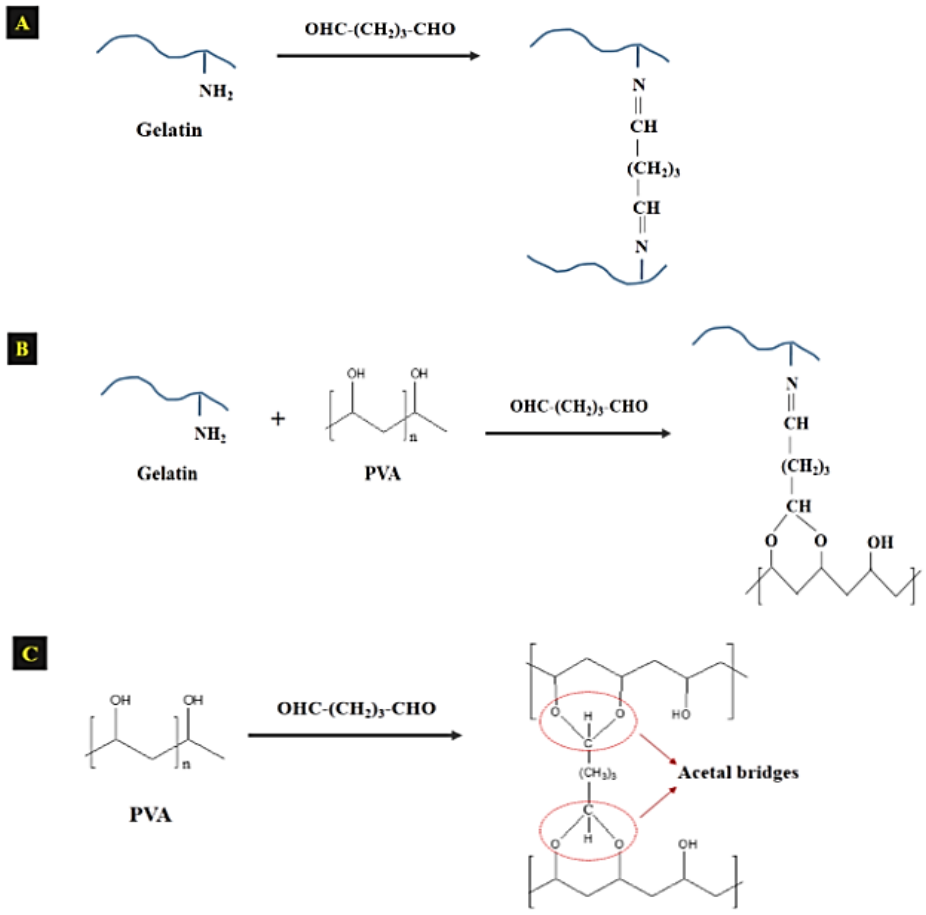

Figure 3.14 The chemical crosslink reactions of (A) gelatin, (B) gelatin/PVA, and (C) PVA with GA crosslinker in the gelatin/PVA hydrogels

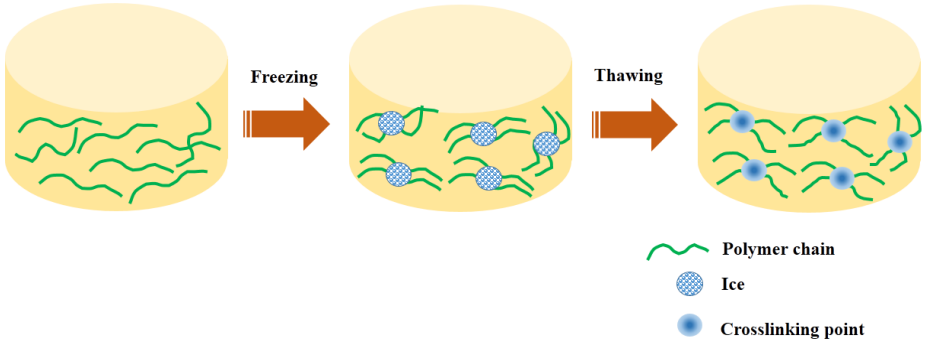

Figure 3.15 Freeze thawing mechanism of hydrogel formation

The mimicked hybrid hydrogel of gelatin/PVA were formed via chemical and physical crosslinking. This can be related to the hydrogel formation of cartilage tissue. The hydrophilic PVA, which shows the unique functionality of a hydrogel similar to hyaluronic acid (HA) in cartilage tissue, was selected to be the base matrix or continuous phase of our mimicked hybrid hydrogels. Gelatin, which has a molecular structure similar to collagen in cartilage, was chosen to be the non-continuous phase in the mimicked hybrid hydrogels. Importantly, chemical crosslinking is the process during formation of the ECM particularly in collagen fibril formation (31). Therefore, chemical crosslinking is the mimicked *in situ* formation of collagen fibril formation in the ECM. Physical crosslinking occurs in the glycosaminoglycan which is a component of the ECM in cartilage tissue (32). HA especially has showed unique physical crosslinking which leads to hydrogel formation (33). In this research, the physical crosslinking of PVA is the mimicked *in situ* hydrogel formation which is similar to HA in cartilage tissue. Our results demonstrated the chemical and physical crosslinking of the gelatin/PVA mimicked *in situ* collagen fibrillation and HA hydrogel formation in cartilage tissue.

3.5.2 Physical performance of mimicked hybrid hydrogels of gelatin/PVA

After mimicking, the physical performance of the hybrid hydrogels of gelatin/PVA were tested to determine the necessary ability to connect to subchondral bone. Some research studies proposed cartilage tissue scaffolds which have the ability

to induce tissue formation of subchondral bone on the surface (3,34–36). In this research, the swelling behavior, degradation, and mechanical properties of the mimicked hydrogels were selected for testing to determine the similars to natural cartilage tissue. In the main, the physical performance results of our research explained the relationship of molecular structure-morphology-physical performance. Some research studies demonstrated that the crosslinking affects the morphological formation and properties of hydrogels such as porous formation, swelling, degradation time, and mechanical properties (3,34–37). For instance, the swelling behavior in hydrogels is associated with permeability, fluid flow, and the compressive stiffness in articular cartilage applications. An increase in the water content reduces the load bearing capacity of articular cartilage (38). Our data presented that a high swelling ratio which was found in the higher gelatin concentrations of the gelatin/PVA hydrogels, i.e. 100:0 and 70:30. This result was due to the lower crosslink density in the gelatin hydrogels. The free amino groups, which uncrosslinked with aldehyde of GA, in the gelatin could interact with water which resulted in a high swelling ratio (39). The other cause relates to the addition of gelatin in the hydrogels which makes the hydrogel structures becoming looser. The macromolecular chains of gelatin can then extend easily compared to PVA polymer chains. The highly swollen hydrogels resulted from lower degree of crosslinking and the not so tight structure which resulted in faster penetration of fluid into the highly porous structure (40). This higher swelling leads to higher degradation and lower mechanical strength. The degradation and mechanical properties of gelatin/PVA hydrogels can be tuned to match the cartilage and subchondral bone regeneration. If the degradation rate is too rapid, it causes mechanical failure of the hydrogels and damages the reconstructed subchondral bone as the underlying support (41). Our results showed that higher gelatin content in the hydrogels had greater swelling and degradation and lower compressive strength. However, lower swelling behavior in the higher PVA content of the gelatin/PVA hydrogels, i.e. 50:50, 30:70, and 0:100, can maintain stable shapes for more than two months. However, for articular cartilage repair at the subchondral bone interface, the hydrogels should degrade slightly to allow cell and blood invasion after maintaining mechanical stability in the first two months (3). This is a point for further development of our hydrogels in the future.

It is known that the crosslinking density of polymer chains can improve the mechanical properties. Since articular cartilage is primarily loaded under compressive force, a guideline for the design of cartilage replacement material should consider the mechanical properties, such as compressive stress or Young' modulus, to be similar to the adjacent cartilage to distribute the load bearing at the joint (42). Our results showed that higher compressive stress and Young's modulus were obtained as the concentration of PVA increased. This results from the stronger and higher chemical and physical crosslinks in the PVA chains. The physical crosslinked hydrogels containing PVA come from the hydrogen bonded PVA crystallites in the network (43). In the compressive test, the hydrogels were compressed in one direction. The increased crosslinked polymer fraction supports the hydrogel network and thus gave more resistance to the compressive force (40). According to Watase *et al*.,(44) increased crystallinity due to the freeze-thaw cycles in PVA hydrogels caused an increased elastic modulus.

However, a greater stiffness or smaller pore size of hydrogels may limit nutrient flow and decrease the viscoelastic properties and the shock absorbance capacity in subchondral bone, leading to the breakdown of the overlying cartilage (15). Therefore, controlling the pore size and interconnected pore network are ways to improve tissue formation at the defects to be similar to the natural tissue.

3.5.3 Biological properties of mimicked hybrid hydrogels of gelatin/PVA

The biological properties are important to evaluate the potential to induce tissue formation of subchondral bone at the surface of mimicked hybrid hydrogels of gelatin/PVA. Principally, the hydrogels must provide cell adhesion and migration which influence cell proliferation (31). Our research focused on gelatin and PVA because of their molecular structures and functionalities, and the morphologies that affect the biological properties. In the view of molecular structure and functionality, good cell proliferation was obtained from hydrogels with a high amount of gelatin, i.e. 100:0 and 70:30, because of the RGD amino sequence. The interaction between the RGD amino sequence on the surface of the gelatin and cellular integrin receptors can regulate the intracellular signal pathway that resulted in the enhancement of cell binding

(45). At the early stage of testing, the contour forms of the hydrogels were stable. This also promotes cell adhesion which leads to inducing cell proliferation. The hydrogels that had lower contents of gelatin, i.e. 50:50, 30:70, and 0:100, had fewer biding sites to support cell attachment. The PVA hydrogel appeared to have a quite low cell density because it has no RGD amino sequences as a binding site for cell recognition (22,27). Some research studies (22,43,46) proposed that cells cultured on gelatin and PVA hydrogels were still viable which indicated that the gelatin, gelatin/PVA, and PVA hydrogels were non-toxic. Importantly, at the later stage of testing, the hydrogels with higher amount of PVA, i.e. 50:50, 30:70, and 0:100, had sufficient stability to maintain their contour shape. Therefore, they still showed cell proliferation. On the other hand, hydrogel with low amounts of PVA, i.e. 100:0 and 70:30, had insufficient stability to maintain the contour shape and for this reason they could not display cell proliferation. The results demonstrated that the mimicked hybrid hydrogel with a certain ratio of gelatin and PVA showed suitable molecular structure and functionality for cell attachment and proliferation.

In the view of morphological structure, the crosslink density also affects the interconnected pores and pore size in hydrogel. Smaller pore size were observed in the SEM images of the gelatin/PVA hydrogels with higher PVA content. It is possible that the gelatin molecules prevent the PVA chains from moving close to each other to form hydrogen bonds during the freeze-thaw cycles (42). The pore sizes of the gelatin/PVA hydrogels were in the range of 50-120 μm, which is suitable for cell attachment. Interestingly, pore interconnectivity allows for cell migration and attachment and the larger pore sizes could allow osteoblast migration from the subchondral bone to the articular cartilage (4). Some research studies have proposed that if the pore size is too large, the specific surface area decreases which resulted in the reduction of ligand density for cell binding (43).

ALP is an important component of hard tissue formation, including tissue formation in subchondral bone development. Generally, ALP enzyme is expressed in the early state during osteogenic activity. ALP can be used to identify the osteoblast differentiation. Interestingly, at day 7, the 50:50 and 30:70 gelatin/PVA hydrogels were higher in ALP activity than the others. For the other days, no differences in the ALP activity were observed any of the groups. This comes from two reasons. First, a

sufficient number of RGD binding groups in the gelatin of the hydrogel is the major cause to induce ALP activity expression (3,34). Second, stability of the hydrogel is the minor cause to induce ALP activity expression (47). Interestingly, after day 7 no significant differences were observed in the ALP activity between any of the groups. This resulted from the insufficient number of RGD biding groups and instability of the hydrogels.

Alizarin red staining and calcium assay were performed to investigate the calcium deposition and calcium content of the hydrogels. Alizarin red, which is an anthraquinone derivative, was used to detect the calcium compounds. The calcium cations react with alizarin red by covalent linkages to oxygen and hydroxyl groups. This mechanism causes the orange-red precipitate on the hydrogel (48). The hydrogel with gelatin showed better calcium deposition than without gelatin. A sufficient number of RGD binding groups and the stability were the causes to enhance calcium content in the hydrogels, particular in the 30:70 gelatin/PVA hydrogel.

According to the biological properties, the mimicked gelatin/PVA hydrogel at a ratio of 30:70 was the most suitable as a cartilage scaffold to induce subchondral bone formation at the interface area. This was due to the sufficient number of RGD binding groups and the stability that caused the induction of the biological functions of the mimicked hydrogel.

3.6 Conclusions

The hybrid hydrogels of gelatin/PVA were fabricated with the mimicking concept and were proposed as cartilage scaffolds of osteoarthritis surgery. The molecular organization, morphology, and performance of the hybrid hydrogels were characterized, observed, and tested for evaluation of the potential to induce tissue formation of subchondral bone at the surface. The results demonstrated that hydrogels produced by a combination of gelatin/PVA solutions were successfully prepared by the chemically and physically crosslinked interactions. The crosslinking network on hydrogels controls the swelling behavior, degradation rate, mechanical properties, and pore size as well as the biological properties of hydrogels. Although the mechanical properties of gelatin/PVA hydrogels are not sufficient to support the subchondral bone

interface, the excellent swelling behavior, degradation rate, pore size, and biological properties of these hydrogels, especially at a gelatin/PVA hydrogel ratio of 30:70, could be decent candidates since they could maintain the structure shape with proper swelling and degradation rate. Moreover, these hydrogels showed appropriate cell biocompatibility and cell adhesion. The osteogenic potential of gelatin/PVA hydrogel was confirmed by ALP activity, alizarin red, and calcium content assay. The outcomes of this work may be helpful to design the hydrogels in tissue engineering to induce subchondral bone formation for OA surgery.

3.7 Acknowledgments

This work was partially supported by Institute of Biomedical Engineering, Faculty of Medicine, Prince of Songkla University. A. Thangprasert would like to acknowledge the scholarship supported by the Development and Promotion of Science and Technology Talents Project (DPST).

3.8 References

1. Tat SK, Lajeunesse D, Pelletier J-P, Martel-Pelletier J. Targeting subchondral bone for treating osteoarthritis: what is the evidence? Best Pract Res Clin Rheumatol. 2010 Feb;24(1):51–70.
2. Seo S-J, Mahapatra C, Singh RK, Knowles JC, Kim H-W. Strategies for osteochondral repair: Focus on scaffolds. J Tissue Eng. 2014 Jan 1;5:2041731414541850.
3. Witte F, Reifenrath J, Müller PP, Crostack H-A, Nellesen J, Bach FW, et al. Cartilage repair on magnesium scaffolds used as a subchondral bone replacement. Mater Werkst. 2006 Jun 1;37(6):504–8.
4. Vega S, Kwon M, Burdick J. Recent advances in hydrogels for cartilage tissue engineering. Eur Cell Mater. 2017 Jan 30;33:59–75.
5. Choi SM, Singh D, Kumar A, Oh TH, Cho YW, Han SS. Porous Three-Dimensional PVA/Gelatin Sponge for Skin Tissue Engineering. Int J Polym Mater Polym Biomater. 2013 Mar 1;62(7):384–9.

6. Gu Z-Q, Xiao J-M, Zhang X-H. The development of artificial articular cartilage – PVA-hydrogel. Biomed Mater Eng. 1998 Jan 1;8(2):75–81.
7. Pal K, Banthia AK, Majumdar DK. Preparation and characterization of polyvinyl alcohol-gelatin hydrogel membranes for biomedical applications. AAPS PharmSciTech. 2007 Mar 1;8(1):E142–6.
8. Baker MI, Walsh SP, Schwartz Z, Boyan BD. A review of polyvinyl alcohol and its uses in cartilage and orthopedic applications. J Biomed Mater Res B Appl Biomater. 2012 Jul 1;100B(5):1451–7.
9. Bahrami B, Kordestani SS, Mirzadeh H, Mansoori P. Poly (vinyl alcohol)-Chitosan Blends : Preparation , Mechanical and Physical Properties. 2002 Dec 17; 12(2):139-146.
10. Kobayashi M, Hyu HS, Kobayashi M, Hyu HS. Development and Evaluation of Polyvinyl Alcohol-Hydrogels as an Artificial Atrticular Cartilage for Orthopedic Implants. Materials. 2010 Apr;3(4):2753–71.
11. Mahnama H, Dadbin S, Frounchi M, Rajabi S. Preparation of biodegradable gelatin/PVA porous scaffolds for skin regeneration. Artif Cells Nanomedicine Biotechnol. 2017 Jul 4;45(5):928–35.
12. Miao T, Miller EJ, McKenzie C, Oldinski RA. Physically crosslinked polyvinyl alcohol and gelatin interpenetrating polymer network theta-gels for cartilage regeneration. J Mater Chem B. 2015 Dec 2;3(48):9242–9.
13. Ponticiello MS, Schinagl RM, Kadiyala S, Barry FP. Gelatin-based resorbable sponge as a carrier matrix for human mesenchymal stem cells in cartilage regeneration therapy. J Biomed Mater Res. 2000 Nov 1;52(2):246–55.
14. Lien S-M, Ko L-Y, Huang T-J. Effect of pore size on ECM secretion and cell growth in gelatin scaffold for articular cartilage tissue engineering. Acta Biomater. 2009 Feb;5(2):670–9.
15. Castañeda SR, Román-Blas JA, Largo R, Herrero-Beaumont G. Subchondral bone as a key target for osteoarthritis treatment. Biochem Pharmacol. 2012 Feb 1;83(3):315-23.
16. Clark JM. The structure of vascular channels in the subchondral plate. J Anat. 1990 Aug;171:105–15.

17. Deng C, Zhu H, Li J, Feng C, Yao Q, Wang L, et al. Bioactive Scaffolds for Regeneration of Cartilage and Subchondral Bone Interface. Theranostics. 2018 Feb 15;8(7):1940–55.
18. Ma L, Gao C, Mao Z, Zhou J, Shen J, Hu X, et al. Collagen/chitosan porous scaffolds with improved biostability for skin tissue engineering. Biomaterials. 2003 Nov;24(26):4833–41.
19. Jing X, Mi H-Y, Salick MR, Cordie T, Crone WC, Peng X-F, et al. Morphology, mechanical properties, and shape memory effects of poly(lactic acid)/ thermoplastic polyurethane blend scaffolds prepared by thermally induced phase separation. J Cell Plast. 2014 Jul 1;50(4):361–79.
20. Behera BC, Yadav H, Singh SK, Sethi BK, Mishra RR, Kumari S, et al. Alkaline phosphatase activity of a phosphate solubilizing Alcaligenes faecalis, isolated from Mangrove soil. Biotechnol Res Innov. 2017;1(1):101–11.
21. Ponez L, Sentanin FC, Majid SR, Arof AK, Pawlicka A. Ion-Conducting Membranes Based on Gelatin and Containing LiI/I2 for Electrochromic Devices. Mol Cryst Liq Cryst. 2012 Mar 1;554(1):239–51.
22. Huang C-Y, Hu K-H, Wei Z-H. Comparison of cell behavior on pva/pva-gelatin electrospun nanofibers with random and aligned configuration. Sci Rep. 2016 Dec 5;6:37960.
23. Silva ARP da, Macedo TL, Coletta DJ, Feldman S, Pereira M de M. Synthesis, characterization and cytotoxicity of Chitosan/Polyvinyl Alcohol/Bioactive Glass hybrid scaffolds obtained by lyophilization. Matér Rio Jan. 2016 Dec;21(4):964–73.
24. Azami M, Rabiee M, Moztarzadeh F. Glutaraldehyde crosslinked gelatin/hydroxyapatite nanocomposite scaffold, engineered via compound techniques. Polym Compos. 2010 Dec 1;31(12):2112–20.
25. Nichol JW, Koshy ST, Bae H, Hwang CM, Yamanlar S, Khademhosseini A. Cell-laden microengineered gelatin methacrylate hydrogels. Biomaterials. 2010;31(21):5536–44.
26. Loh QL, Choong C. Three-dimensional scaffolds for tissue engineering applications: role of porosity and pore size. Tissue Eng Part B Rev. 2013 Dec;19(6):485–502.

27. Yang C, Wu X, Zhao Y, Xu L, Wei S. Nanofibrous scaffold prepared by electrospinning of poly(vinyl alcohol)/gelatin aqueous solutions. J Appl Polym Sci. 2011 Sep 5;121(5):3047–55.
28. Farris S, Song J, Huang Q. Alternative reaction mechanism for the cross-linking of gelatin with glutaraldehyde. J Agric Food Chem. 2010 Jan 27;58(2):998–1003.
29. Bajpai A, Saini R. Preparation and characterization of biocompatible spongy cryogels of poly(vinyl alcohol)–gelatin and study of water sorption behaviour. Polym Int. 2005 Sep 1;54(9):1233–42.
30. Hassan CM, Peppas NA. Cellular PVA hydrogels produced by freeze/thawing. J Appl Polym Sci. 2000 Jun 28;76(14):2075–9.
31. Chung HJ, Steplewski A, Chung KY, Uitto J, Fertala A. Collagen Fibril Formation. J Biol Chem. 2008 Sep 19;283(38):25879–86.
32. Roughley PJ, Lee ER. Cartilage proteoglycans: Structure and potential functions. Microsc Res Tech. 1994 Aug 1;28(5):385–97.
33. Bulpitt P, Aeschlimann D. New strategy for chemical modification of hyaluronic acid: Preparation of functionalized derivatives and their use in the formation of novel biocompatible hydrogels. J Biomed Mater Res. 1999;47(2):152–69.
34. Chen J, Chen H, Li P, Diao H, Zhu S, Dong L, et al. Simultaneous regeneration of articular cartilage and subchondral bone in vivo using MSCs induced by a spatially controlled gene delivery system in bilayered integrated scaffolds. Biomaterials. 2011;32(21):4793–805.
35. Panseri S, Russo A, Cunha C, Bondi A, Martino AD, Patella S, et al. Osteochondral tissue engineering approaches for articular cartilage and subchondral bone regeneration. Knee Surg Sports Traumatol Arthrosc. 2012 Jun 1;20(6):1182–91.
36. Liu M, Yu X, Huang F, Cen S, Zhong G, Xiang Z. Tissue Engineering Stratified Scaffolds for Articular Cartilage and Subchondral Bone Defects Repair. Orthopedics. 2013 Nov 1;36(11):868–73.
37. Hennink WE, Nostrum CF van. Novel crosslinking methods to design hydrogels. Adv Drug Deliv Rev. 2012;64:223–36.

38. Cohen NP, Foster RJ, Mow VC. Composition and dynamics of articular cartilage: structure, function, and maintaining healthy state. J Orthop Sports Phys Ther. 1998 Oct;28(4):203–15.
39. Matsuda S, Iwata H, Se N, Ikada Y. Bioadhesion of gelatin films crosslinked with glutaraldehyde. J Biomed Mater Res. 1999 Apr 1;45(1):20–7.
40. Liu Y, Vrana NE, Cahill PA, McGuinness GB. Physically crosslinked composite hydrogels of PVA with natural macromolecules: structure, mechanical properties, and endothelial cell compatibility. J Biomed Mater Res B Appl Biomater. 2009 Aug;90(2):492–502.
41. Schlichting K, Schell H, Kleemann RU, Schill A, Weiler A, Duda GN, et al. Influence of scaffold stiffness on subchondral bone and subsequent cartilage regeneration in an ovine model of osteochondral defect healing. Am J Sports Med. 2008 Dec;36(12):2379–91.
42. Beddoes CM, Whitehouse MR, Briscoe WH, Su B. Hydrogels as a Replacement Material for Damaged Articular Hyaline Cartilage. Mater Basel Switz. 2016 Jun 3;9(6).
43. Ino JM, Sju E, Ollivier V, Yim EKF, Letourneur D, Le Visage C. Evaluation of hemocompatibility and endothelialization of hybrid poly(vinyl alcohol) (PVA)/gelatin polymer films. J Biomed Mater Res B Appl Biomater. 2013 Nov 1;101(8):1549–59.
44. Watase M.; Nishinari K.; Nambu M. Anomalous increase of the elastic modulus of frozen poly vinyl alcohol gels. Cryo Letters. 1983;4(3):197-200
45. Sedaghati T, Seifalian AM. Nanotechnology and bio-functionalisation for peripheral nerve regeneration. Neural Regen Res. 2015 Aug;10(8):1191–4.
46. Liu Y, Vrana NE, Cahill PA, McGuinness GB. Physically crosslinked composite hydrogels of PVA with natural macromolecules: Structure, mechanical properties, and endothelial cell compatibility. J Biomed Mater Res B Appl Biomater. 2009 Aug 1;90B(2):492–502.
47. Yamamoto M, Takahashi Y, Tabata Y. Controlled release by biodegradable hydrogels enhances the ectopic bone formation of bone morphogenetic protein. Biomaterials. 2003;24(24):4375–83.

48. Paul H, Reginato AJ, Ralph Schumacher H. Alizarin red s staining as a screening test to detect calcium compounds in synovial fluid. Arthritis Rheum. 1983 Feb 1;26(2):191–200.

CHAPTER 4
SMART BASEMENT MEMBRANE EXTRACELLULAR MATRIX BASED ON THERMO-RESPONSIVE HYALURONIC-POLY (*N*-ISOPROPYLACRYLAMIDE) AS THE MODEL TO ENGINEER THE MORPHOLOGY OF TISSUES

Abstract

Morphological formation of tissue is important for regenerative medicine. In this research the smart basement membrane extracellular matrix (ECM) was created as the model to engineer the morphology of tissue. Poly (*N*-isopropylacrylamide) (PNIPAM) was grafted to hyaluronic acid (HA) via coupling reaction to form amide bond. Then, the molecular structure of grafted HA-PNIPAMs were characterized by ^{1}H-NMR, GPC, and FT-IR techniques. The structural formation was characterized with DSC. The physical behavior was observed by rheological properties. Osteoblast cells of MC3T3-E1 were cultured on the grafted HA-PNIPAM. Then, cell toxicity and proliferation on the HA grafted PINIPAM were evaluated. Afterward, cell detachment and cell viability after detachment was observed. The results showed that PNIPAM was partially grafted to HA. The rheological properties demonstrated that the grafted HA-PNIPAM showed the highest viscosity at around 30^{o}C. The grafted HA-PNIPAM showed non-toxicity, good cell proliferation into the sheet form. The cell sheet of the grafted HA-PNIPAM detached and arranged into the rolled form. Finally, the results demonstrated that the grafted HA-PINIPAM showed the suitable physical behavior, non-cell toxicity, cell proliferation, cell detachment, and cell viability after detachment which is promising for model to engineer the morphology of tissue.

4.1 Introduction

Morphological formation of tissue is the important stage for regenerative medicine (1–3). For some cases, the non-completed morphological formation has an effect on the irregular regeneration which lead to malfunction of tissue (1,2).Therefore, some researches are often emphasized to create the approach to regulate morphological formation of tissue (4). Those researches are mainly focused on morphological formation by activation with the biological signals; growth factors, cytokines, and extracellular matrix (ECM) (1–3,5). Especially, ECM has the performance of the biological signal which also shows the structural function to support cell behavior; cell adhesion, proliferation, and migration(6). Some literatures demonstrate that ECM self-organizes into different forms which act as the structure to regulate the different morphological formation of tissue (1,2). According to the unique performance of ECM, it was emphasized in this research.

Extracellular matrix (ECM) is the component in tissue (7). ECMs are mainly composed of protein and polysaccharide that self-organize into the complicated structure (7). Especially, basement membrane ECM showed the function to support the cell sheet formation (6). Some reports demonstrate the use of the basement membrane EMC as the natural scaffold, which is successful to regulate two dimensional (2D) morphological formation of tissue (8). Therefore, the basement membrane ECM was focused on this research.

Hyaluronic acid (HA) is an important component in ECM (9). Based on the distinguished physical property and bio-function, HA has been often used as based materials for biomedical applications (10). Interestingly, some research presented bio-function of HA to induce cell behaviors leading to different morphogenesis of tissue regeneration (1,2). This has been used to engineer tissue morphogenesis into different forms (1,2). Based the biological function, HA was chosen as based bio-functional materials in this research.

Poly (*N*-isopropylacrylamide) (PNIPAM) is the unique polymer, which has the thermo-responsive function. PNIPAM has been often used for grafting on substrate to engineer cell sheet membranes. At the transition temperature around 32^{o}C of human

body, the polymer chains intact to exhibit the hydrophobicity of PNIPAM at the grafted surface (11). This leads to the cell layer detaches from the grafted surface (12). Owing to the thermo-responsive function, PNIPAM was selected as based smart materials incorporated with HA in this research.

Generally, PNIPAMs incorporated with HA have been often used for biomedical application; regenerative medicine (11), drug delivery (13,14), and tissue engineering (15). There is rarely study on grafted HA-PNIPAMs, which act as the smart basement membrane ECM to engineer morphology of tissue. In this research, the grafted HA-PNIPAM was synthesized via coupling reaction to form amide bond, and characterized. Physical property and bio-function of the grafted HA-PNIPAM were tested. Then, performance of the grafted HA-PNIPAM as smart basement membrane ECM was evaluated for promising material to engineer morphology of tissue.

4.2 Materials and methods

4.2.1 Materials

A 95 % hyaluronic acid sodium salt (HA), 98% adipic dihydrazide (ADH), and 3-Mercaptopropionic acid (MPA) chain transfer were purchased from Acros Organics (Geel, Belgium), *N*-isopropylacrylamide (NIPAM) monomer with a molecular weight of 113.2 g and 1-ethyl-3-(3 dimethylaminopropyl) carbodiimide hydrochloride (EDC) were obtained from Tokyo Chemical Industry (TCI, Tokyo, Japan) (TCL), *N*-Hydroxysuccinimide (NHS) and Azobisisobutyronitrile (AIBN) initiator were purchased from Merck (Darmstadt, Germany), and *N,N'*-methylenebis(acrylamide) (MBA) crosslinking agent was obtained from Sigma-Aldrich (St. Louis, Missouri, US).

4.2.2 Synthesis of HA-NH_2

HA-NH_2 was synthesized following the previously reported procedure (16). HA-NH_2 was prepared by dissolving HA 0.5 g in 100 ml DI water to obtain HA solution at concentration of 5 mg/ml. Then, 10 g of ADH was added into HA solution. 0.8 g of EDC and 0.7g of NHS dissolved in DMSO/H_2O (5 ml:5ml) were then added into the reaction

mixture of HA and ADH solution. The pH of the mixture was adjusted to about 4-5 by adding 1 molar hydrochloric acid (HCl) solution. The reaction was stirred at room temperature overnight and dialyzed (molecular weight cut-off [MWCO] 3500) against with DI water to remove unreacted molecules. NaCl was added into reactant solution to produce 5% w/v solution and HA-NH_2 was precipitated in ethanol. The precipitated HA-NH_2 was dissolved again in DI water and dialyzed for 3 days to remove the salt. The HA-NH_2 product was lyophilized and kept at 4°C for further use.

4.2.3 Synthesis of PNIPAM-COOH

The carboxylic acid terminated PNIPAM was synthesized by free radical polymerization of NIPAM monomer. The synthesis of PNIPAM-COOH was slightly modified from procedures of R. Yu *et al,* and J.-P. Chen *et al* (17,18). 10g NIPAM was dissolved in 50 ml THF. 0.073 g AIBN, 0.62 ml MBA and 136.5 mg MPA were added into NIPAM solution with stirring under nitrogen atmosphere for 30 min. The reaction was carried out at 60°C overnight. After polymerization, the viscous solution was formed and then the solution was evaporated to remove THF. The PNIPAM-COOH was purified by washing with hot water and finally lyophilized to obtain dried PNIPAM-COOH polymer.

4.2.4 Synthesis of HA-PNIPAM copolymer

The HA-PNIPAM copolymer was synthesized by conjugating the amine groups of 0.1 g HA-NH_2 to the carboxylic groups of PNIPAM-COOH with different weights of PNIPAM-COOH. Before grafting HA-NH_2 with PNIPAM-COOH, PNIPAM-COOH (3 g and 5 g) was dissolved in DI water and incubated with EDC and NHS at 4°C for 48 h. EDC can form an intermediate of an amide linkage between HA-NH_2 and PNIPAM-COOH while NHS was used to increase the stability this amide intermediate. To graft PNIPAM-COOH to HA-NH_2, HA-NH_2 (0.1 g) was dissolved in DI water and added into

PNIPAM-COOH/EDC/NHS solution. The mixture was stirred overnight at room temperature, dialyzed for 3 days against DI water to remove unreacted PNIPAM-COOH, and then lyophilized to obtain the desired copolymer.

The synthetic routes of HA-NH_2, PNIPAM-COOH, and HA-PNIPAM copolymer were shown in Figure 4.1.

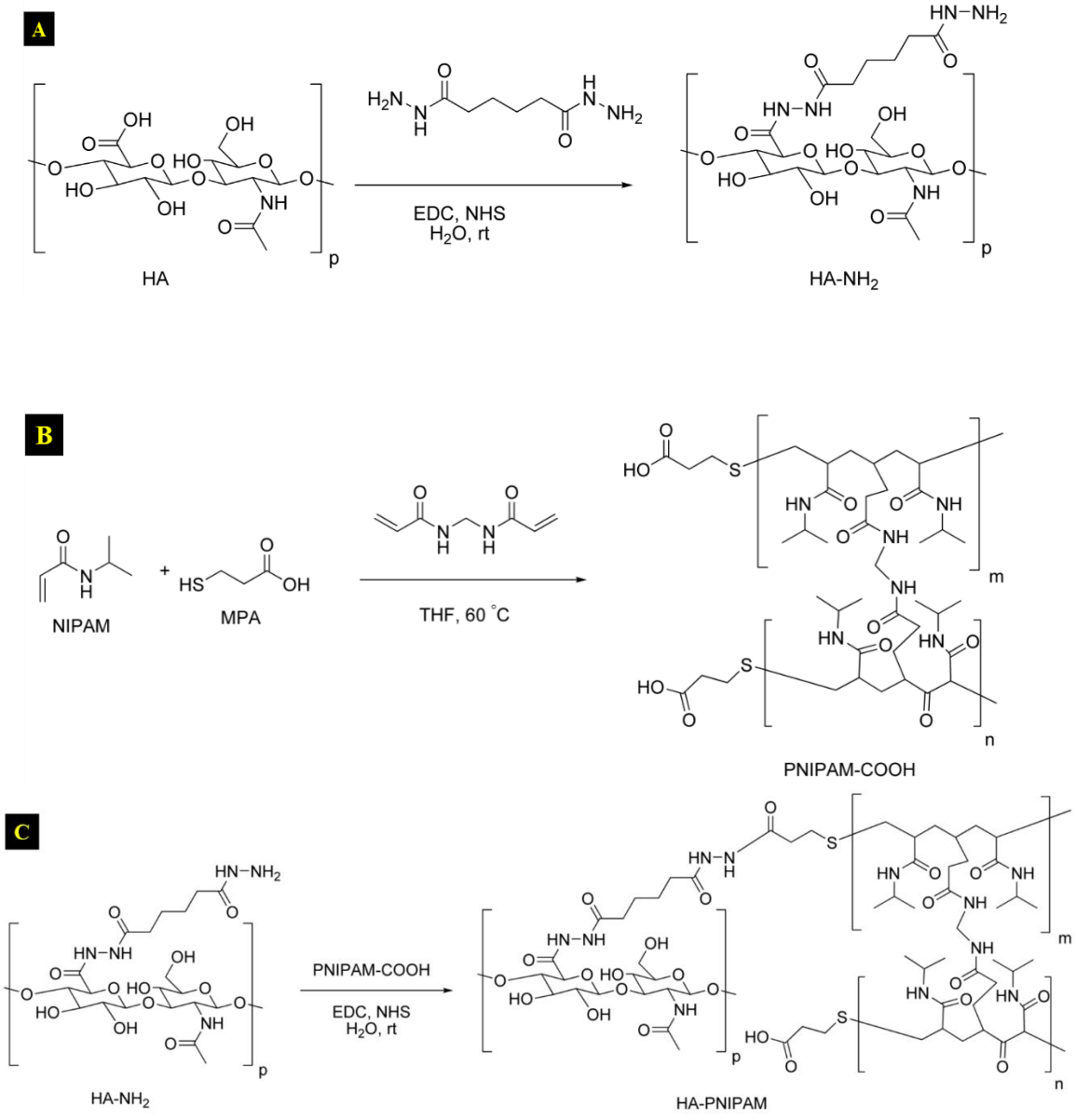

Figure 4.1 Synthetic route of (A) HA-NH_2, (B) PNIPAM-COOH, and (C) HA-PNIPAM grafted-copolymer

4.3 Characterizations

4.3.1 Proton nuclear magnetic resonance (^{1}H-NMR) characterization

The chemical structures of synthesized polymers were determined by ^{1}H-NMR spectrometer (Bruker Advance FT-NMR 300 MHz machine using tetramethylsilane (TMS) as internal standard). Deuterium oxide (D_2O) was used as a solvent for all samples.

4.3.2 Gel permeation chromatography (GPC) measurement

The weight average molecular weight (M_w), number average molecular weight (M_n), and polydispersity index (PDI=M_w/M_n) of HA-NH_2, PNIPAM-COOH, HA-PNIPAM-3, HA-PNIPAM-5 were measured using GPC technique. The sample polymers were prepared by dissolving in DI water for HA-NH_2, HA-PNIPAM-3, and HA-PNIPAM-5 and in THF for PNIPAM-COOH. The GPC measurement condition was as the following: column 7.8x300 mm, flow rate of 1 mL/min, temperature of the column set to 40 °C and injection quantity of test sample and standard was 20 µL.

4.3.3 Graft yield measurement

The %graft yield of HA-PNIPAM copolymers was calculated based on the weight change using the following equation (18).

$$\text{Graft yield (\%)} = \frac{(W_{\text{HA-PNIPAM}} - W_{\text{HA-NH2}})}{W_{\text{PNIPAM-COOH}}} \times 100$$

4.3.4 Fourier transform infrared spectroscopy (FT-IR)

FT-IR (EQUINOX 55, Bruker Optics, Germany) with the mode of Attenuated Total Reflectance (ATR) was used to study the chemical structure of the synthesized polymers of HA-NH_2, PNIPAM-COOH, HA-PNIPAM-3, and HA-PNIPAM-5. Dried samples were mixed with KBr powder, compressed as a pellet, and measured over the range of 4000-400 cm^{-1} wavenumbers.

4.3.5 Differential scanning calorimetry (DSC)

To determine LCST and thermal profiles of the synthesized polymers, 10% w/v polymer solutions of PNIPAM-COOH, HA-PNIPAM-3, and HA-PNIPAM-5 were dissolved in DI water and the DSC (DSC7, Perkin Elmer, USA) analysis of these polymers solution was performed by heating the temperature from 20 to 50^{o}C at a heating rate 2^{o}C/min under nitrogen flow.

4.3.6 Rheological properties

To study LCST and the rheological behavior of polymers at varied temperatures, the aqueous solution of PNIPAM-COOH, HA-PNIPAM-3, and HA-PNIPAM-5 were prepared at 10% w/v concentration. For each polymer, 0.3 ml of 10% w/v polymer solution was added between plate and the polymer viscosity was measured using Brookfield DV2T viscometer (Middleboro, USA) using plate-plate geometry. The viscosity data was recorded by increasing the temperature from 25 to 39^{o}C and water was used as a control.

4.3.7 Cell culture

Osteoblast cells of MC3T3-E1 were cultured in a 75 cm^3 flask with alpha Minimal essential medium-α-modification (α-MEM) medium (Gibco, Invitrogen, Carlsbad, CA, USA) and supplemented with 1% penicillin/streptomycin, 0.1% fungizone, and 10% fetal bovine serum (FBS). The MC3T3-E1 cell cultures were kept in a 37^{o}C incubator with 5% CO_2 and the medium was changed every 2-3 days.

4.3.8 Cell toxicity and cell proliferation

300 µl of HA-NH_2, PNIPAM-COOH, HA-PNIPAM-3, and HA-PNIPAM-5 polymers solutions were seeded on 24-well plate before cell cultivation. After UV sterilization for 3 h, 100 µl MC3T3-E1 cell suspension with $5x10^4$ cells density per well were carefully mixed with the synthesized polymers on well plates. Then, the polymers containing cells were incubated at 37^{o}C in a CO_2 incubator. The PNIPAM-COOH, HA-PNIPAM-3, and HA-PNIPAM-5 polymer solution turned into a white

sheet covered on the bottom of well plates. Then, one milliliter of the culture medium was added to each well plate and the cell culture was carried out at 37°C in a CO_2 incubator. To determine cell toxicity and cell proliferation, PrestoBlue reagent (PrestoBlue® cell viability regent, Invitrogen, USA) was prepared by mixing with the fresh medium at a ratio of 1:10, added into the polymer hydrogels, incubated at 37°c for 1 h, and transferred 200 µl solution into 96 well plate. Colorimetric measurement was studied at the wavelength of 570 nm using an ELISA plate reader. Cell proliferation in triplicates was measured with triplicates at day 1, 3, 5 and 10 after cell cultivation.

4.3.9 Cell detachment

After polymer sterilization under UV light, MC3T3-E1 with $5x10^4$ cell density were seeded onto with the synthesized polymer coated on the commercial culture sterilized dish (Nunclon™ Surface). Cells were cultured for 3 days and the dishes were incubated at room temperature until the cell sheet membrane started to detach from the culture dish.

4.3.10 Cell viability after detachment

Cell viability after detachment was transferred to the new sterilized dish. Then, cells were further cultured for 10 min, 3 day, and 5 day and cell viability was observed by microscope (Axio Observer 7 Carl Zeiss, Sweden) at room temperature. Tissue culture polystyrene (TPS) was used as control group.

4.3.11 Statistical analysis

All data were statically analyzed using one-way ANOVA, Turkey's HDS test (SPSS 20.0 software package). The data were presented as mean ± standard deviation was shown. P values less than 0.05 were considered to be significant.

4.4 Results

4.4.1 ^{1}H-NMR characterization

^{1}H-NMR spectra of HA-NH_2 and PNIPAM-COOH polymers were showed in Figure 4.2. For the ^{1}H-NMR spectrum of HA-NH_2, the multiplet signal between 3.2 and 3.7 ppm was assigned to the protons in the glycosides. Moreover, the chemical shift around 1.9 ppm indicated to the proton of *N*-acetyl groups in HA-NH_2.

^{1}H-NMR spectra of PNIPAM-COOH showed the chemical shift at 3.78 ppm, which was the methine proton (-CH-) of isopropyl group. The peak at 1.99 ppm was indicated to the methine proton (-CH-) on PNIPAM-COOH backbone. The multiplet signal between 2.5 and 2.7 ppm was assigned to the methylene protons (-CH_2-) next to the carbonyl group in the cross linker. The peak at around 1.47 to 1.57 ppm was the methylene protons (-CH_2-) located on polymer backbone, and peak at 1.03 ppm was the methyl protons (-CH_3-) in isopropyl groups (19).

PNIPAM-COOH characteristic peaks was not presented in ^{1}H-NMR spectra of HA-PNIPAM-3 and HA-PNIPAM-5 (data not shown) since the molecular weight of HA-NH_2 was much higher than PNIPAM-COOH. Therefore, GPC and FT-IR techniques will be used to get more information and to confirm the grafting reaction to synthesize HA-PNIPAM copolymers instead of ^{1}H-NMR technique.

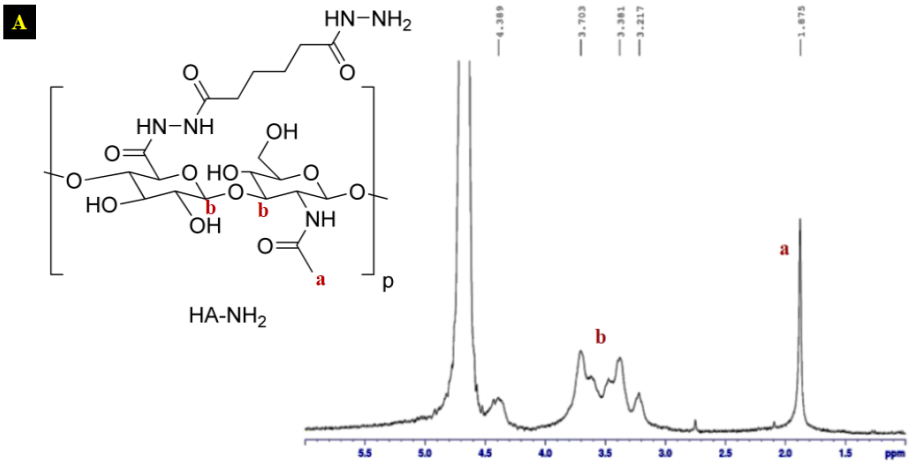

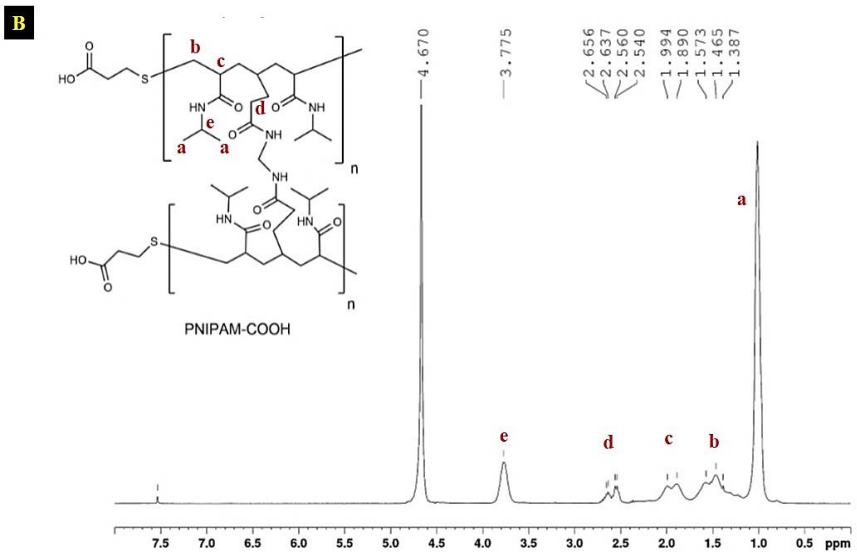

Figure 4.2 ^{1}H-NMR spectra of (A) HA-NH_2 and (B) PNIPAM-COOH

Grafting yield of HA-PNIPAM with different weight of PNIPAM-COOH content was calculated. The grafting yield of HA-PNIPAM copolymer increased with increasing the amount of PNIPAM-COOH to HA-NH_2. In addition, M_n, M_w and PDI were calculated using GPC technique. Table 4.1 showed the feed compositions, grafting yield, M_n, M_w, and PDI of synthesized polymers.

Table 4.1 Grafting yield, M_n, M_w, and PDI of synthesized polymers

Sample	Weight of HA-NH_2 (g)	Weight of PNIPAM-COOH (g)	Grafting yield (%)	M_n	M_w	PDI
HA-NH_2	-	-	-	24970	29419	1.18
PNIPAM-COOH	-	-	-	2746	3633	1.32
HA-PNIPAM-3	0.1	3	55.34 ± 1.51	96914	201755	2.08
HA-PNIPAM-5	0.1	5	60.12 ± 3.96	277428	1798083	6.48

4.4.2 FT-IR characterization

The FT-IR spectra of HA-NH_2, NIPAM, PNIPAM-COOH, HA-PNIPAM-3, and HA-PNIPAM-5 showed the characteristic peaks in Figure 4.3. The FT-IR spectra of NIPAM monomer displayed at 1654 cm^{-1} and 1617 cm^{-1} which related to the carbonyl group (C=O) bond stretching vibration and the C=C bond stretching vibration, respectively. The absorbance band at 1544 cm^{-1} was the secondary amide (N-H) bending and the amine N–H stretching was shown at 3500-3250 cm^{-1} (20). Characteristic peaks of PNIPAM-COOH appeared in the range 3200-3600 cm^{-1}, corresponding to N-H stretching vibration band. Moreover, the small shoulder at 1713 cm^{-1} indicated the carboxylic groups of MPA on the PNIPAM-COOH side chain. The C-H vibrations of isopropyl groups (-CH $(CH_3)_2$) PNIPAM repeating unit presented at 1387 and 1367 cm^{-1} and the disappearance of C=C peak in PNIPAM-COOH spectra indicated the successful polymerization of NIPAM monomer. Moreover, the amide I and amide II bands also represented the C=O stretching and N-H vibration bands at 1648 and 1547

cm^{-1}, respectively (21). The symmetric and asymmetric vibrations of methyl groups (-CH_3) of PNIPAM-COOH polymer were presented at 2974 and 2875 cm^{-1} and the vibration of C-H bond at 2934 cm^{-1} were also appeared (22). The FTIR spectra of PNIPAM-COOH indicated that this PNIPAM-COOH polymer was successfully synthesized by radical polymerization.

The FT-IR spectrum of HA conjugated with PNIPAM revealed a shift of the carbonyl stretching peak from 1611 cm^{-1} in HA-NH_2 to about 1650 cm^{-1} in HA-PNIPAM, and the shift of the bands at 1405 and 1376 cm^{-1} in HA-NH_2 to 1387 and 1368 cm^{-1} in HA-PNIPAM attributed to the amide bond formation between HA-NH_2 and PNIPAM-COOH (23). Similar results were reported by W. Wei *et al.* for PNIPAM/salecan hydrogel (21) and by R. Hernandez and C. Mijangos for alginate/PNIPAM semi-IPNs (24).

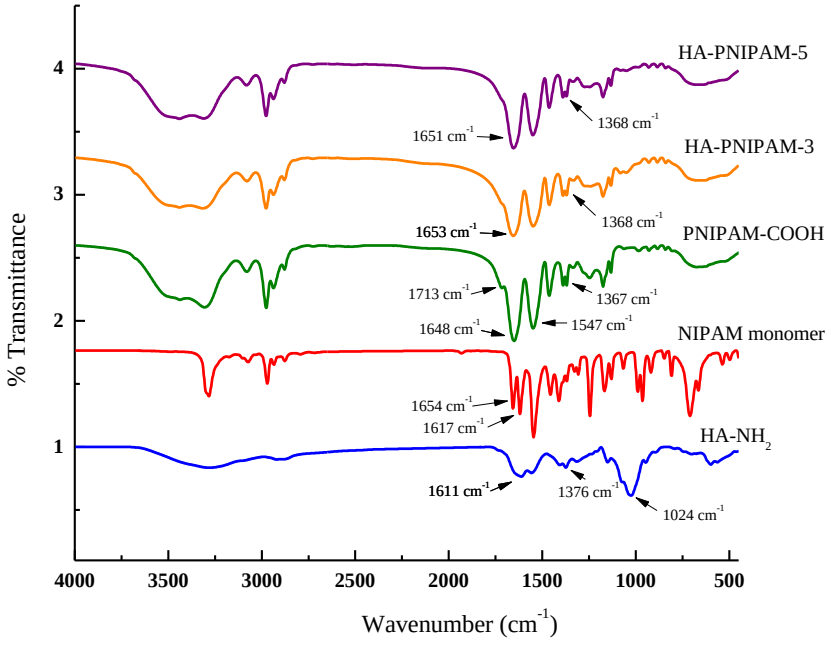

Figure 4.3 FT-IR spectra of HA-NH_2, NIPAM monomer, PNIPAM-COOH, HA-PNIPAM-3, and HA-PNIPAM-5

4.4.3 Thermo-responsive behavior of copolymer

Thermo-responsive behavior of PNIPAM, HA-PNIPAM-3, and HA-PNIPAM-5 polymers were studied since the solubility of these polymers depends on the temperature. Therefore, the thermal properties of these polymers as a function of temperature were studied. The LCST of polymers in this work was characterized by rheological behavior and DSC analysis. All synthesized polymers (10% w/v) were soluble in water at room temperature. For rheological behavior, the LCST determined by viscosity measurement with varying the temperature from 20 to 39°C was showed in Figure 4.4. The viscosity of synthesized PNIPAM-COOH solution increased rapidly at the temperature around 29.9°C. The phase transition of PNIPAM-COOH, HA-PNIPAM-3 and HA-PNIPAM-5 solution changed from a transparent solution to more turbid and formed an elastic gel when temperature increased to approximately 30°C.

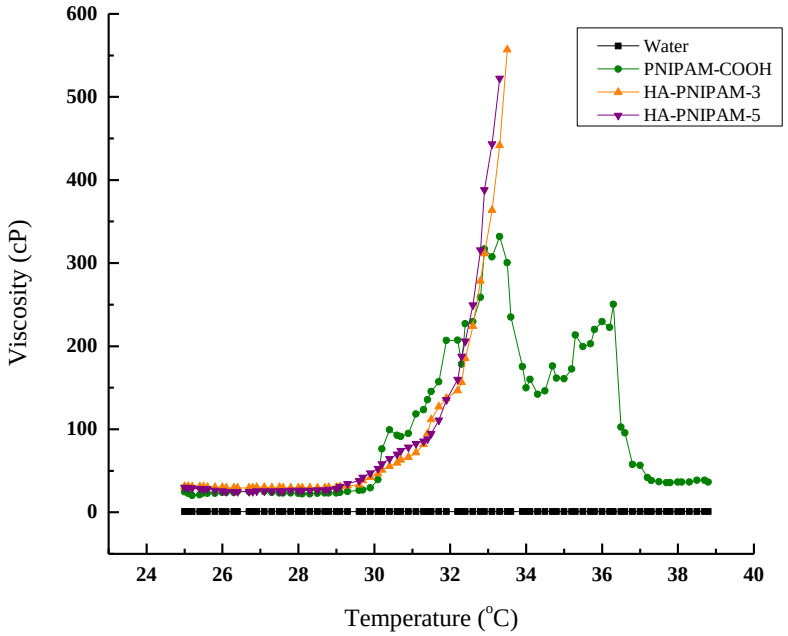

Figure 4.4 Viscosity behavior of the different synthesized polymers at concentration of 10% w/v

DSC is a technique to study sol-gel transition upon heating and cooling cycles. For the DSC results (Figure 4.5), the DSC thermograms showed a single endothermic peak for all of synthesized polymers. The onset temperature (T_t onset) was determined as a transition temperature (T_{trans} or LCST) of polymer. When coupling HA to the

PNIPAM polymer, the transition temperature was shifted to slightly higher temperature. All synthesized polymers showed the LCST at about 30 °C which is similar to the LCST determined from viscosity measurement. The LCST of HA-PNIPAM-5 obtained from viscosity and DSC measurement was higher than the LCST of HA-PNIPAM-3 due to the stronger hydrophobic interactions from increasing amount of PNIPAM (16). These LCST results were summarized in Table 4.2.

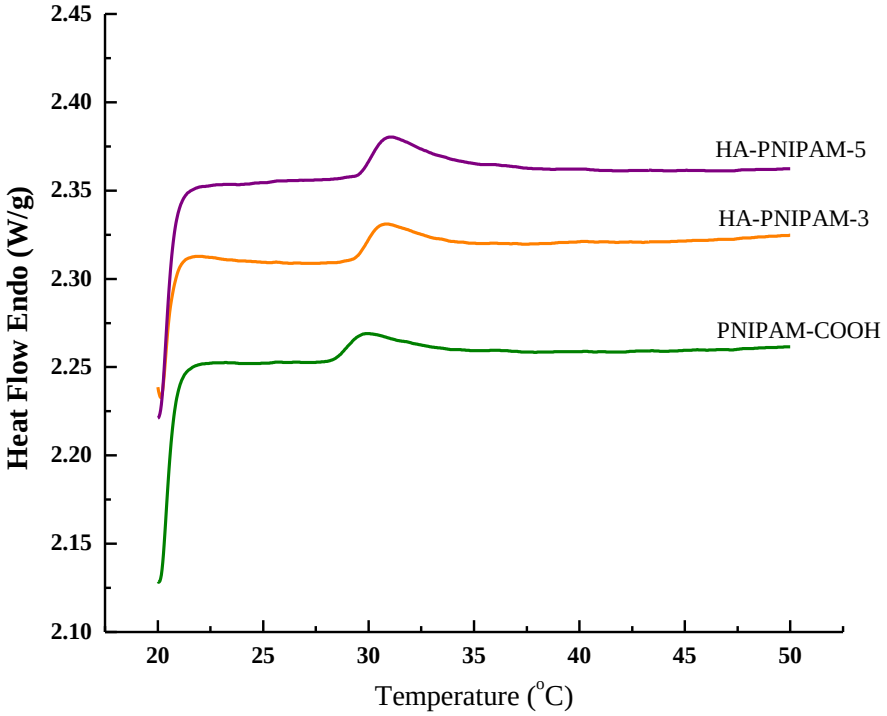

Figure 4.5 DSC thermograms of PNIPAM-COOH, HA-PNIPAM-3, and HA-PNIPAM-5 in solution state (10% w/v)

Table 4.2 The sol-gel transition temperature (°C) of synthesized polymers (10%w/v)

Method	PNIPAM-COOH	HA-PNIPAM-3	HA-PNIPAM-5
DSC	30.2	31.4	31.7
Viscosity	29.3	29.6	29.8

4.4.4 Cell toxicity and cell proliferation

Cell toxicity and cell proliferation of HA-NH_2, PNIPAM-COOH, HA-PNIPAM-3, and HA-PNIPAM-5 were evaluated at day 1, 3, 5, and 10 using PrestoBlue reagent (Figure 4.6). Cell proliferation of HA-PNIPAM-3 and HA-PNIPAM-5 was increased from day 1 to day 10. HA-NH_2 polymer was measured only day 1 and day 3 due to its dissolution into medium which resulted in no cell proliferation on another day. Cells cultured on PNIPAM-COOH polymer were not well to proliferate compared to HA-PNIPAM-3 and HA-PNIPAM-5 copolymer.

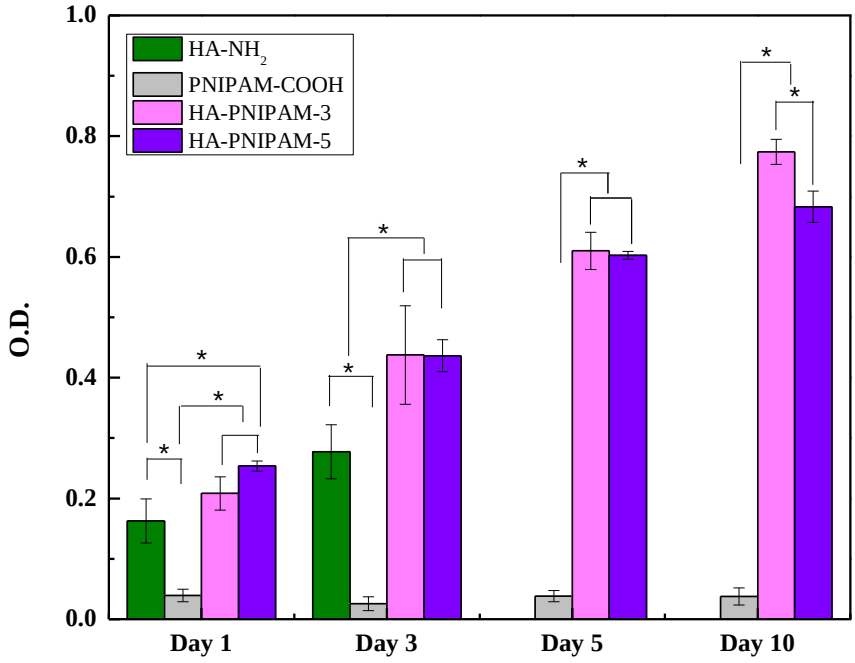

Figure 4.6 Cell toxicity and cell proliferation of synthesized polymer. The symbol (*) presented significant changes (*$p < 0.05$)

4.4.5 Cell detachment

Cells detachment cultured on synthesized polymers was observed at room temperature. Cell sheet membrane containing PNIPAM-COOH polymer start to detach from the TPS substrate after 10 min incubation (Figure 4.7). On the other hand, cells cultured on HA-NH_2 polymer did not appear a cell sheet membrane. This results indicated that the cell sheet membrane come from the ability of PNIPAM-COOH

polymer. Moreover, cells-cultured polymers containing PNIPAM can reverse and form as a cell sheet membrane again after incubation at 37°C.

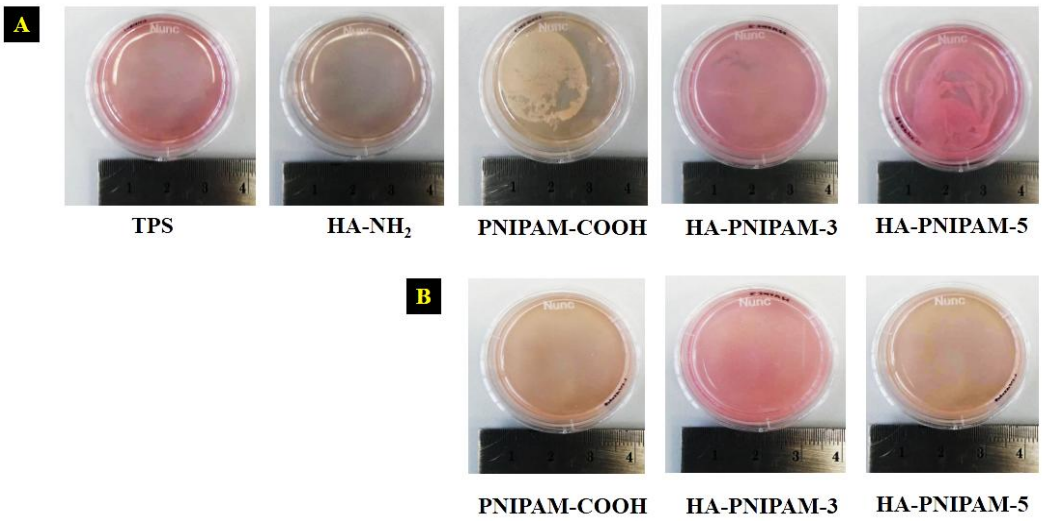

Figure 4.7 (A) Cell sheet with PNIPAM hydrogel detached from the TPS surface after incubating at room temperature (B) Revised attachment of cell sheet with PNIPAM hydrogel on the TPS surface after incubation at 37°C

4.4.6 Cell viability after detachment

Cell sheet membranes of PNIPAM-COOH, HA-PNIPAM-3, and HA-PNIPAM-5 were further cultured after cell detachment from TPS substrate for 10 min, 3 day, and 5 day (Figure 4.8). Cells viability was observed at room temperature. The result showed that cells can live, growth, and proliferate in the time cultured periods. At day 5, the amount of cells was higher compared to other days. The higher cells number were observed in HA-PNIPAM-3 and HA-PNIPAM-5 which was similar to cell toxicity and cell proliferation result measured by PrestoBlue reagent. Moreover, there was only a few numbers of cells left on the plate after transferring to new plate. According to this result, it was a proof of cell attachment on the synthesized polymer before TPS plate.

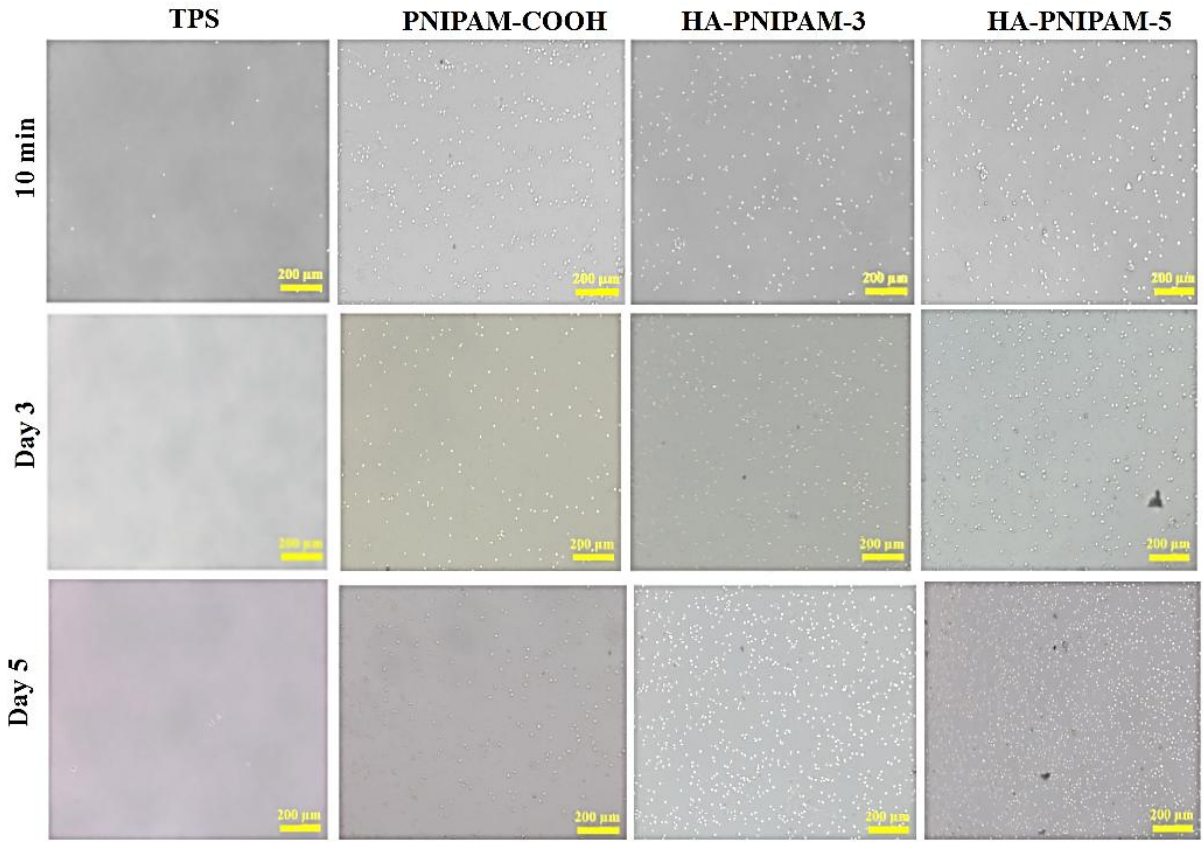

Figure 4.8 Cell culturing at 10 min, day 3, and day 5 in PNIPAM-COOH, HA-PNIPAM-3, and HA-PNIPAM-5

4.5 Discussions

4.5.1 Molecular formation and structural organization of smart basement membrane ECM

Smart basement membrane ECM based on thermo-responsive HA-PINIPAM copolymer was synthesized by grafting PNIPAM-COOH on HA-NH_2 chain through amide bond formation. The higher PNIPAM-COOH content in HA-PNIPAM-5, the more amount of PNIPAM-COOH grafted to HA-NH_2 chain. From this result, the molecular weight of HA-PNIPAM copolymer can be controlled by varying the amount of PNIPAM-COOH polymer during grafting process. Similar results have also reported

by J.P. Chen and T.H.Cheng who prepared PNIPAM-gelatin hydrogels with different PNIPAM graft chain densities (25).

4.5.2 Physical behaviors of smart basement membrane ECM

The LCST was used to define the rheological properties of polymer hydrogel into two parts. First, below LCST, the polymer solution maintain the chain mobility which resulted in no change in viscosity. At the temperature above LCST, the viscosity of polymer dramatically rise and polymer solution turns into a rigid gel, which come from the action of PNIPAM-COOH chain (18). In this study, the LCST of PNIPAM-COOH polymer solution increased slightly with the coupling of HA-NH_2 in the copolymer chain. This possibly is the more hydrophilic effect. The hydrophilic HA-NH_2 backbone prevented the dehydration of PNIAPM-COOH chain (16). Since the LCST was depended on the water interaction with the polymer and hydrophilic/hydrophobic moieties within polymer molecules(26), the increasing of temperature was required to break hydrogen bond between polymer and solvent. This causes the increasing of LCST in HA-PNIPAM copolymer. The result was also demonstrates that the LCST of HA-PNIPAM-5 was slightly higher than that in HA-PNIPAM-3. It was indicated that the stronger hydrophobic interaction between polymer chains in HA-PNIPAM-5 and the complicated chain entanglement of copolymer (18). However, the LCST of PNIPAM-COOH, HA-PNIPAM-3, and HA-PNIPAM-5 were still lower than the physiological temperature, indicating the possibility for cell sheet membrane. This demonstrates that our smart basement membrane ECM is suitable as the substrate to engineer the cell sheet morphogenesis in similar environment to human body.

4.5.3 Bio-functionality of smart basement membrane ECM

After cell culturing with the smart basement membrane ECM, its bio-functionality is tested. The results demonstrated that the incorporating HA-NH_2 in PNIPAM-COOH can improve the biocompatibility of polymers. This is due to the increasing hydrophilicity of HA-NH_2 in copolymer. Such hydrophilic copolymer allows an array of protein conformations to reside and interact with a variety of

hydrophilicity. This result was similar to C.H.Chen *et al*., who prepared HA-chitosan-PNIPAM injectable hydrogels for prevention of postoperative peritoneal adhesion (27). They proposed that HA and chitosan can improve biocompatibility of PNIPAM hydrogel. V. Laukkanen *et al.,* also reported that the increasing of biocompatibility of polymers corresponds to the increasing of hydrophilicity or positive charges (28). Our research demonstrated that the basement membrane ECM showed suitable bio-functionality to induce the cell behavior leading to the enhancement of tissue formation. This showed that our basement membrane ECM had the suitable bio-functionality for engineering of tissue with the different morphology.

4.5.4 Smart basement membrane ECM to engineer the morphology of tissue

To evaluate the performance of smart basement membrane ECM to engineer the morphology of tissue, cell sheet was heated to 37 ^{o}C. Then, morphology of cell sheet was observed. The morphological formation of cell sheet on smart basement membrane was shown in figure 4.9. For the first stage, the thermo-responsive behavior of HA-PNIPAM cell sheet for detachment and adhesion was presented. When the temperature was reduced to room temperature, the solution was presented due to the intermolecular interaction between polar groups of HA-PNIPAM and water molecules. This interaction between polymer and water caused hydration of the HA-PNIPAM chain to form expanded structure. This hydrophilic surface of polymer caused the cells detachment. This was due to the more difficult adsorption of the extracellular matrix, protein, or other specific agents on hydrophilic polymer surface. Therefore, cell adhesion was impeded (29). When the temperature was increased to LCST, hydrogen bonds were broken and the hydrophobic interaction between HA-PNIPAM took place (30). Then, the copolymer chains collapsed and precipitated out of the aqueous solution. Transparent solution at temperature lower than LCST became cloudy, opalescent and achieved to the white sheet membrane when temperature was higher than LCST. This hydrophobic structure of HA-PNIPAM caused the cells adhesion.

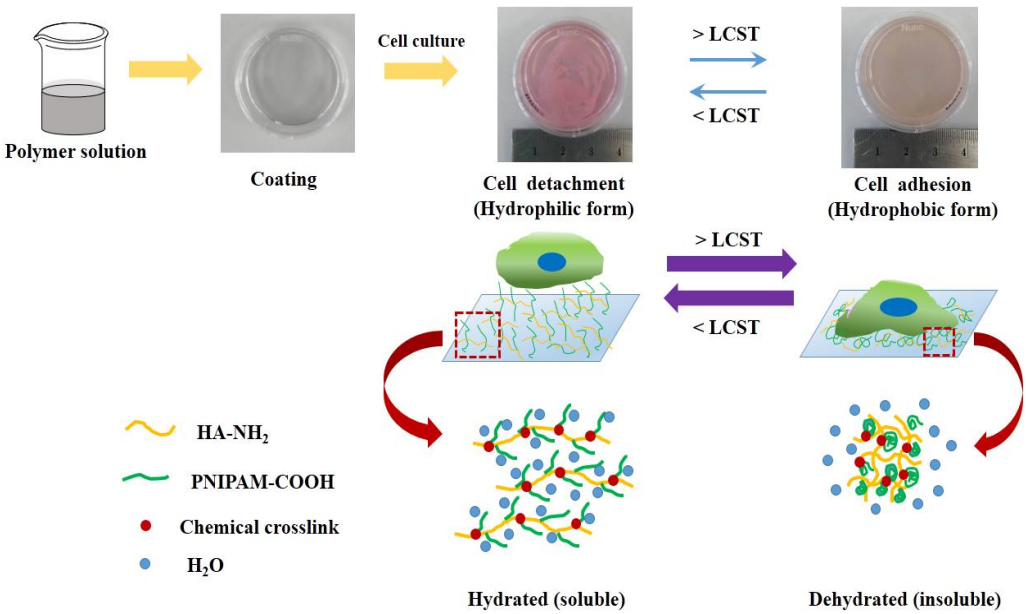

Figure 4.9 Thermo-responsive behavior of HA-PNIPAM copolymer for cell sheet membrane

Some researches demonstrate the suitable scaffolds which are used to engineer the complicate morphology of tissue (31). Interestingly, our ECM can be used as the alternative model to design the complicate morphology of tissues for instance; muscle, blood vessel, trachea, *etc*. The suggested model is to use the positive mold for adhesion of our ECM which acts as the substrate for cell attachment (Figure 4.10). Then, the suitable approach was used to culture attached cells leading to morphology of hollow sheet with a certain size. Afterward, the formed hollow sheet was detached from the mold by decreasing of temperature. Notably, the suitable approach for culturing is often used by bioreactors, which mimic the similar environment to natural tissue formation (1–3,5). Furthermore, to mimic signals which are grafted to the PINIPAM is the second development to create biological function similar to the complicated tissues.

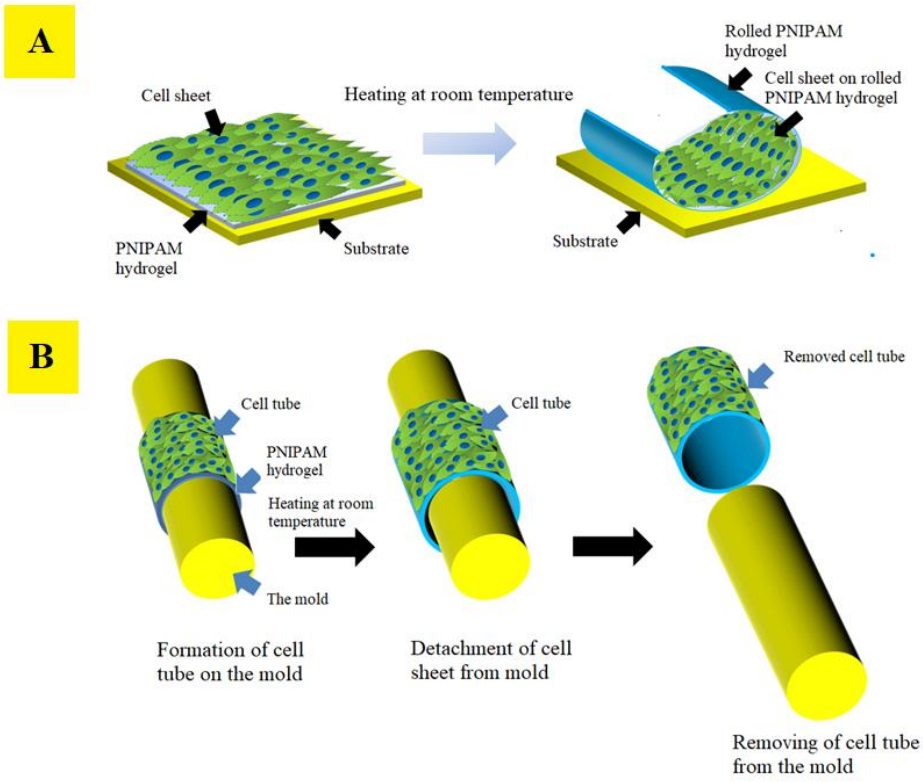

Figure 4.10 The proposed model of engineered complicate tissue based on the smart basement membrane ECM (A) Morphological formation of two dimensional (2D) tissue (B) Morphological formation of three dimensional (3D) tissue

4.6 Conclusions

In this research, the thermo-sensitive grafted HA-PNIPAM copolymer was synthesized for using as the smart basement membrane ECM to engineer morphology of tissue. The molecular structure of copolymer was characterized before physical behaviors and biological properties were tested. The results demonstrated that the copolymer showed the structure of HA-NH_2 partially grafted with PNIPAM-COOH. The physical behaviors showed that the copolymer self-organized into hydrogel at 37 ^{o}C. The copolymer was coated on the substrate for cell culturing. Cell viability on copolymer coated substrate showed good adhesion. Cells sheet was detached at room temperature. Then, the cell sheet arranged itself into rolled form. This research demonstrated that the thermo-sensitive grafted HA-PNIPAM copolymer showed the

unique performance which can serve as pioneer model to engineer morphology of tissue.

4.7 Acknowledgements

This work was partially supported by Institute of Biomedical Engineering, Faculty of Medicine, Prince of Songkla University. A. Thangprasert would like to acknowledge the scholarship supported by the Development and Promotion of Science and Technology Talents Project (DPST).

4.8 References

1. Kusuhara H, Isogai N, Enjo M, Otani H, Ikada Y, Jacquet R, et al. Tissue engineering a model for the human ear: Assessment of size, shape, morphology, and gene expression following seeding of different chondrocytes. Wound Repair Regen. 2009;17(1):136–46.
2. Zhang X, Reagan MR, Kaplan DL. Electrospun silk biomaterial scaffolds for regenerative medicine. Adv Drug Deliv Rev. 2009 Oct 5;61(12):988–1006.
3. Kim HN, Jiao A, Hwang NS, Kim MS, Kang DH, Kim D-H, et al. Nanotopography-guided tissue engineering and regenerative medicine. Adv Drug Deliv Rev. 2013 Apr 1;65(4):536–58.
4. Aubin JE. Regulation of Osteoblast Formation and Function. Rev Endocr Metab Disord. 2001 Jan 1;2(1):81–94.
5. Senoo H, Hata R. Extracellular matrix regulates cell morphology, proliferation, and tissue formation. Kaibogaku Zasshi. 1994 Dec;69(6):719–33.
6. Canavan HE, Cheng X, Graham DJ, Ratner BD, Castner DG. Cell sheet detachment affects the extracellular matrix: A surface science study comparing thermal liftoff, enzymatic, and mechanical methods. J Biomed Mater Res A. 2005;75A(1):1–13.
7. Badylak SF. The extracellular matrix as a scaffold for tissue reconstruction. Semin Cell Dev Biol. 2002 Oct 1;13(5):377–83.
8. Li Y, Kilian KA. Bridging the Gap: From 2D Cell Culture to 3D Microengineered Extracellular Matrices. Adv Healthc Mater. 2015;4(18):2780–96.

9. Collins MN, Birkinshaw C. Hyaluronic acid based scaffolds for tissue engineering—A review. Carbohydr Polym. 2013 Feb 15;92(2):1262–79.
10. Burdick JA, Prestwich GD. Hyaluronic Acid Hydrogels for Biomedical Applications. Adv Mater. 2011;23(12):H41–56.
11. Elloumi-Hannachi I, Yamato M, Okano T. Cell sheet engineering: a unique nanotechnology for scaffold-free tissue reconstruction with clinical applications in regenerative medicine. J Intern Med. 2010;267(1):54–70.
12. Nash ME, Healy D, Carroll WM, Elvira C, Rochev YA. Cell and cell sheet recovery from pNIPAm coatings; motivation and history to present day approaches. J Mater Chem. 2012 Aug 28;22(37):19376–89.
13. Yadavalli T, Ramasamy S, Chandrasekaran G, Michael I, Therese HA, Chennakesavulu R. Dual responsive PNIPAM–chitosan targeted magnetic nanopolymers for targeted drug delivery. J Magn Magn Mater. 2015 Apr 15;380:315–20.
14. Ashraf S, Park H-K, Park H, Lee S-H. Snapshot of phase transition in thermoresponsive hydrogel PNIPAM: Role in drug delivery and tissue engineering. Macromol Res. 2016 Apr 1;24(4):297–304.
15. Ohya S, Nakayama Y, Matsuda T. Thermoresponsive Artificial Extracellular Matrix for Tissue Engineering: Hyaluronic Acid Bioconjugated with Poly(N-isopropylacrylamide) Grafts. Biomacromolecules. 2001 Sep 1;2(3):856–63.
16. Tan H, Ramirez CM, Miljkovic N, Li H, Rubin JP, Marra KG. Thermosensitive injectable hyaluronic acid hydrogel for adipose tissue engineering. Biomaterials. 2009 Dec 1;30(36):6844–53.
17. Yu R, Zheng S. Poly(acrylic acid)-grafted Poly(N-isopropyl acrylamide) Networks: Preparation, Characterization and Hydrogel Behavior. J Biomater Sci Polym Ed. 2011 Jan 1;22(17):2305–24.
18. Chen J-P, Cheng T-H. Thermo-Responsive Chitosan-graft-poly(N-isopropylacrylamide) Injectable Hydrogel for Cultivation of Chondrocytes and Meniscus Cells. Macromol Biosci. 2006;6(12):1026–39.

19. Coronado R, Pekerar S, Lorenzo AT, Sabino MA. Characterization of thermo-sensitive hydrogels based on poly(N-isopropylacrylamide)/hyaluronic acid. Polym Bull. 2011 Jun 1;67(1):101–24.
20. Maheswari B, Babu PEJ, Agarwal M. Role of N-vinyl-2-pyrrolidinone on the thermoresponsive behavior of PNIPAm hydrogel and its release kinetics using dye and vitamin-B12 as model drug. J Biomater Sci Polym Ed. 2014 Feb 11;25(3):269–86.
21. Wei W, Hu X, Qi X, Yu H, Liu Y, Li J, et al. A novel thermo-responsive hydrogel based on salecan and poly(N-isopropylacrylamide): Synthesis and characterization. Colloids Surf B Biointerfaces. 2015 Jan 1;125:1–11.
22. Wu Y, Yao J, Zhou J, Dahmani FZ. Enhanced and sustained topical ocular delivery of cyclosporine A in thermosensitive hyaluronic acid-based in situ forming microgels. Int J Nanomedicine. 2013;8:3587–601.
23. D'Este M, Alini M, Eglin D. Single step synthesis and characterization of thermoresponsive hyaluronan hydrogels. Carbohydr Polym. 2012 Oct 15;90(3):1378–85.
24. Hernández R, Mijangos C. In situ Synthesis of Magnetic Iron Oxide Nanoparticles in Thermally Responsive Alginate-Poly(N-isopropylacrylamide) Semi-Interpenetrating Polymer Networks. Macromol Rapid Commun. 2009;30(3):176–81.
25. Ohya S, Kidoaki S, Matsuda T. Poly(N-isopropylacrylamide) (PNIPAM)-grafted gelatin hydrogel surfaces: interrelationship between microscopic structure and mechanical property of surface regions and cell adhesiveness. Biomaterials. 2005 Jun 1;26(16):3105–11.
26. Gandhi A, Paul A, Sen SO, Sen KK. Studies on thermoresponsive polymers: Phase behaviour, drug delivery and biomedical applications. Asian J Pharm Sci. 2015 Apr 1;10(2):99–107.
27. Chen C-H, Chen S-H, Mao S-H, Tsai M-J, Chou P-Y, Liao C-H, et al. Injectable thermosensitive hydrogel containing hyaluronic acid and chitosan as a barrier for prevention of postoperative peritoneal adhesion. Carbohydr Polym. 2017 Oct 1;173:721–31.

28. Vihola H, Laukkanen A, Valtola L, Tenhu H, Hirvonen J. Cytotoxicity of thermosensitive polymers poly(N-isopropylacrylamide), poly(N-vinylcaprolactam) and amphiphilically modified poly(N-vinylcaprolactam). Biomaterials. 2005 Jun 1;26(16):3055–64.
29. Liu H, Wang S. Poly(N-isopropylacrylamide)-based thermo-responsive surfaces with controllable cell adhesion. Sci China Chem. 2014 Apr 1;57(4):552–7.
30. Lencina MMS, Ciolino AE, Andreucetti NA, Villar MA. Thermoresponsive hydrogels based on alginate-g-poly(N-isopropylacrylamide) copolymers obtained by low doses of gamma radiation. Eur Polym J. 2015 Jul 1;68:641–9.
31. Wu L, Zhang H, Zhang J, Ding J. Fabrication of Three-Dimensional Porous Scaffolds of Complicated Shape for Tissue Engineering. I. Compression Molding Based on Flexible–Rigid Combined Mold. Tissue Eng. 2005 Jul 1;11(7–8):1105–14.

CHAPTER 5
CONCLUSIONS AND FUTURE WORKS

This thesis is focused on the fabrication and characterization of functional mimicked hydrogels in bone tissue engineering for orthopedic applications. There are three types of fabricated hydrogels in this research. The first study is to fabricate the combination of gelatin, chitosan, and calcium phosphate (CCP) hydrogel with different CCP content. This hydrogel is designed to mimic ECM of calcified soft tissue. The results show that the addition of CCP into gelatin/chitosan hydrogel can enhance cell proliferation and viability. This hydrogel will be used as a model for heterotopic ossification (OH) evaluation. However, the mechanical properties, gene expression, and in vivo testing are important factors for further study.

The hybrid hydrogels of gelatin/PVA with different ratios are successfully produced by the chemical and physical crosslink network. This hydrogel is designed to mimic collagen fibril and glycosaminoglycan formation in ECM of cartilage tissue. The results demonstrate that the pore size decreased as the proportion of PVA increased. The swelling behavior and degradation rate increased as the proportion of gelatin increased. The compressive strength increased as the proportion of PVA increased. The biological properties of this gelatin/PVA hydrogel indicate that the hydrogel promote cell adhesion and cell proliferation. Moreover, the gelatin/PVA hydrogel also increase ALP activity and calcium content, which are important biomarkers in osteogenic cell formation. Although the mechanical properties of gelatin/PVA hydrogel are not sufficient to support subchondral bone interface, the swelling behavior, degradation rate, pore size, and biological properties of this gelatin/PVA hydrogel are suitable for applications at subchondral bone interface. To develop this hydrogel, varying the freeze-thaw cycles and the amount of gelatin and PVA was studied. Moreover, gene expression and in vivo tests are necessary in future work.

Cell sheet membrane obtained from hyaluronic acid grafted with thermo-responsive PNIPAM polymer is fabricated. ^{1}H-NMR, GPC, and FT-IR spectrum confirmed the synthesized polymer structures. The molecular weight increased as a proportion of PNIPAM-COOH increased. This results suggest that PNIPAM-COOH

successfully grafted on HA-NH_2 chain. LCST of polymers is in the range of 29-32^oC, which comes from the ability of PNIPAM-COOH. Moreover, LCST is lower than biological temperature, which is suitable for clinical and tissue regeneration applications. For biological properties, cells can adhere and detach on synthesized polymers by controlling temperature. Moreover, cells can proliferate after transferring to the new plate. These synthesized polymers are not only applied for cell sheet applications but also trigger the information of complicated morphology of tissue.

According to this research, it was deduced that our mimicked hydrogel is promising to orthopedic application; 1) model for disease evaluation, 2) surgical applications, 3) to engineer the morphology of tissue. For the future works, to create the multifunctional hydrogel for specific application is challenge for the materials scientist and physician.

Appendix

^{1}H-NMR spectra of HA-PNIPAM-3

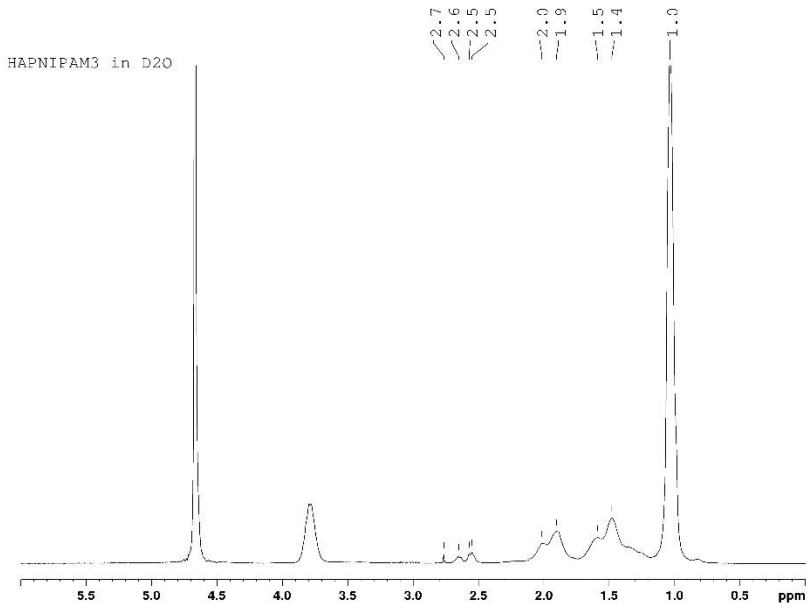

^{1}H-NMR spectra of HA-PNIPAM-5

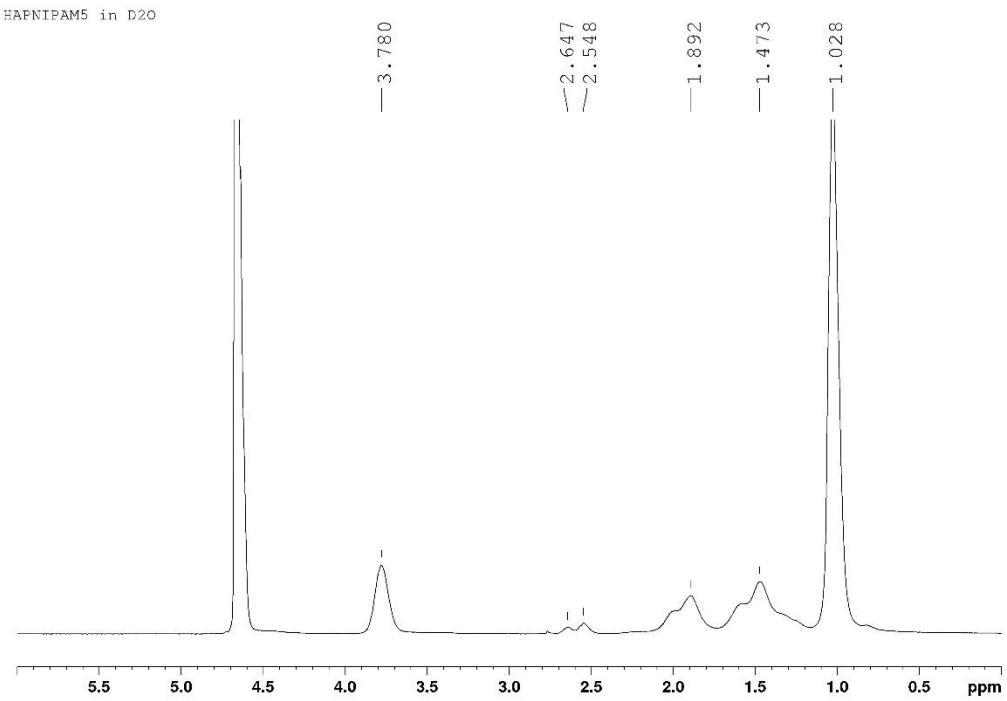

GPC Information

1. HA-NH_2

Sample name	: HA-NH_2	Run time	: 50.00 minutes
Sample type	: Broad unknown	Acquired by	: Water Phase
Injection	: 1	Acq method	: Pullulans method
Injection volume	: 20.00 µl		

BROAD UNKNOWN RELATIVE CHROMATOGRAM

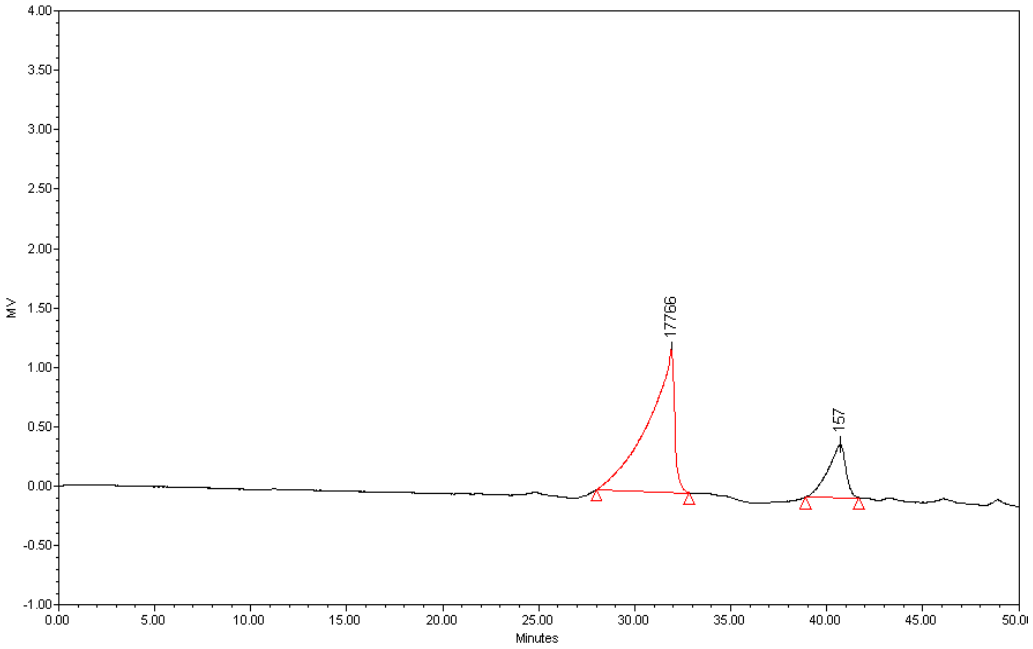

	Name	Retention Time (min)	Mn (Daltons)	Mw (Daltons)	MP (Daltons)	Mv (Daltons)	Mz (Daltons)	Mz+1 (Daltons)	Polydispersity	Mz/Mw	Mz+1/Mw	Id	Area (?V*sec)	% Area	Height (?V)	Int Type
1	Broad	31.901	24970	29419	17766		36141	44783	1.178167	1.228488	1.522258	0	114330	79.55	1201	BB
2	Peak2	40.700	179	199	157		224	253	1.111709	1.124640	1.269143	0	29393	20.45	450	BB

2. PNIPAM-COOH

Sample name : PNIPAM-COOH	Run time : 45.00 minutes
Sample type : Broad unknown	Acquired by : Tetrahydrofuran (THF)
Injection : 1	Acq method : Polystyrene method
Injection volume : 20.00 µl	

BROAD UNKNOWN RELATIVE CHROMATOGRAM

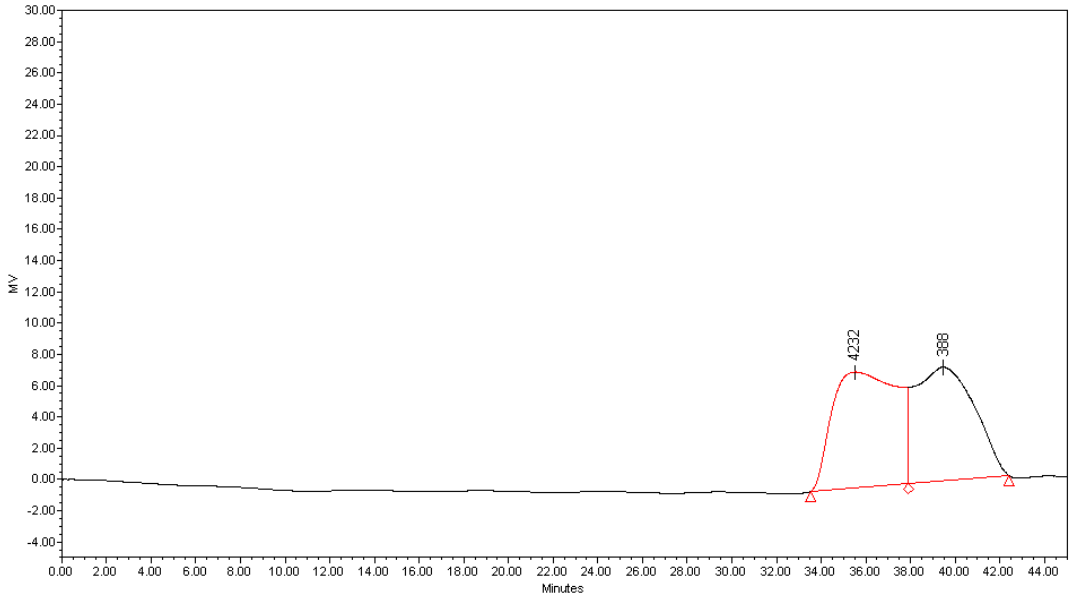

	Name	Retention Time (min)	Peak Codes	Mn (Daltons)	Mw (Daltons)	MP (Daltons)	Mv (Daltons)	Mz (Daltons)	Mz+1 (Daltons)	Polydispersity	Mz/Mw	Mz+1/Mw	Id	Area (?V*sec)	% Area	Height (?V)	Int Type
1	Peak4	35.500	I08	2746	3633	4232		4568	5345	1.322885	1.257167	1.471265	0	1498655	52.90	7404	BV
2	Peak3	39.471		318	479	388		652	781	1.509107	1.360129	1.630843	0	1334102	47.10	7276	VB

3. HA-PNIPAM-3

Sample name	: HA-PNIPAM-3	Run time	: 50.00 minutes
Sample type	: Broad unknown	Acquired by	: Water Phase
Injection	: 2	Acq method	: Pullulans method
Injection volume	: 20.00 µl		

BROAD UNKNOWN RELATIVE CHROMATOGRAM

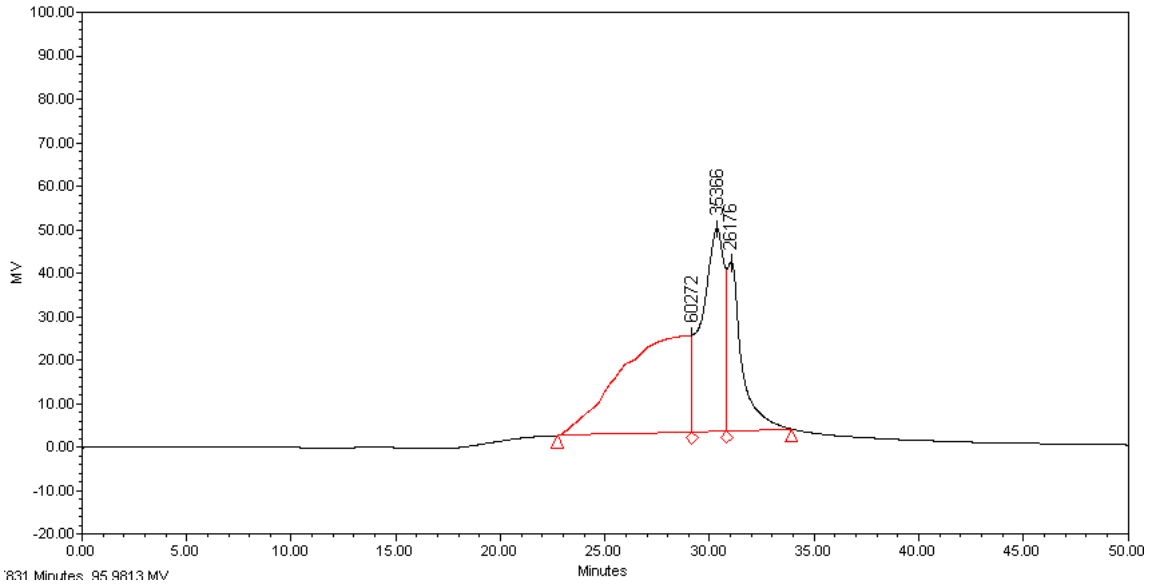

	Name	Retention Time (min)	Mn (Daltons)	Mw (Daltons)	MP (Daltons)	Mv (Daltons)	Mz (Daltons)	Mz+1 (Daltons)	Polydispersity	Mz/Mw	Mz+1/Mw	Id	Area (?V*sec)	% Area	Height (?V)	Int Type
1	Peak5	29.150	135834	221516	60272		393946	614661	1.630779	1.778408	2.774795	0	5140234	49.07	22182	BV
2	Peak3	30.347	38862	40485	35366		42254	44097	1.041762	1.043697	1.089205	0	3446177	32.90	46652	VV
3	Peak6	31.027	21401	22733	26176		23687	24377	1.062223	1.041972	1.072311	0	1889431	18.04	38767	VB

4. HA-PNIPAM-5

Sample name	: HA-PNIPAM-5	Run time	: 50.00 minutes
Sample type	: Broad unknown	Acquired by	: Water Phase
Injection	: 3	Acq method	: Pullulans method
Injection volume	: 20.00 µl		

BROAD UNKNOWN RELATIVE CHROMATOGRAM

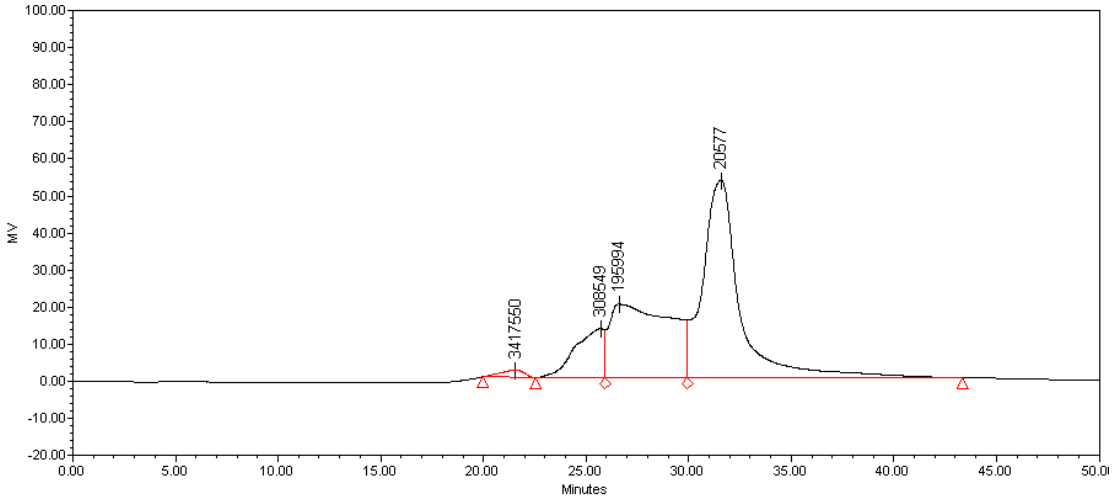

	Name	Retention Time (min)	Mn (Daltons)	Mw (Daltons)	MP (Daltons)	Mv (Daltons)	Mz (Daltons)	Mz+1 (Daltons)	Polydispersity	Mz/Mw	Mz+1/Mw	Id	Area (?V*sec)	% Area	Height (?V)	Int Type
1	Peak5	21.547	3760094	4246209	3417550		4843561	5504952	1.129283	1.140679	1.296439	0	161705	1.32	2011	BB
2	Peak3	25.705	427769	486087	308549		569826	680960	1.136331	1.172272	1.400902	0	1297335	10.56	13216	BV
3	Peak4	26.617	93853	123410	195994		155618	182283	1.314933	1.260979	1.477050	0	4130212	33.61	19847	VV
4	Broad	31.570	5080	19710	20577		24098	26804	3.879890	1.222639	1.359919	0	6698089	54.51	53259	VB

VITAE

Name Miss Atsadaporn Thangprasert

Student ID 5710330019

Educational Attainment

Degree	Name of Institution	Year of Graduation
Bachelor of Science (Chemistry)	Prince of Songkla University	2010
Master of Science (Material Science and Engineering)	Mahidol University	2013

Scholarship Award during Enrollment

Development and Promotion of Science and Technology Talents Project (DPST)

List of publications

Atsadaporn Thangprasert, Chittreeya Tansakul, Nuttawut Thuaksubun, Jirut Meesane, Mimicked extracellular matrix of calcified soft tissue based on chitosan/gelatin/compounded calcium phosphate hydrogel to design ex vivo model for heterotopic ossification, Materials and Design 134 (2017) 486–493.

Proceeding and international conferences

Atsadaporn Thangprasert, Chittreeya Tansakul, Jirut Meesane. Synthesis of Novel pH- and Temperature-Controlled Composite Hydrogels for Tissue Engineering, 9th World Congress Biomaterials, May2016, Montreal, Canada.

Atsadaporn Thangprasert, Chittreeya Tansakul, Nuttawut Thuaksubun, Jirut Meesane, Gelatin-based hybrid hydrogels as mimicked extracellular matrix scaffolds for bone healing in maxillofacial defects. The 7th National and International Graduate Study Conference “Thailand 4.0 Creative Innovation for Sustainable Development”